ASPECTS OF NEUTRON EMISSION FOLLOWING THE CH[illegible] PARTICLE BOMBARDMENT OF NUCLEI

Bruce Wakefield

Pembroke College

A thesis submitted for the Degree of Doctor of Philosophy in the University of Oxford.

Michaelmas Term, 1967.

C O N T E N T S

A B S T R A C T

A study of the nuclei Be^6, Be^9 and Cl^{33} has been made. These nuclei have been investigated by observing the neutrons emitted during or after their formation by charged induced reactions. The neutron energies have been measured by the "time of flight" technique, using both the pulsed beam and associated particle methods.

The first chapter contains an outline of the Distorted Wave Born Approximation and the application of this theory to the calculation of the angular distributions of neutrons emitted from a (p,n) reaction, which is treated as a special case of inelastic scattering, and also from the single and double stripping reactions (d,n) and (He^3,n).

In Chapter II is a description of the pulsed beam and associated particle time of flight techniques. A detailed account of the design, construction and mode of operation of the beam pulsing device used for the (p,n) experiments is given. Also included is a description of the neutron detector used together with an account of a method of pulse shape discrimination against gamma rays.

The reaction Li^6(p,n)Be^6 is reported in Chapter III. The reaction has been studied using the pulsed beam method

with proton energies ranging from 7 MeV to 18 MeV. At all incident energies the ground state of Be^6 was excited. For incident energies between 10.0 and 11.3 MeV there was evidence for an excited state in Be^6 at 1.7 MeV. Measurements with proton energies between 15.0 and 18.0 MeV confirmed this. The excitation and width of the first excited state has been found to be :-

$$E_x = 1.67 \pm 0.05 \text{ MeV}; \qquad \Gamma = 1.18 \pm 0.07 \text{ MeV}.$$

At incident energies of 16.55 and 18.0 MeV evidence has also been found for a second excited state in Be^6 at an excitation of about 3 MeV. Angular distributions for the ground state neutrons have been measured at incident energies of 8.3, 9.0, 9.6, 10.0, 10.5, 15.0, 16.55 and 18.0 MeV, and for the first excited state at 15.0 MeV. The angular distributions measured at 10.5 MeV and below could be fitted very well by a series of the first three Legendre polynomials, and have been interpreted in terms of compound nucleus theory. It is concluded that for these energies the reaction proceeds through two interfering states in Be^7 at about 10 MeV excitation with spins of $\frac{1}{2}^+$ and $3/2^-$. An attempt has been made to explain the results obtained at 15.0 MeV and above in terms of a direct reaction theory. The direct reaction

theory however gave no semblance of a fit. Calculations have been made in terms of pure phase space considerations in order to explain the nature of the neutron continuum seen in the reaction. It is concluded that the continuum arises chiefly from the four body break-up reaction

$$Li^6 + p \Rightarrow He^4 + p + p + n$$

with a small contribution from the reaction

$$Li^6 + p \Rightarrow Li^5 + p + n \quad .$$

An experiment performed to study the neutron decay of excited states in Be^9 populated by the beta decay of Li^9 is reported in Chapter IV. The neutron energies were measured by the associated particle time of flight technique. It has been found from this experiment that the beta decay of Li^9 populates not only the ground state and 2.43 MeV state of Be^9, but also states at 3.35 and 4.6 MeV. These two states, which have not previously been observed, have been given spin assignments of $\frac{1}{2}^-$ and $3/2^-$. Assuming that the beta decay branching ratio of Li^9 to the 2.43 MeV state in Be^9 is 20 per cent, the branching ratios to the 3.35 and 4.6 MeV states is found to be (7 ± 4) per cent and > 1.5 per cent, compared to shell model predictions of (10 ± 2) per cent and

(12 ± 3) per cent.

Finally, in Chapter V is reported the reaction $P^{31}(He^3,n)Cl^{33}$. This experiment was performed to measure the spin of the first $T = 3/2$ state in Cl^{33}. From the angular distribution of the neutrons, which is characteristic of an $L = 0$ angular momentum transfer, the spin of the analogue state has been found to be $\frac{1}{2}^+$. In addition tentative spin assignments of $3/2^+$ and $\frac{1}{2}^+$ have been given to two other states in Cl^{33} at 6.30 and 7.45 MeV respectively.

ACKNOWLEDGEMENTS

There are many people whose assistance has been invaluable during the course of my research at Oxford. But first I must thank Professor D.H. Wilkinson, F.R.S. for having allowed me the use of the facilities of the Oxford Nuclear Physics Laboratory.

Secondly, I must thank my supervisor, Dr. B.E. Macefield, for his help and encouragement, which was always available when needed.

A research project such as I have undertaken would not have been possible without the full co-operation of the technical staff of the Oxford Electrostatic Generators. They coped admirably with the task of operating the accelerators under the very exacting conditions demanded by the experiments.

I am also grateful to Dr. H.M. Hulme for allowing me the use of the research facilities at A.W.R.E. Aldermaston and to the staff of the tandem and 6 MeV Van de Graaff accelerators at A.W.R.E. for their assistance.

My colleague throughout most of this work has been Samar Mubarakmand. His assistance with the construction of apparatus and with the running of experiments was invaluable. It was a pleasure to work with him.

A special mention must be made of Mr. D. Waine for his unfailing help in the research workshop. He made the most impossible-looking job appear easy.

The analysis of the experimental data has involved the use of several computer programmes. I therefore wish to thank Dr. B.J. Macefield, Mr. M.J.L. Yates, Dr. J.C. Hardy, Dr. I.S. Towner and Dr. A.D. Hill for the use of their programmes.

I am grateful to the Science Research Council for financial assistance.

Finally, I must thank Mrs. M. Browne for typing this thesis.

C H A P T E R I

REACTION MECHANISMS

The term "nuclear reaction" is applied to a variety of processes involving the collisions of nuclei. In a typical nuclear reaction a particle x collides with another particle A and as the result of some interaction between them two new particles y and B are produced. Such a process can be written as

$$x + A \rightarrow y + B$$

or as $A(x,y)B$

The incident and outgoing particles x and y are usually light nuclei such as protons, neutrons, deuterons or helium nuclei while the target and residual nuclei A and B are generally heavier. Examples of nuclear reactions are $Li^6(p,n)Be^6$, $Li^7(t,p)Li^9$ and $P^{31}(He^3,n)Cl^{33}$. Nuclear reactions may also lead to more than two final nuclei. For example the reaction 10 MeV protons onto Li^6 can lead to the following reactions :- $Li^6(p,n)Be^6$, $Li^6(p,pn)Li^5$ and $Li^6(p,2pn)He^4$. Particles x and y may also be identical particles in which case we have a reaction known as scattering.

A reaction A(x,y)B can generally proceed in many ways. The particle x can interact with the nucleus A as a whole and get captured by it to form a compound nucleus. Its energy is quickly shared among all the constituent nucleons in A well before any re-emission can occur. The compound nucleus (A + x), which is left in an excited state, eventually breaks up into particles B and y. A reaction which proceeds by this mechanism is known as a "compound nucleus" reaction. Another way in which the reaction A(x,y)B can proceed is by what is known as a "direct reaction" mechanism. In this the particle x can interact with just one of the nucleons in A and in doing so can knock particle y out of B, being captured itself, or else be scattered back away from A. Alternatively, it can capture a nucleon or a cluster of nucleons from A to form a composite particle y. Another possibility occurs if x itself is a composite particle, when the target A can capture one or more of the constituents of x leaving the remaining particle to escape. These processes are characterized by the fact that a compound nucleus (A + x) is not formed.

It is by the study of nuclear reactions that the structure of atomic nuclei can be investigated. In a reaction the residual nucleus B can be left in an excited state, and

by measuring the energies of the outgoing particle y and from a knowledge of the total energy of the system one can determine the energy level structure of the nucleus B. If the reaction proceeds via a compound nucleus, one can investigate the structure of the compound nucleus by measuring the reaction cross section as a function of incident particle energy. Spins and parities of nuclear states can be determined from studies of the angular distributions of the emitted particles. In general compound nucleus reactions yield information about the compound state while direct reactions yield information about the residual nucleus.

In this thesis we will be using both compound nucleus theory and direct reaction theory. The results of the reaction $Li^6(p,n)Be^6$ obtained with incident proton energies below 11.3 MeV will be interpreted in terms of the compound nucleus theory. The compound nucleus formed by this reaction is Be^7. For incident energies above 15.0 MeV the compound nucleus theory does not appear to explain the results, and for these a direct reaction mechanism is assumed. The results will be compared with the predictions of a direct reaction model which treats the process as a special form of inelastic scattering. We shall also be using a direct reaction theory to interpret the results of the reaction $P^{31}(He^3,n)Cl^{33}$.

The direct reaction applicable to this case is one known as stripping. The target nucleus strips off and captures the two protons in the incident He^3 nucleus as it brushes past the target, leaving the neutron free to escape. In the next section is given an outline of the distorted wave Born approximation direct reaction theory, together with its application to inelastic scattering reactions and stripping reactions.

Distorted wave theory of direct reactions

A class of reactions known as direct reactions has become a good source of information about nuclear structure. These reactions are characterised by proceeding on a very short time scale without the formation of a compound nucleus. Examples of direct reactions are inelastic scattering and stripping. The first can be pictured as occurring when an incident nucleon enters the nucleus, collides with a target nucleon, loses some energy and then proceeds to escape from the nucleus. In a stripping reaction, for example a (d,p) reaction, the incident deuteron brushes past the nucleus and in doing so the loosely bound neutron is captured by the target. The proton carries on, being scattered by its interaction with the captured neutron.

The transition amplitude for a reaction i → f or A(a,b)B is

$$S_{fi} = \langle \phi_f(\underline{k}_f) | V_f | \psi(\underline{k}_i) \rangle$$

$\psi(\underline{k}_i)$ is the total wave function of the system in which a particle a is incident on a target A with a wave vector $\underline{k}_i$. It is the solution of the Schrodinger equation

$$H\psi = E\psi$$

where H is the total Hamiltonian of the system.

$\phi_f(\underline{k}_f)$ is the wave function that describes the motion of the two product particles after the interaction, namely that of a particle b being scattered by the residual nucleus B.

It is an eigenstate of the Hamiltonian H_o^f which gives such a motion, i.e.,

$$H_o^f \phi_f = E \phi_f$$

V_f is the interaction which induces the transition i → f and is related to H by

$$H = H_o^f + V_f$$

H may also be decomposed into $H_o^i + V_i$ where H_o^i is the

Hamiltonian which represents elastic motion in the incident channel, and V_i is the remaining part of H, and is the interaction which induces transitions into all open channels (except the elastic scattering channel).

The distorted wave Born approximation is introduced by replacing $\Psi(\underline{k}_i)$ in the expression for the transition amplitude by $\phi_i(\underline{k}_i)$, the wave function for the elastic scattering in channel i. In other words the complete wave function is written as

$$\Psi(\underline{k}_i) = \phi_i(\underline{k}_i) + \left\{\text{outgoing waves in other channels}\right\}$$

and in the Born approximation we assume that

$$\left\{\text{outgoing waves in other channels}\right\} \approx 0.$$

The physical meaning of this approximation is that the coupling of the incident channel to other channels is assumed to be small, so that all other cross sections are small compared to the cross section for the transition $i \to f$. The transition amplitude for the transition $i \to f$ in the D.W.B.A. can therefore be written as

$$T_{fi} = \left\langle \phi_f^{(-)}(\underline{k}_f) \middle| V_f \middle| \phi_i^{(+)}(\underline{k}_i) \right\rangle$$

where the superscripts (+) and (-) denote incoming and outgoing wave boundary conditions. The differential cross

section for the reaction can be expressed in terms of S_{fi} as

$$\frac{d\sigma}{d\Omega} = \frac{M_i M_f}{(2\pi\hbar^2)^2} \frac{k_f}{k_i} \sum |S_{fi}|^2$$

where the sum is over z components of angular momentum in the final state and an average over those in the initial state, and the M's are the reduced masses for the initial and final pairs of particles.

The wave functions ϕ_i and ϕ_f can be written as

$$\phi_i^{(+)}(\underline{k}_i) = \chi_a \chi_A \psi_i^{(+)}(\underline{k}_i, \underline{r}_i)$$

and

$$\phi_f^{(-)}(\underline{k}_f) = \chi_b \chi_B \psi_f^{(-)}(\underline{k}_f, \underline{r}_f)$$

where $\chi_a \chi_A \chi_b \chi_B$ are the internal wavefunctions of the particles a, A, b and B, and the $\psi(\underline{k},\underline{r})$ are distorted waves which describe the relative motion in the entrance and exit channels. These are Coulomb waves incident in the direction $\underline{k}$ together with outgoing spherical waves scattered by the Coulomb field plus spherical waves scattered by the optical nuclear potential. They are usually generated by solving the Schrodinger equation for an optical potential

which reproduces the observed elastic scattering at the same energy; i.e., the waves satisfy the equation

$$\left\{\nabla^2 + k^2 - \frac{2M}{\hbar^2}\left[U(r) + U_c(r)\right]\right\}\psi(\underline{k},\underline{r}) = 0$$

where $U(r)$ is the optical potential, $U_c(r)$ is the Coulomb potential and M is the reduced mass of the pair of interacting particles.

The form of the transition amplitude for the reaction A(a,b)B can now be written as

$$T = \iint \psi_b^{(-)*}(\underline{k}_b,\underline{r}_b) \left\langle B,b \middle| V \middle| A,a \right\rangle \psi_a^{(+)}(\underline{k}_a,\underline{r}_a)\, d\underline{r}_a\, d\underline{r}_b$$

The factor $\left\langle B,b \middle| V \middle| A,a \right\rangle$ is known as the nuclear form factor and is given by

$$\left\langle B,b \middle| V \middle| A,a \right\rangle = \int \chi_B^* \chi_b^* V \chi_A \chi_a \, d\xi$$

where ξ represents all coordinates independent of $\underline{r}_a$ and $\underline{r}_b$. It is therefore a function of $\underline{r}_a$ and $\underline{r}_b$ and contains all the information on nuclear structure, angular momentum selection rules and even the type of reaction being considered (i.e., whether stripping, inelastic scattering etc.).

The general treatment of this nuclear form factor is given in a paper by Satchler [Sa 64]. Here the matrix element is expanded into terms which correspond to the transfer to the nucleus of a definite amount of angular momentum J, which in turn is comprised of an orbital part L and a spin part S, where

$$\underline{J} = \underline{J}_B - \underline{J}_A \; ; \quad \underline{S} = \underline{S}_a - \underline{S}_b \; ; \quad \underline{L} = \underline{J} - \underline{S}$$

This series is written with Clebsh-Gordon coefficients corresponding to this vector coupling. The matrix element then becomes

$$\left\langle J_B M_B, S_b m_b \left| V \right| J_A M_A S_a m_a \right\rangle = \sum_{LSJ} i^{-L} G_{LSJ,M}(\underline{r}_b \underline{r}_a ; bB, aA)$$

$$\times (-)^{S_b - m_b} \left\langle J_A J M_A, M_B - M_A \middle| J_B M_B \right\rangle \left\langle S_a S_b m_a, -m_b \middle| S M_a - m_b \right\rangle$$

$$\times \left\langle L M, m_a - m_b \middle| J M_B - M_A \right\rangle$$

where $M = M_B - M_A + m_b - m_a$, and the symbols bB and aA denote the dependence on the various nuclear quantum numbers other than the z components of spin.

The amplitude T involves an integration over the space

of both $\underline{r}_a$ and $\underline{r}_b$ and the numerical integration of such an integral is difficult. Consequently the "zero range" approximation is introduced. This has the physical meaning that particle b is emitted at the same point as particle a is absorbed, so that $\underline{r}_b = \frac{A}{B}\underline{r}_a$ where A and B are the masses of the corresponding nuclei. As a result the integral for T is reduced to a three dimensional one. The form factor $G_{LSJ,M}(\underline{r})$ can then usually be factored into three parts

$$G_{LSJ,M}(\underline{r}) = A_{LSJ} F_{LSJ}(r) Y_L^M(\theta,\phi)$$

where A_{LSJ} is a spectroscopic factor and includes such quantities as fractional parentage coefficients and the interaction strength, and where $F_{LSJ}(r)$ is a radial form factor. If we now substitute this expression for G into the expansion for the nuclear form factor, and then substitute the expansion for the nuclear form factor into T we obtain the expression for the transition amplitude

$$T = \sum_{LSJ}(2J+1)^{\frac{1}{2}} A_{LSJ} \left\langle J_A J M_A, M_B - M_A \middle| J_B M_B \right\rangle \beta_{SJ}^{LMm_b m_a}(\underline{k}_b, \underline{k}_a)$$

where $M = M_B - M_A + m_b - m_a$, and where β is given by

$$(2J+1)^{\frac{1}{2}}\, i^{L}\, \beta_{SJ}^{LMm_b m_a}(\underline{k}_b,\underline{k}_a) = \left\langle LSM, m_a - m_b \,\middle|\, JM - m_b + m_a \right\rangle$$

$$\times \left\langle S_a\, S_b\, m_a, -m_b \,\middle|\, S\, m_a - m_b \right\rangle \times (-)^{S_b - m_b} (2L+1)^{\frac{1}{2}}$$

$$\times \int \psi_b^{(-)*}(\underline{k}_b, \tfrac{A}{B}\underline{r})\, F_{LSJ}(r)\, Y_L^M(\hat{r})\, \psi_a^{(+)}(\underline{k}_a, \underline{r})\, d\underline{r}$$

As mentioned before, all the information on nuclear structure, and the type of reaction is contained in the nuclear form factor. The types of reactions with which we are concerned in this thesis are inelastic scattering, for which p,n reactions are a special case, and stripping reactions. The treatment of the nuclear form factors for these reactions is given in papers by Satchler [Sa 64; Sa 66] and we will here outline the procedure.

a) Inelastic Scattering

The interaction producing the scattering may be expanded into multipoles.

$$V = V(r, \xi_a \xi_A) = \sum_{LSJ} (-)^{J-\mu} V_{LSJ,\mu}(\xi_A, r)\, T_{LSJ,-\mu}(\hat{r}, \xi_a)$$

where ξ_a and ξ_A represent the internal coordinates of the projectile and target. $T_{LSJ,-\mu}$ is a spin-angle tensor

constructed as

$$T_{LSJ,\mu}(\theta,\xi_a) = \sum_m \langle LSm\,\mu-m \mid J\ \mu\rangle\, i^L\, Y_L^m(\theta,\phi)\, \mathcal{S}_{S,\mu-m}(\xi_a)$$

$\mathcal{S}_S$ is a tensor of rank S in the projectile coordinates and can be expressed in terms of the spin operator $\underline{s}_a$ for a; e.g., we may put $\mathcal{S}_0 = 1$ and $\mathcal{S}_1 = \underline{s}_a$. The various terms in the expansion of $T_{LSJ,\mu}$ correspond to various amounts of the angular momenta L, S and J which can be transferred to the target during the reaction. L arises from a change in the orbital motion of the projectile while S comes from coupling to the projectile spin. L also determines the parity change in the transition $\Delta\pi = (-)^L$.

If we include isobaric spin in the interaction then V must be modified slightly to be

$$V = \sum_T \underline{V}^{(T)} \cdot \underline{\mathcal{C}}_T = \sum_{T\tau} (-)^\tau\ V^{T\tau}\ \mathcal{C}_{T-\tau}$$

where $V^T = V^T(\underline{r}, \xi_a\ \xi_A)$ is given above with $V_{LSJ,\mu}$ replaced by $V^T_{LSJ,\mu}(r, \xi_A)$. $\underline{\mathcal{C}}_T$ is a tensor of rank T in the isospin of the projectile and we can put $\mathcal{C}_0 = 1$ and $\underline{\mathcal{C}}_1 = t_a$. V^T may produce a change in the isospin of the target nucleus.

Inserting the interaction V into the nuclear form factor we obtain with $S_b = s_a$, and $t_b = t_a$

$$\langle bB \mid V \mid aA \rangle \equiv \langle S_a m_b, t_a \tau_b, J_B M_B T_B \tau_B \mid V \mid S_a m_a t_a \tau_a J_A M_A T_A \tau_A \rangle$$

$$= \sum_{TLSJ} i^{-L} G^{T}_{LSJ}(\underline{r}) (-)^{S_a - m_b} \langle S_a S_a m_a - m_b \mid S\ m_a - m_b \rangle$$

$$\times \langle J_A J M_A, \cdots - M_A \mid J_B \cdots_B \rangle \langle \cdots M, m_a - m_b \mid J M_B - A \rangle$$

$$\times \langle T_A \cdots \tau_A, \tau_B - \tau_A \mid \cdots_B \tau_B \rangle \langle t_a \cdots \tau_b, \tau_B - \tau_A \mid t_a \tau_a \rangle$$

where $G^{T}_{LSJ}(\underline{r}) = G^{T}_{LSJ}(r)\ Y^{L*}_{\cdots}(\omega r)$

and $G^{T}_{LSJ}(r) = (-)^{S} \hat{\ }_a \hat{\ }^{-1} \langle S_a \| S_b \| S_a \rangle \langle t_a \| \cdots \| t_a \rangle$

$$\times \langle J_B \cdots \| V^{T}_{LSJ}(r) \| J_A \cdots \rangle$$

$\hat{S}$ denotes $(2S + 1)^{\frac{1}{2}}$.

We assume that the interaction V is a sum of two body interactions between the projectile and the target nucleons.

i.e., $V = \sum_i v_{ia} - U$

where the subscript i stands for a target nucleon. U is the optical potential used to generate the distorted waves but

since it is diagonal in the nuclear states it does not contribute to inelastic scattering. The interaction v_{ia} depends on the separation $\rho = |\underline{r}_i - \underline{r}|$ where $\underline{r}$ is the position of the centre of mass of the projectile, and this dependence ($g(\rho)$) may be expanded in multipoles

$$g(\rho) = \sum_{L=0}^{\infty} (2L+1)\, g_L(r_i, r)\, P_L(\cos \theta_{ia})$$

$$= 4\pi \sum_{LM} g_L(r_i, r)\, Y_L^M(\theta_i \phi_i)\, Y_L^{M*}(\theta \phi)$$

v_{ia} is also a spin and isospin dependent interaction which for nucleons as projectiles can be written as

$$v_{ia} = -V_N [a_0 + a_1\, \underline{\sigma}_i \cdot \underline{\sigma}_a]\, g(\rho)$$

The $\underline{\sigma}$ are the Pauli spin operators, while the a_β include the isospin dependence

$$a_\beta = a_{\beta a} + a_{\beta p}\, \underline{\tau}_i \cdot \underline{\tau}_a$$

The $\underline{\tau}$ are also Pauli spin operators with z components ± 1 for neutrons and protons respectively. The a_β are also normalised so that

$$a_{o\alpha} + a_{1\alpha} \hat{\tau}_3 (a_{o\beta} + a_{1\beta}) = 1$$

We may now perform the separation $V = \sum_T \underline{V}^T \cdot \underline{\tau}_T$

if we identify $\underline{\tau}_0 = 1$ and $\underline{\tau}_1 = \underline{t}_a$. Then

$$V^0 = - V_N \sum_i [a_{o\alpha} + a_{1\alpha} \underline{\sigma}_i \cdot \underline{\sigma}_a] g(\rho)$$

and

$$V' = - V_N \sum_i \underline{\tau}_i [a_{o\beta} + a_{1\beta} \underline{\sigma}_i \cdot \underline{\sigma}_a] g(\rho)$$

Also if we choose $\underline{S}_0 = 1$ and $\underline{S}_1 = \underline{\sigma}_a$ we find

$$V^T_{LSJ,\mu} = - (-)^S 4\pi V_N \sum_i g_{LSJ} (r_i, r) T_{LSJ,\mu} (\theta_i \phi_i \sigma_i)$$

$$\times \begin{cases} a_{o\alpha} & \text{if } T = 0 \\ a_{1\alpha} \underline{\tau}_i & \text{if } T = 1 \end{cases}$$

Using explicit values for the spin and isospin reduced matrix elements, the radial part of the nuclear form factors can be written as

$$G^{T}_{L,J}(r) = (-)^{S}\, 2^{\frac{1}{2}}\, \hat{T}\, \langle J_B T_B \| V^{T}_{L,J}(r) \| J_A T_A \rangle$$

$$= -\, 2^{\frac{1}{2}}\, 4\pi\, V_N \langle J_B T_B \| \sum_i (a_{S\alpha}\, \delta_{T,0} + 3^{\frac{1}{2}}\, a_{S\beta}\, \tau_i\, \delta_{T,1})\, g_L\, Y^{T}_{L,J} \| J_A T_A \rangle$$

$$= \kappa^{T}_{LSJ}\, F^{T}_{LSJ}(r)$$

Details of the evaluation of these reduced matrix elements are given in Satchler's paper (Sa 66) for a number of examples in particular :-

1) Single particle transitions which correspond to the excitation of a single particle outside a closed shell from an orbit n, ℓ, j to another orbit n', ℓ', j'.

2) The j^n configurations which correspond to the recoupling of n nucleons which occupy the j orbit.

3) The transitions of j^n to $j^{n-1}\, j'$ corresponding to the excitation of one of the particles in the j orbit to the j' orbit.

In each case radial integrals of the form

$$I_L(r) \equiv I_{L;1,2}(r) = \int_0^\infty j_L(r_i r)\, \psi_1(r_i)\, \psi_2(r_i)\, r_i^2\, dr_i$$

appear in the matrix element, where $U_k(r)$ are the radial parts of single particle bound state wavefunctions. The subscript k stands for the quantum numbers N_k, ℓ_k and j_k. In the zero range approximation $g(\rho) = \delta(\rho)$, and so $g_L(r_i,r) = \delta(r_i-r)/4\pi r^2$. Thus the $I_L(r)$ for a given pair of $U_k(r_i)$ are the same for all L namely

$$I_L(r,4\pi) = U_1(r)U_2(r) / 4\pi$$

The radial factor $I_L(r)$ is identified as the radial form factor $F^T_{L,J}(r)$ in the expression for $G^T_{L,J}(r)$

(b)

Stripping reactions

In the stripping reaction A(a,b)B, the projectile is assumed to be made up of the emitted particle b and another particle x which is captured by the target. The interaction is usually taken to be V_{bx} which is the potential binding b and x to form a. The nuclear form factor then becomes

$$\langle J_B M_B S_b m_b \mid V \mid J_A M_A S_a m_a \rangle$$

$$= \int \Psi^*_{J_B M_B}(\underline{r}_x \xi_x \xi_A) \phi^*_{S_b m_b}(\xi_b)\, V_{bx}(r_{bx} \xi_b \xi_x) \Psi_{J_A M_A}(\xi_A)$$

$$\times \phi_{S_a m_a}(r_{bx} \xi_b \xi_x)\, d\xi_A\, d\xi_b\, d\xi_x$$

where ξ_A, ξ_x and ξ_b represent the internal coordinates of the corresponding particles. The spin transfer S is now seen to be the spin of the captured particle and need not have a unique value since in general x is a cluster of nucleons. To evaluate this matrix element the wave function of the residual nucleus is first expanded in terms of the eigenstates of the target.

$$\Psi^{J_B M_B}(\underline{r}_{xA}\xi_x\xi_A) = \sum_{J\mu J_A' M_A'} \Psi^{J_A' M_A'}(\xi_A)\, \mathcal{Q}^{BA'}_{J\mu}(\underline{r}_{xA}\xi_x)$$

$$\times \langle J_A' J M_A' \mu \,|\, J_B M_B \rangle$$

Since V_{bx} does not depend on $\underline{r}_{xA}$ the only terms in this expansion which will contribute to the matrix element are the ones with $J_A' = J_A$ and $M_A' = M_A$.

$\mathcal{Q}_{J\mu}$ is the associated wavefunction for particle x and may be expanded into spherical harmonics in $\underline{r}_{xA}$

$$\mathcal{Q}^{BA}_{J\mu}(r_{xA},\xi_x) = \sum_{LSM} i^L Y^M_L(\hat{r}_{xA}) \Phi^{BA,LJ}_{S,\mu-M}(r_{xA},\xi_x)$$

$$\times \langle LSM, \mu-M \,|\, J\,\mu \rangle$$

The function Φ cannot in general be factored into functions depending on r_{xA} and ξ_x separately although it can always be expanded in such a form. If x is a single nucleon, or if its structure does not change during its transfer from a to A then it can be factored. Whether Φ is simply factorable or not, the integration over ξ_b and ξ_x can be performed

$$\iint \chi^{*}_{S_b m_b}(\xi_b)\, \Phi^{BAJ\mu *}_{S,\mu-m}(r_{xA}\,\xi_x)\, V_{bx}(r_{bx}\,\xi_b\,\xi_x)\, \chi_{S_a m_a}(r_{bx}\,\xi_b\,\xi_x)\, d\xi_b\, d\xi_x$$

$$= \langle S_b S\, m_b, \mu-m \mid S_a m_a \rangle \; H_{LSJ}(r_{xA}, r_{bx})$$

Hence $G_{LSJ,M}(\underline{r}_b, \underline{r}_a) = \mathcal{J} \hat{a}\, \hat{S}^{-1}\, Y_L^{m*}(\hat{r}_{xA})\, \chi_{xA}\, H_{LSJ}(r_{xA}, r_{bx})$

where $\mathcal{J}$ is the Jacobian for the transformation from the coordinates $\underline{r}_{xA}$ and $\underline{r}_{bx}$ to $\underline{r}_b$ and $\underline{r}_a$ used in the distorted waves

$\mathcal{J} = [aA/x\,(a+A)]^3$ where the letters refer to the masses of the corresponding particles.

For single nucleon transfer such as (d,n) reactions the expansion of $\Psi_{J_B L_B}$ may be described in shell model

terms. The function Ψ can be identified as the wave function for the single nucleon orbit (L,J) times a spectroscopic factor.

$$\Psi^{BA}_{J\mu} = a^{BA}_{LJ} \Psi_{LJ\mu}(r_{xA}, \xi_x)$$

There is no sum over L and S since $S = \frac{1}{2}$ only and $L = J \pm \frac{1}{2}$ according to the parity change. The function Φ is factorable

$$\Phi^{BnLJ}_{b\sigma}(r_{xA}, \xi_x) = a^{BA}_{LJ} U_{LJ}(r_{xA}) \chi_{n\sigma}(\xi_x)$$

where U_{LJ} is the radial function for the L orbit and $\chi_{n\sigma}$ is the nucleon spin function. As a result h is also factorable

$$h_{LJ}(r_{xA}, r_{bx}) = a^{BA}_{LJ} U_{LJ}(r_{xA}) D(r_{bx}) \quad \text{where}$$

$$\langle S_b m_b \sigma \mid S_a m_a \rangle D(r_{bx}) = \iint \Psi^*_{S_b m_b}(\xi_b) \chi^*_{n\sigma}(\xi_x)$$

$$\times V(r_{bx}, \xi_b \xi_x) \Psi_{S_a m_a}(r_{bx}, \xi_b \xi_x) \, d\xi_b \, d\xi_x$$

If the wavefunction for a is also factorable as it is for the deuteron, i.e., if

$$\Psi_{S_a m_a}(r_{bx}, \xi_b, \xi_x) = \phi_a(r_{bx})\, \chi_{S_a m_a}(\xi_b \xi_x)$$

then D becomes

$$D(r_{bx}) = V_{bx}^{(S_a)}(r_{bx})\, \phi_a(r_{bx})$$

where $V^{(S_a)}$ is the value of V in the spin state S_a.

In the zero range approximation $D(r_{bx})$ is replaced by a delta function

$$D(r_{bx}) = D_o\, \delta(\underline{r}_{bx})$$

Since $\underline{r}_{bx} = (\underline{r}_b - \frac{A}{B}\, \underline{r}_a)\ (aB/x(a+A))$, then

$$\delta(\underline{r}_{bx}) = \delta(\underline{r}_b - \frac{A}{B}\, \underline{r}_a)\ (aB/x(x+A))^{-3}$$

$G_{LSJ,n}(\underline{r})$ then becomes

$$G_{LSJ,n}(\underline{r}) = A_{LSJ}\, F_{LSJ}(r)\, Y_L^n(-,\chi)$$

with $F_{LSJ}(r) = b(r)$ the radial function of the captured particle and $A_{LSJ} = \hat{a}^{-1}\, C_{LJ}^{BA} \cdot n^{\frac{1}{2}}\, D_o$ where n is the number of equivalent nucleons in orbit LJ.

Double stripping is treated by Hook and Mitra [no 64] . The associated wavefunction of the captured particles is written as the sum of products of two single particle wavefunctions.

$$\zeta^{BA}_{J\mu} = \sum \langle lSm, \mu-m \,|\, J\mu \rangle \langle \ell_1 \ell_2 m_1, M-m_1 \,|\, lM \rangle$$

$$\times \langle s_1 s_2 \sigma_1, \mu-m-\sigma_1 \,|\, S\ \mu-m \rangle\ i^{\ell_1+\ell_2}\ Y^{m_1}_{\ell_1}(r_1\phi_1) Y^{m_2}_{\ell_2}(r_2\phi_2)$$

$$\times \chi^{\sigma_1}_{s_1} \chi^{\mu-m-\sigma_1}_{s_2}\ u_{\ell_1}(r_1) u_{\ell_2}(r_2)$$

where the sum is over all quantum numbers except J and μ. The subscripts 1 and 2 refer to the two captured particles. The interaction in this case is the interaction between the outgoing particles and the stripped particles

$$\text{i.e.,} \quad V = V_{b1} + V_{b2}$$

In order to facilitate calculations the zero range approximation for the incident particle is made. To do this we write $\underline{r}_b = \underline{r}_1 = \underline{r}_2 = \underline{r}$, i.e., we treat the projectile as a point particle. Also if we consider only (He^3,n) reactions, the captured particles are both protons and so in

the projectile they must be in an s state. The transferred spin can then only be $S = 0$ and so we must also have $J = L$. The wave function of the final nucleus is now

$$\Psi_{J_B M_B} = \sum \langle J_A J M_A \mu \mid J_B M_B \rangle \langle L 0 M 0 \mid J M \rangle \langle \tfrac{1}{2} \tfrac{1}{2} \sigma_1, -\sigma_2 \mid 0 0 \rangle$$

$$\times \langle \ell_1 \ell_2 \, m_1, M-m_1 \mid L M \rangle \; i^{\ell_1+\ell_2} \, Y^{m_1}_{\ell_1}(\theta\phi) \, Y^{M-m_1}_{\ell_2}(\theta\phi)$$

$$\times \chi^{\sigma_1}_{s_1} \chi^{-\sigma_1}_{s_2} \, U_{\ell_1}(r) U_{\ell_2}(r) \, \theta_{J_B J'_A}(J 0 L \ell_1 \ell_2) \Psi_{J'_A M'_A}$$

where the sum is over all quantum numbers except J_B and M_B, and where $\theta(J 0 L \ell_1 \ell_2)$ is a two particle fractional parentage coefficient. The integrations can now be carried out and after some manipulation the final expression for the differential cross section is [see No74]

$$\frac{d\sigma}{d\Omega} = \frac{k_b}{k_a} \frac{(2J_B+1)}{(2J_A+1)} \sum_M \left| \sum_{\ell_a} D^M_{\ell_a}(\theta) \, I^M_{\ell_a}(\theta,0) \right|^2$$

where $D^M_{\ell_a}(\theta) = \sum_{\ell_1 \ell_2 \ell_b} i^{\ell_a - \ell_b - \ell_1 - \ell_2} \frac{\hat{\ell}_1 \hat{\ell}_2 \hat{\ell}_b}{\hat{L} \hat{\ell}_a} \langle \ell_1 \ell_2 \, 0 0 \mid L 0 \rangle$

$$\times \langle L \ell_b \, 0 0 \mid \ell_a 0 \rangle \langle L \ell_b \, M 0 \mid \ell_a M \rangle \times I(\ell_a \ell_b \ell_1 \ell_2) \sigma_L(\ell_1 \ell_2)$$

In this formula $\Theta_L(\ell_1\ell_2)$ is given by

$$\Theta_L(\ell'_1\ell'_2)\,\Theta_L(\ell_1\ell_2) = \sum_{SJ} \hat{S}^2 C^2(J_t L \ell'_1\ell'_2)\, G_t^2(S)\, \hat{J}^{-2} C^2(J_t L \ell_1\ell_2)$$

and $G_t^2(S)$ denotes the probability that the two captured particles in the projectile have spin S. As mentioned before for (He^3,n) reactions S = 0 and L = 0. The radial integral I is given by

$$I(\ell_a\ell_b\ell_1\ell_2) = \int_0^\infty U_{\ell_a}(r)\, U_{\ell_b}(r)\, U_{\ell_1}(r)\, U_{\ell_2}(r)\, r^2\, dr$$

where U_{ℓ_a} and U_{ℓ_b} are the radial wave functions which arise when the distorted waves are expanded in spherical harmonics.

The above expression for the cross section does not give the absolute value, since to obtain this involves evaluating an overlap integral between the interaction operator V and a product of He^3 and diproton wavefunctions. This factor is given by

$$D(\underline{r}_{bx}) = \iint \chi_s^{\sigma *} \Psi^*_{b^m b}(\xi_b) V_{bx}(\underline{r}_{bx}, \xi_b \xi_x)\, \Psi_{a^m a}(\underline{r}_{bx} \xi_b \xi_x)$$

$$\times \; d\xi_b\, d\xi_x$$

where χ_S^σ is the spin function of the captured pair.

Assuming that $D(\underline{r}_{bx})$ has a short range we can write in the zero range approximation [Ma 67]

$$D(\underline{r}_{bx}) = g \left\langle \ell_b \; m_b \; \sigma \middle| S_a \; m_a \right\rangle \delta(\underline{r}_{bx})$$

where the Clebsh Gordon coefficient appears as the result of extracting the magnetic quantum number dependence of $D(\underline{r}_{bx})$, and where g is a constant which depends on the strength of the interaction and the structure of particles a and b. The expression given above for the cross section should be multiplied by the factor ^{2} which is used as a parameter in fixing the absolute magnitude of the cross section.

The selection rules determining the value of L in double stripping are

$$\underline{J}_f = \underline{J}_i + \underline{L} + \underline{S} \; ; \quad \underline{L} = \underline{\ell}_1 + \underline{\ell} \; ; \quad \underline{S} = \underline{s}_1 + \underline{s}_2$$

The value of L is even if the parities of the initial and final states are the same, but odd if they are different. In the case of the (He^3,n) or (t,p) reactions there is an additional selection rule

$$S = 0 \; .$$

C H A P T E R II

EXPERIMENTAL TECHNIQUE

Introduction

Neutrons can be detected quite efficiently, but the measurement of their energies is not so straightforward. This is because the neutron itself is not an ionizing particle. In order to detect neutrons they have to be made to undergo some form of nuclear interaction in order to produce a fast moving charged particle. The charged particle is then detected through its ionizing properties. The interactions commonly used are (n, p) scattering and the reactions

1) $n + Li^6 \rightarrow He^4 + H^3$

2) $n + B^{10} \rightarrow Li^7 + He^4$

3) $n + He^3 \rightarrow H^3 + h$

Detectors relying on (n, p) scattering are cloud-chambers, photographic plates, recoil telescopes and the organic scintillators. Detectors using reactions 1, 2 and 3 are Li^6I crystals, BF_3 counters and He^3 proportional counters

respectively. The energies of the neutrons have to be deduced from the kinematics of the induced reactions. Complications arise in the case of (n, p) scattering because the energy of the recoiling proton depends on its angle of recoil.

In principle the most straightforward method of measuring neutron energies is to measure their velocities. This is known as the "time of flight" technique. This method of energy measurement was first applied to neutrons with energies in the eV range. However with the development of neutron detectors with a very fast response, and the development of electronic equipment capable of handling pulses in the nanosecond region it has been possible to extend time of flight measurements into the MeV range of energies.

The time of flight technique was used in the experiments described in this thesis. In order to measure the velocity of a neutron one must know the time at which it left the target, the time at which it reached the detector and the distance travelled between the target and the detector. Measuring the time of detection, and the flightpath is easy; the problem is to determine the starting time. There are two ways of doing this. The most versatile way is to bombard the target with short bursts of particles. The time of

arrival of a burst of particles at the target then determines the time of departure of the neutron. The other method involves detecting a charged particle or gamma ray which is released from the target in coincidence with the neutron, and using the time of detection of this particle as the starting time. This latter method has the advantage that expensive beam pulsing equipment is not required but obviously cannot be used to study neutrons which arise from transitions to the ground state of particle stable nuclei unless the recoiling nucleus can be detected. It is however a useful tool for measuring the angular correlation between neutrons and gamma rays or neutrons and charged particles, but one of the major problems associated with angular correlation experiments, namely, the ratio of real to random coincidences, is likely to be more acute for correlations with neutrons since in order to get reasonable neutron energy resolution, neutron flight paths of several meters are required. This will mean that the neutron flux entering the detector from the target will be small, while the general background remains the same. Both of these time of flight techniques were used for the experiments reported in this thesis.

The Pulsed Beam Method

In order to perform time of flight experiments with

the pulsed beam method, a means of producing pulses of charged particles is required. There are two ways of doing this with Van de Graaff accelerators. The easiest way is to chop the D.C. beam from the accelerator after acceleration by sweeping it across a narrow slit with an r.f. electric field. A better method is to produce the pulses before acceleration by pulsing the source. At Oxford where the (p, n) experiments were done the former method of pulsing is used, while the 6 MeV Van de Graaff at A.W.R.E. Aldermaston, where the (He^3,n) experiments were performed, has pulsed source.

At Oxford the pulses are produced by passing the accelerated beam between a pair of parallel deflector plates to which a strong r.f. electric field, with a frequency of 10 mc/sec. is applied. This field sweeps the beam across the entrance slit of the analysing magnet. A short burst of particles passes through the magnet everytime the beam crosses the slit. From this arrangement alone, bursts are produced every 50 nanoseconds. Because this time interval between pulses is too short to measure the time of flight of the neutrons to be studied a way of increasing this time must be found. Another disadvantage of this simple system is that there are two image points produced on the target, one arising when the beam is swept from left to right, and

the other when it is swept from right to left. One way of increasing the time interval between pulses is to run the deflector plates at a lower frequency, but now a larger electric field would be needed to produce the same pulse length. The double image would still be produced, and in fact would be worse than before since the separation is proportional to the applied field.

The method we have used to increase the time interval between successive pulses, which also removes the double image, is as follows. After passing between the main deflector plates the beam passes between a second but smaller set of deflector plates. An r.f. electric field with a frequency of 5 mc/sec. is applied to the secondary deflectors. The direction of this field is at right angles to that of the main field and also at right angles to the direction of the beam. If the relative phase of the two r.f. fields is adjusted correctly the beam after passing through both sets of deflectors will trace out a figure of eight in space, the centre of the figure lying on the D.C. beam axis. This again is undesirable since with this arrangement the beam would still cross the slit from left to right and vice-versa, although the pulse repetition rate is now one pulse every 100 m.sec.. The repetition rate is still further reduced,

and the double image finally removed by applying a negative D.C. bias to the upper one of the two secondary deflectors. The beam of positive ions is therefore deflected upwards. The figure of eight traced out by the beam is also moved upwards so that the centre is no longer on the axis. The magnitude of the bias is adjusted until only the bottom of the figure of eight crosses the axis and hence the magnet slit. The beam will now cross the slit in one direction only, and only once every 200 n.s. which is the period of the secondary r.f. field. The speed with which the beam crosses the slit and hence the pulse length is governed by the frequency and magnitude of the main field. A detailed description of the beam chopper will now follow.

The Main Deflectors

The main deflector plates are two hollow bars 80 cms. long, 2.2 cms. wide and separated by 1.9 cms. They are orientated such that the field between them is horizontal. Cooling water can be circulated through them. The plates are mounted on P.T.F.E. insulators inside an aluminium pipe 20 cms. in diameter which is coupled to the beam line between the tandem accelerator and the analysing magnet. Micrometer adjusting screws enable the plates to be aligned accurately parallel to the beam axis.

The r.f. power is applied to the plates from a 8 kW, 10 kc/sec. power amplifier. The circuit diagram of this amplifier is shown in Fig. (2.1). The plates themselves form part of the amplifier's tank circuit. The rest of the tank circuit consists of a coil 12" long and 4" in diameter wound from 12 turns of 1/4" bore copper tube, and a parallel plate variable air condenser (TC1) with a maximum working capacity of about 8 pf used for fine tuning. The amplifier uses a water cooled triode (Mullard TY7-600W) which will stand a maximum power dissipation on its anode of 6 kW. The maximum power developed in the tank circuit when the valve is operated with an anode voltage of 6 kV is estimated to be 8 kW, and the efficiency estimated to be 70 per cent. The tank coil is an autotransformer with a step up ratio of 4 : 1, so when the amplifier is run at full power the r.f. voltage developed across the deflector plates is 24 kV. The condenser C1 connected between the tank circuit and the grid of the triode is similar in construction to TC1 and is used to neutralize the 11 pf grid-anode capacity of the triode to prevent feedback from the output to the input. The resistance-capacity combination R1, C1 provides a self biasing circuit for the triode, their values having been chosen so as to give a mean D.C. grid bias of - 450 V. The relay is included to protect the valve in the

FIG 2·1

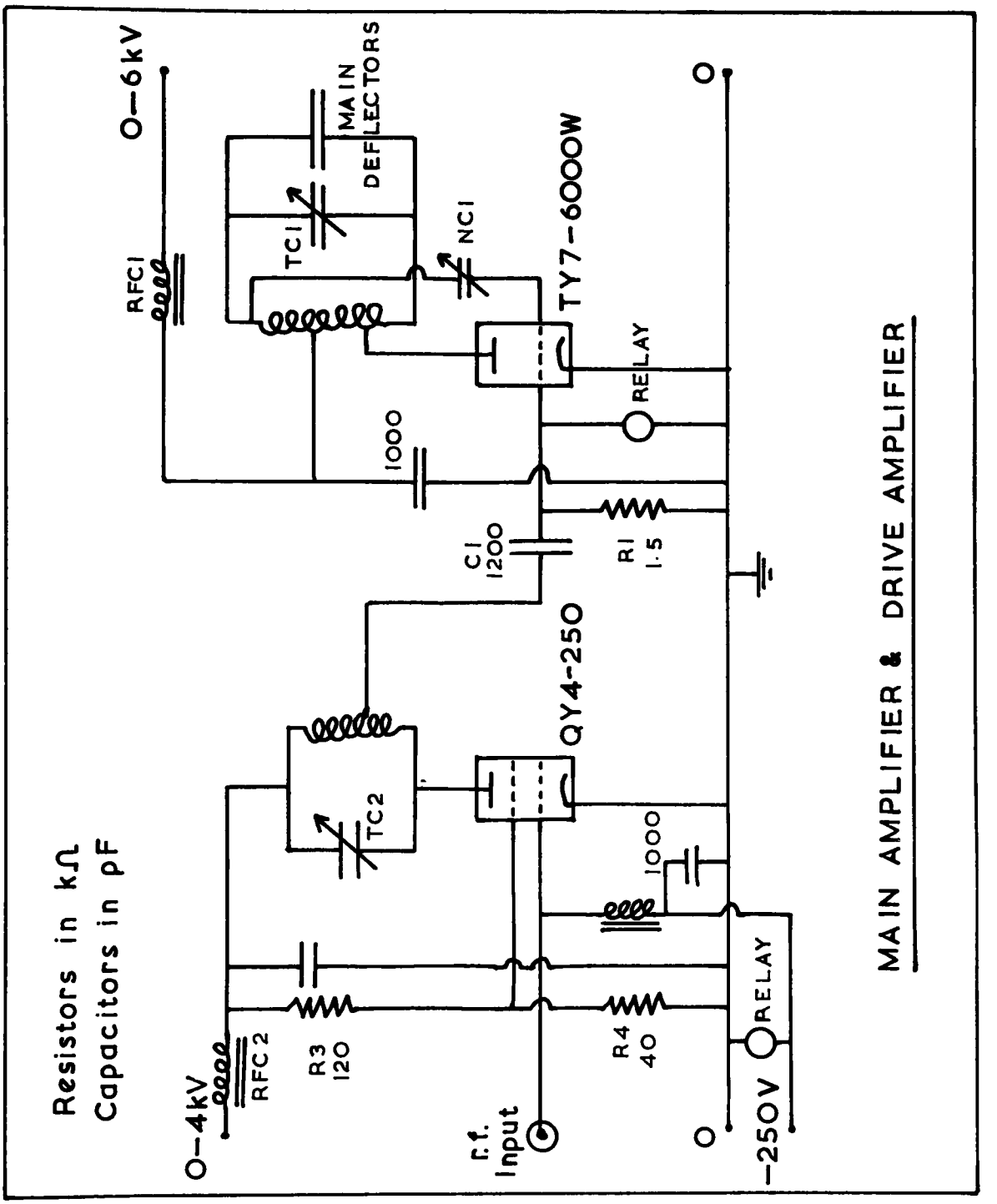
MAIN AMPLIFIER & DRIVE AMPLIFIER
Resistors in kΩ
Capacitors in pF
0—6kV
RFC1
TC1
MAIN DEFLECTORS
NC1
TY7-6000W
RELAY
1000
C1 1200
R1 1·5
QY4-250
TC2
1000
RELAY
0—4kV
RFC2
R3 120
R4 40
r.f. Input
0
-250V
0

event of failure of the input to the valve resulting in the loss of grid bias. If the grid bias rises above - 300V the relay opens and turns off the EHT supply to the valve.

The power required to drive the main amplifier is about 300W. This is supplied by a smaller power amplifier also shown in Fig. (2.1). This amplifier uses an air cooled tetrode (Mullard QY 4-250) and is capable of providing 750W of power when operated at 4 kV. The tank circuit for this amplifier consists of a coil made from 16 S.W.G. copper wire wound on a 3" diameter former, the input capacity of the triode, the capacity of the coupling cable between the main amplifier and the drive stage and a parallel plate variable air condenser VC2 for tuning. The screen grid is biased at + 500V by the resistor chain R_3, R_4, and the control grid at - 250V by an external stabilized D.C. supply (to be described later). The relay protects the valve in the event of failure of the grid bias supply by switching off the EHT. During the testing of this amplifier it was found that the small grid-anode capacity of 0.2 p.f. was large enough to cause considerable feedback. This necessitated the addition of a small neutralizing condenser connected between the grid and tank coil.

The drive amplifier is itself driven by a third amplifier which contains the standard 10 Mc/sec. crystal

oscillator. The circuit diagram of this amplifier, together with the oscillator, is shown in Fig. (2.2).

When run at full power there is estimated to be heat dissipation of about 10 kW within these amplifiers. Most of this heat is dissipated in the deflector plates and tank coil. To remove this heat water is circulated through the coil and deflector plates. The ends of the coil are connected directly to the inlet pipes of the deflector plates. The cooling water enters through a T junction at the centre of the coil and leaves at the outlets from the deflectors. Another water circuit cools the anode of the triode. Ordinary water from the mains is used for cooling, connections to the various components being made with ½" bore P.T.F.E. pipes. Ideally demineralized water should be used for cooling to reduce power losses, but since the amplifiers had been well overdesigned the power losses actually occurring in the tap water could easily be tolerated, and the complication of installing a demineralized supply was not necessary. At the rear of the chasses containing the amplifiers are mounted 4½" diameter fans each capable of circulating air through the units at a rate of about 80 cu. ft. per minute. These fans maintain a flow of air past the air cooled valves, and also keep the ambient temperature inside the units at a reasonable level.

FIG 2·2

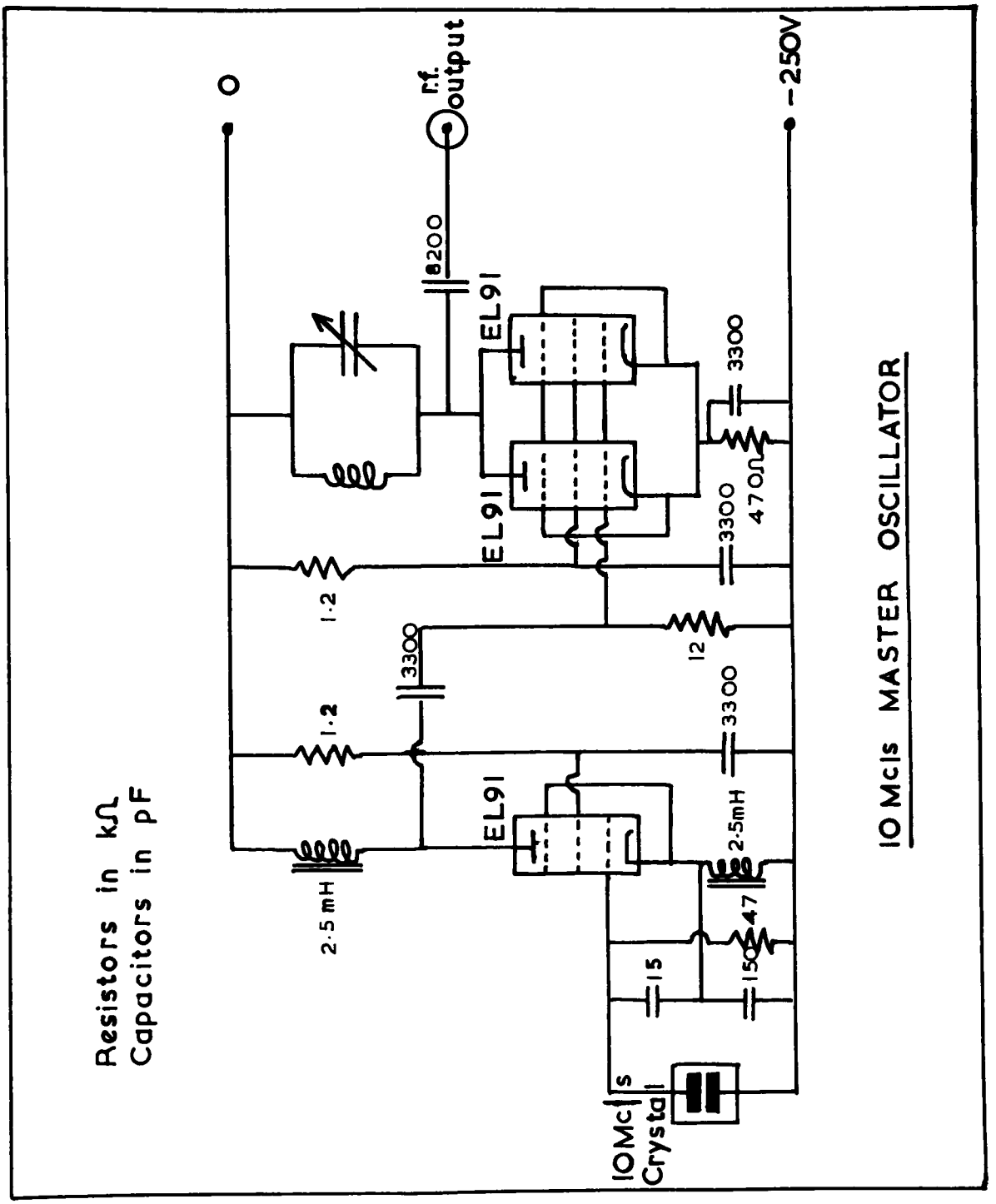
Resistors in kΩ
Capacitors in pF
10 Mc/s MASTER OSCILLATOR
0
r.f. output
-250V
8200
EL91
EL91
EL91
3300
470Ω
3300
1·2
12
3300
1·2
3300
2·5 mH
2·5mH
47
15
150
10Mc/s Crystal

During the testing of the amplifiers problems arose due to the failure of the insulating materials used in the construction. Originally the supports for the tuning condensers were made from "tufnol" and the water pipes made from P.V.C. The reliability of the amplifiers was impaired by the excessive dielectric losses in these materials. Other insulating materials were tried with varying amounts of success. The final choice was polystyrene for the tuning condenser supports, polythene for the tuning knobs and P.T.F.E. for the water pipes. It was also found necessary to mount the current meters on the front of the amplifiers on perspex supports.

The Quadrature Deflectors

The secondary or quadrature deflectors are similar in construction to the main deflectors except that they are only 35 cms. long. They are orientated at right angles to the main plates and so deflect the beam in a vertical plane. The power to these plates is supplied by 2½kw power amplifier which uses an air cooled tetrode valve (Mullard QY5-800). The amplifier is tuned to a frequency of 5 Mc/sec.. The circuit diagram is shown in Fig. (2.3). The tank circuit consists of the quadrature deflectors, the tuning condenser

FIG 2.3

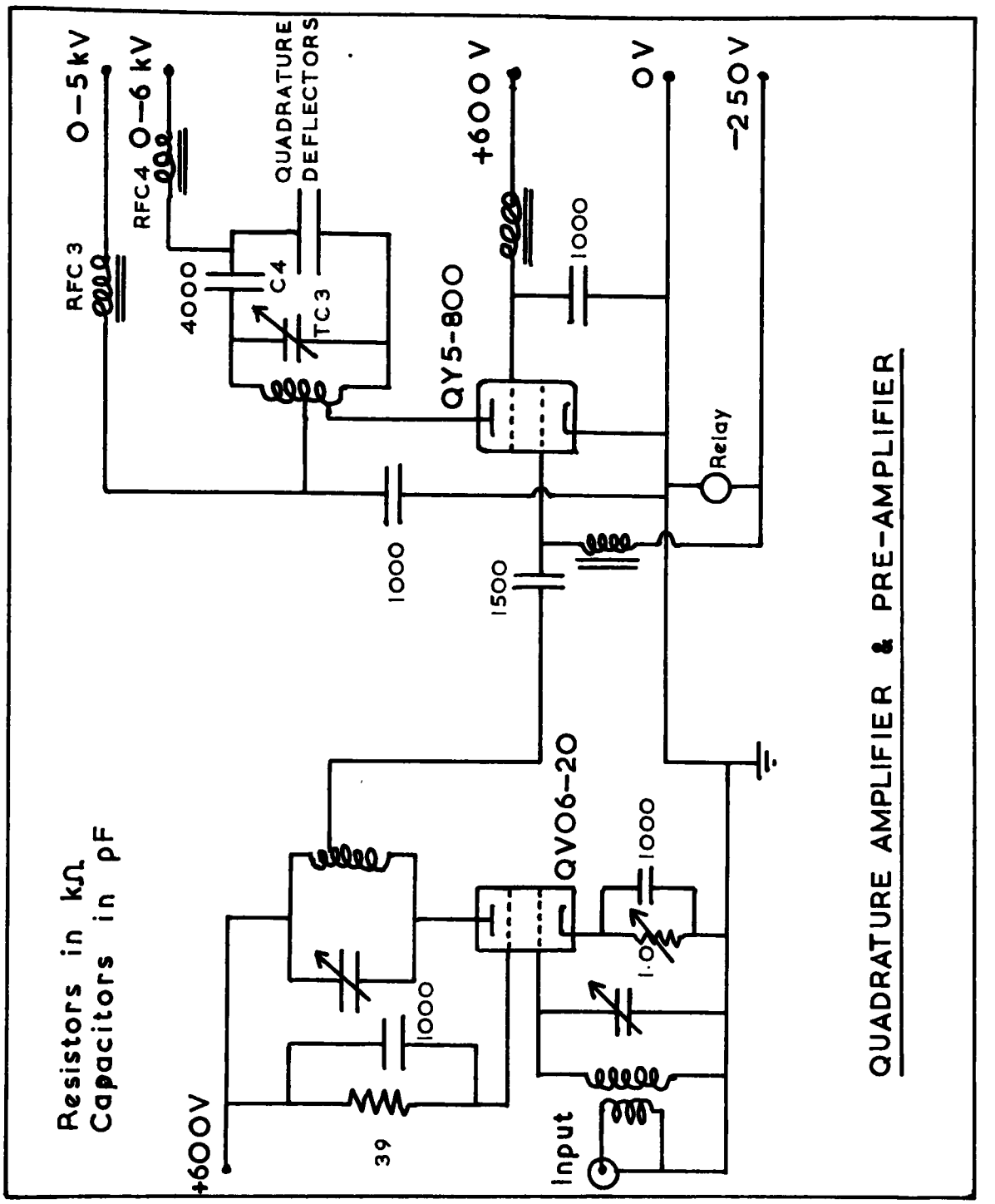
QUADRATURE AMPLIFIER & PRE-AMPLIFIER
Resistors in kΩ
Capacitors in pF
0-5 kV
0-6 kV
RFC 3
RFC 4
QUADRATURE DEFLECTORS
4000
C4
TC3
+600 V
0 V
-250 V
1000
QY5-800
Relay
1500
QV06-20
39
Input
1.0

TC3 and the tank coil. The coil is made from 1/8" bore copper tube wound on a 6" diameter polythene former. One end of the coil is coupled directly to the lower of the two quadrature plates, while the other end is coupled to the upper plate through a 4000 pf 15kV condenser C4. The purpose of C4 is to isolate the upper plate from the EHT to enable a negative bias to be applied to it. The coil has a step up ratio of 3 : 1, thus enabling up to 15 kV of r.f. to be applied to the quadrature deflectors.

Both grids of the tetrode are biased by external supplies. The control grid uses a - 250V D.C. stabilized supply, and the screen grid a + 600V D.C. stabilized supply. A resistor chain could not be used to bias the screen because of the large amount of heat (500 Watts) which would be dissipated in it. As in the case of the QV4-250 a small neutralizing condenser was found necessary to neutralize the 0.1 pf grid-anode capacity. The valve is protected against failure of its control grid bias by a relay which turns off the EHT in the event of such a failure.

The amplifier is cooled by a fan mounted in the back of the unit which directs a stream of cold air over the tetrode. The coil and deflector plates are water cooled, the upper plate being on a separate water circuit from the coil and lower plate.

The negative EHT bias for the upper plate is supplied by an external power pack. Because of the finite resistance of the cooling water this power pack had to be capable of supplying up to 30 mA of current at 6 kV. The r.f. from the plate is prevented from reaching the power pack by the r.f. choke RFC4 made by winding 100 turns of 24 S.W.G. copper wire on to a P.T.F.E. former 5" long and 4½" diameter.

The quadrature amplifier is driven by a pre-amplifier powered by a Mullard tetrode valve QV06-20; also shown in Fig. (2.3). A pick-up loop inside the main amplifier picks up a 10 Mc/sec. signal which is fed into a "phase shifter" (Nu 66). This is a device which scales a 10 Mc/sec. signal down to 5 Mc/sec. and gives a sine wave output whose phase with respect to the input can be varied continuously from 0 to 2π. The output of the phase shifter is then fed to the input of the quadrature preamplifier. By means of the phase shifter the phase of the r.f. applied to the quadrature plates can be varied with respect to the phase of that on the main plates.

Power Supplies

The TT7-600W, QV15-300, and QV14-25A valves require anode EHT supplies of 6 to 7 kV at 2.5A, to 5 kV at 1.5A

and 0 to 4 kV at 1.0A respectively. To obtain these, the three phase mains supply is suitably transformed, full wave rectified and smoothed. Variacs on the input side of the EHT transformers allow the output voltage to be controlled. The rectifiers used are Mullard RM3-1250. Relays are installed inside each unit so that the power supply cannot be switched on unless the grid of the valve, to which the power supply is connected, is biased. They also switch the EHT off in the event of failure of the bias supplies. The three power supplies are housed in a single cabinet which is cooled by three fans mounted at the back. The negative EHT bias supply for the quadrature plate is obtained by full wave rectification of the output of a single phase mains transformer. For this unit the rectifiers used are Ferranti BX33 solid state rectifiers. A Variac on the input to the transformer enables the output of the bias supply to be varied continuously from 0 to 6 kV.

In addition to the EHT supplies two stabilized grid bias supplies are required. One has to supply 50 mA at - 250V and the other 300 mA at + 600V. The - 250V supply is used to bias the grids of the QY4-250 and the QY5-300 and is also used as the H.T. supply for the crystal oscillator and its amplifier. The + 600V supply provides the screen bias for the QY5-300 and also the H.T. supply for the

4V06-20. Figures (2.4) and (2.5) show the circuits for these power supplies. In the original design Zener diodes were used in place of the gas discharge voltage reference tubes, but these were found to be unsatisfactory due to changes in their Zener voltages with changes of temperature and current. The fluctuations with temperature could be reduced by using several Zener diodes with positive and negative temperature coefficients in series, but the fluctuations produced by changes in the current flowing through them could not be removed. Although these fluctuations were only a few millivolts, they were being applied to the input of a high gain amplifier with the result that fluctuations of several volts appeared at the output. Using conventional voltage reference tubes these problems were removed and a high degree of stability was obtained. A 10% change in the mains voltage produced less than 0.5 volt change in the output voltages. Also changes in the output voltages with changes in the loading were negligible.

Arrangement of the Chopper

The main deflectors and the quadrature deflectors are mounted one behind the other with the main deflectors

FIG 2.4

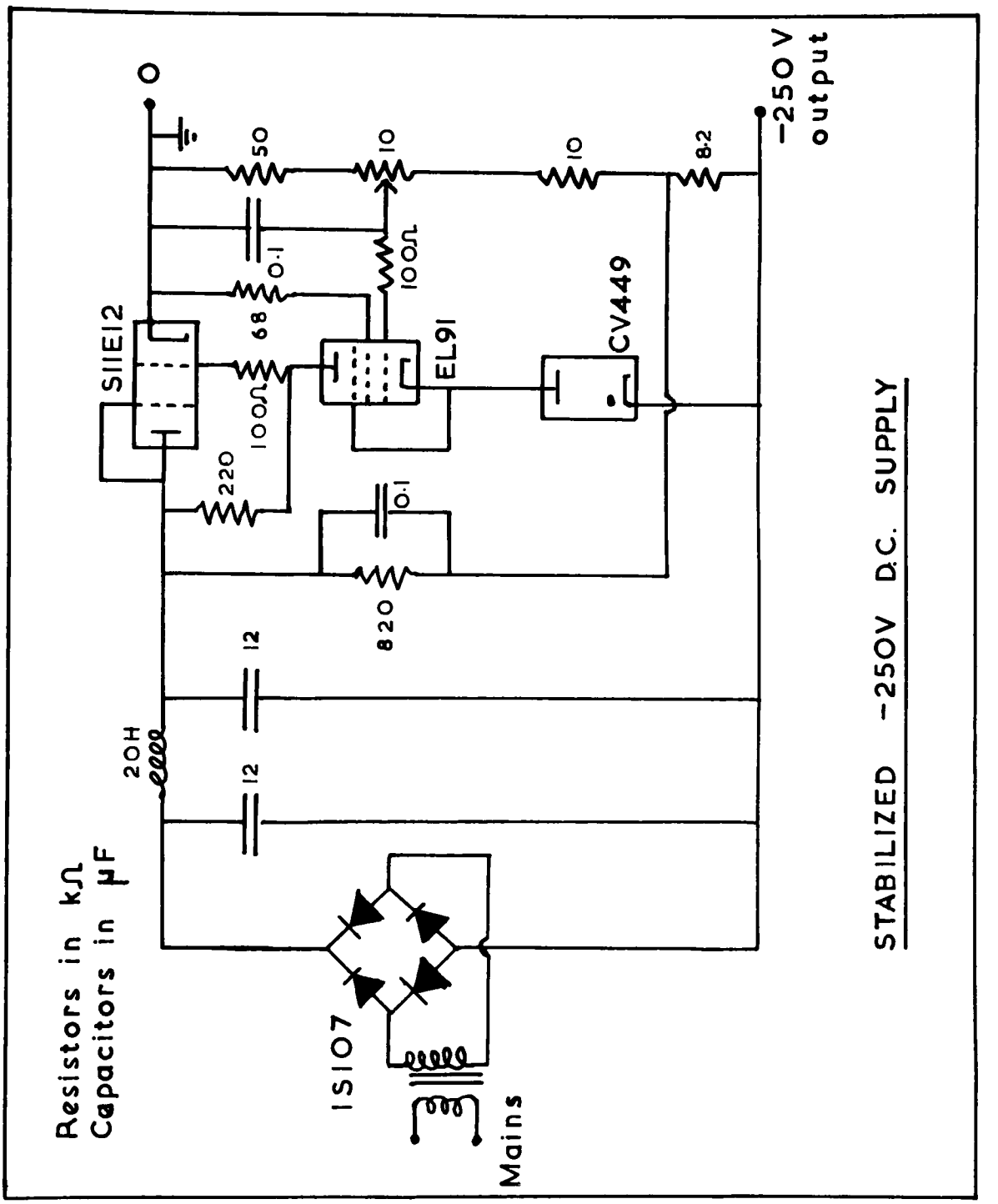
0
50
10
10
8.2
-250 V output
0.1
100Ω
68
100Ω
220
0.1
820
SIIE12
EL91
CV449
12
12
20H
Resistors in kΩ
Capacitors in μF
IS107
Mains
STABILIZED -250V D.C. SUPPLY

FIG 2.5

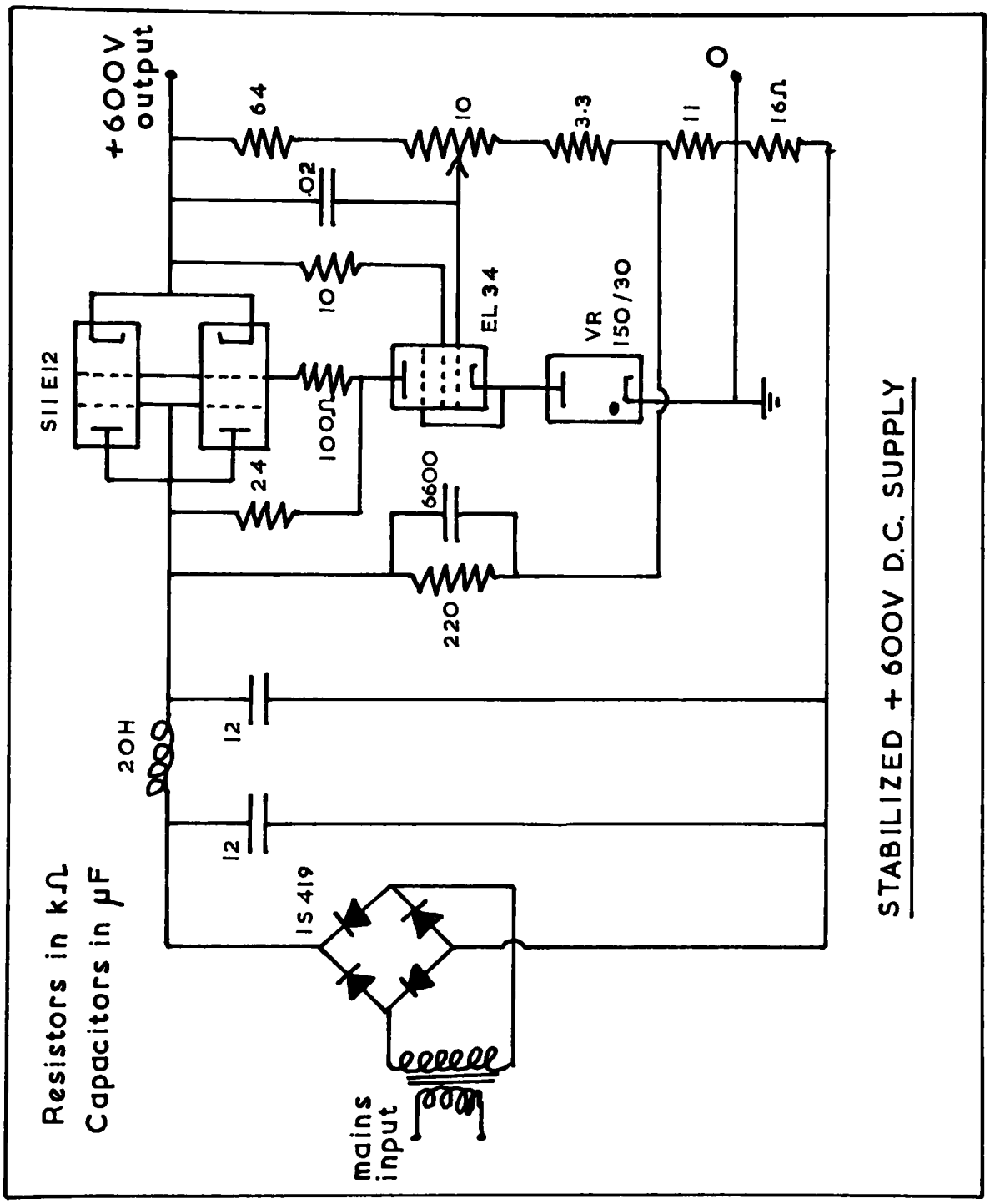
+600V output
64
10
3.3
11
16Ω
0
.02
10
EL 34
VR 150/30
S11 E12
100Ω
24
6600
220
20H
12
12
IS 419
mains input
Resistors in kΩ
Capacitors in μF
STABILIZED + 600V D.C. SUPPLY

nearest to the accelerator. They are electrically screened from each other by an earthed wire mesh which has an aperture in the centre to allow the beam to pass through. The r.f. amplifiers are situated immediately below their respective deflector plates and are coupled to the tank coils by stout copper rods 3/16" diameter. Beneath the main amplifier is its drive stage and the crystal oscillator, and beneath this is the D.C. bias supplies. The quadrature amplifier has its drive stage mounted beneath it, and at the botton of this side of the chopper assembly is a refrigeration unit. When the chopper was being operated on wet days water vapour was found to condense on the water cooled parts resulting in electrical breakdowns. For this reason the refrigeration unit was installed. This removes any water vapour from the air inside the chopper assembly and circulates cold air through it. The complete chopper assembly is enclosed in a steel cabinet with the two halves electrically screened from each other. The unit is fixed to a steel frame and can be lifted into and out of the beam line by means of a pulley. The steel frame fits over four locating pins fixed to the floor of the accelerator vault and ensures that the chopper is correctly aligned between the tandem and the magnet. When in position the centre of the main deflectors is 4 metres

from the entrance slits of the magnet. Figure (2.6) shows the layout of the chopper assembly.

Operating Procedure

The method of pulsing the beam is as follows. First of all a D.C. beam as large as the accelerator will give is analysed by the magnet. The main amplifier is turned on, tuned up and set to a suitable voltage which depends on the energy and nature of the beam used and on the pulse length required. The machine controls are then adjusted to optimize the transmitted beam. The mean D.C. beam will be found to have dropped by a factor of about 50 for pulse lengths of the order of 1 ns. The flight lines on the Oxford accelerator are equipped with beam scanners (Ta 65) which enable the profile of the beam to be observed at selected points along the line. The scanners display on an oscilloscope screen the shape and size of the beam in a horizontal and vertical plane. One of these scanners is situated just in front of the entrance slits of the magnet. This is a focus point for the beam and before pulsing the scanner shows two sharp peaks corresponding to a well-focussed beam in the horizontal and vertical planes. With just the main chopper running the peak on the scanner corresponding to the horizontal size of

FIG 2·6

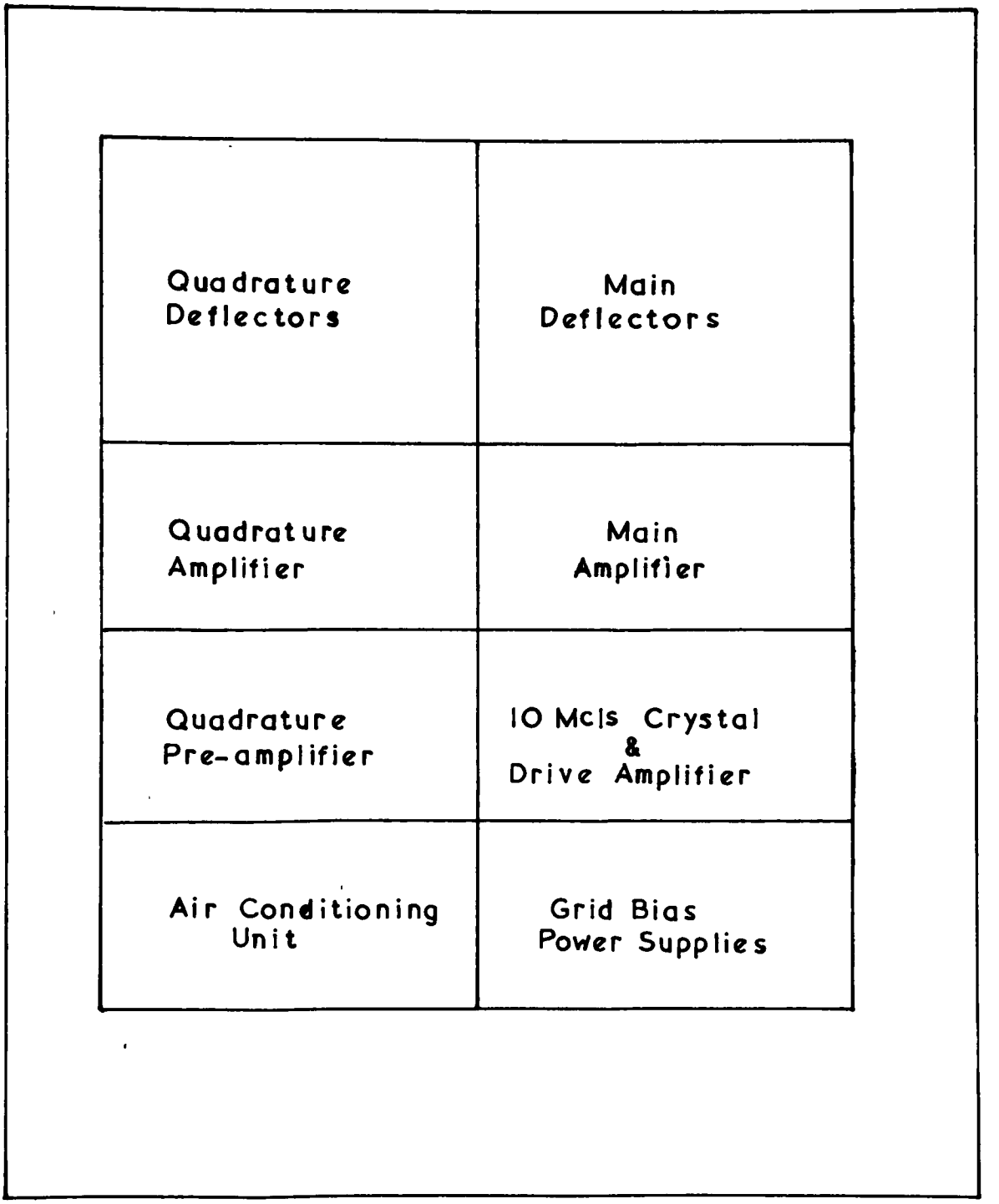

LAYOUT OF THE CHOPPER

the beam is found to widen considerably while the vertical display remains sharp. This is due to the beam being swept backwards and forwards in the horizontal plane. The next stage in the operation is to switch on and tune up the quadrature amplifier. The vertical display on the scanner will now be seen to have changed. Instead of the single sharp peak two or three peaks will be seen. The horizontal display remains broad. The phase of the quadrature amplifier is now altered while watching the scanner. As the phase is varied the vertical scanner shows alternately three peaks and two peaks corresponding to the beam tracing out different Lissajous figures. The phase is adjusted until three peaks are visible and are at their widest separation. The three peaks represent three beams which correspond to the top, centre and bottom of the figure of eight traced out by the original beam. The negative D.C. bias is then applied to the upper quadrature plate until the lowest of the three beams lies on the axis of the flight line, i.e., only the lowest beam crosses the magnet slit. The transmitted current is then optimized by fine adjustments to the phase and bias. The magnitude of the final current will be found to be of the order of 1/200th of that of the initial D.C. beam.

An estimate of the performance of the chopper can be

made in the following way. If the transit time of an ion through the chopper is a small fraction of an r.f. cycle then it can be shown (Ne 60) that for an axial ray the burst width is given by

$$\Delta t = \frac{4 E d. \Delta y}{2\pi f e V_o \ell_1 (\ell_1 + 2\ell_2)}$$

where E = energy of the ions

f = frequency of the r.f. applied to the plates

V_o = peak r.f. voltage

ℓ_1 = length of deflector plates

ℓ_2 = distance of slit from deflectors

Δy = width of the slit.

Because of the finite size of the beam spot Δy should be replaced by $(\Delta y + S)$ where S = diameter of the beam spot at the slit.

For the dimensions of our chopper the burst width turns out to be

$$\Delta t = 1.51 (S + \Delta y) \frac{E}{V_o} \quad \text{n. sec.}$$

if S and Δy are measured in cms., E in MeV and V_o in kV.

Putting in typical values for Δy and S of 0.26 cms. and 0.20 cms. the r.f. voltage required on the chopper plates to chop a 10 MeV proton beam down to 1 ns. is 6.95kV. This is well within the capability of the chopper since it can produce up to 24kV. However the two Oxford accelerators can be coupled together in order to produce protons or deuterons with energies up to 20 MeV. With the same values for the slit width and beam spot diameter as before a 20 MeV proton beam could be chopped down to 0.6 ns. by running the chopper at full power.

Although pulse lengths of much less than 1 ns. can easily be produced, in practice pulse lengths of between 1 and 2 ns. are used. The reason for this is twofold. With a D.C. beam from the accelerator of 3 μA and a pulse length and repetition rate of 1 ns. and 5 Mc/sec. respectively the mean current reaching the target after chopping will only be 15 nA. Reducing the pulse length will reduce the beam intensity still further. Also the resolving time of the detecting equipment (to be discussed later) is at present not better than 2 ns. and nothing is gained by producing pulses with a duration of less than 1 ns. The resolution is not improved and all that happens is a loss of beam intensity resulting in a reduction in the signal to background ratio. The chopper is normally operated at the lowest

voltage for which an increase in voltage does not improve the time resolution of the detection system. The chopper has been used successfully for proton beams with energies up to 18 MeV. At this energy, 12 kV a.c. on the chopper was all that was needed to produce pulses which were short enough not to affect the resolution of the system. Typical operating conditions for the chopper using proton beams with energies of the order of 10 MeV are

R.F. Voltage on main plates = 6 kV
R.F. Voltage on quadrature plates = 6 kV
D.C. Bias on quadrature plate = -3 kV.

The Detector

The main requirements of a neutron detector for time of flight experiments are :-

1) It should have a very fast response of the order of a nanosecond.
2) It should be reasonably efficient.

These two requirements limit the choice of detector to a scintillator-photomultiplier combination. There are now several types of organic scintillators, both liquids and

solids, commercially available which satisfy both requirements. Unfortunately they are often just as sensitive to gamma rays as they are to neutrons. However some of these scintillators have the additional property of producing a different type of light pulse for neutrons than for gamma rays and it is now possible to discriminate completely against gamma rays without reducing the neutron detection efficiency.

One such scintillator is known as Ne213. It is a liquid produced by Nuclear Enterprises Limited. Its decay constant is 3.6 n.s. and it shows excellent pulse shape discrimination properties. Neutrons are detected by producing proton recoils in the scintillator itself, while the response of the scintillator to gamma rays is mainly via the Compton effect. Pulse shape discrimination is possible due to the different response of the scintillator to protons and electrons. The detector we have used is made from this liquid. It is contained in a cell 10" in diameter and 1" thick. Coupled to the scintillator are two Mullard XP1040 photomultiplier tubes. These are 14 stage photomultipliers with a gain of 10^9 and an anode pulse rise time of 2 ns. They have 5" diameter photocathodes. The dynode resistor chain (Fig. 2.7) for the photomultipliers is adapted from the one recommended by Bellettini et. al. (Be 63, Be 64).

A block diagram of the electronic equipment is shown in

FIG 2.7

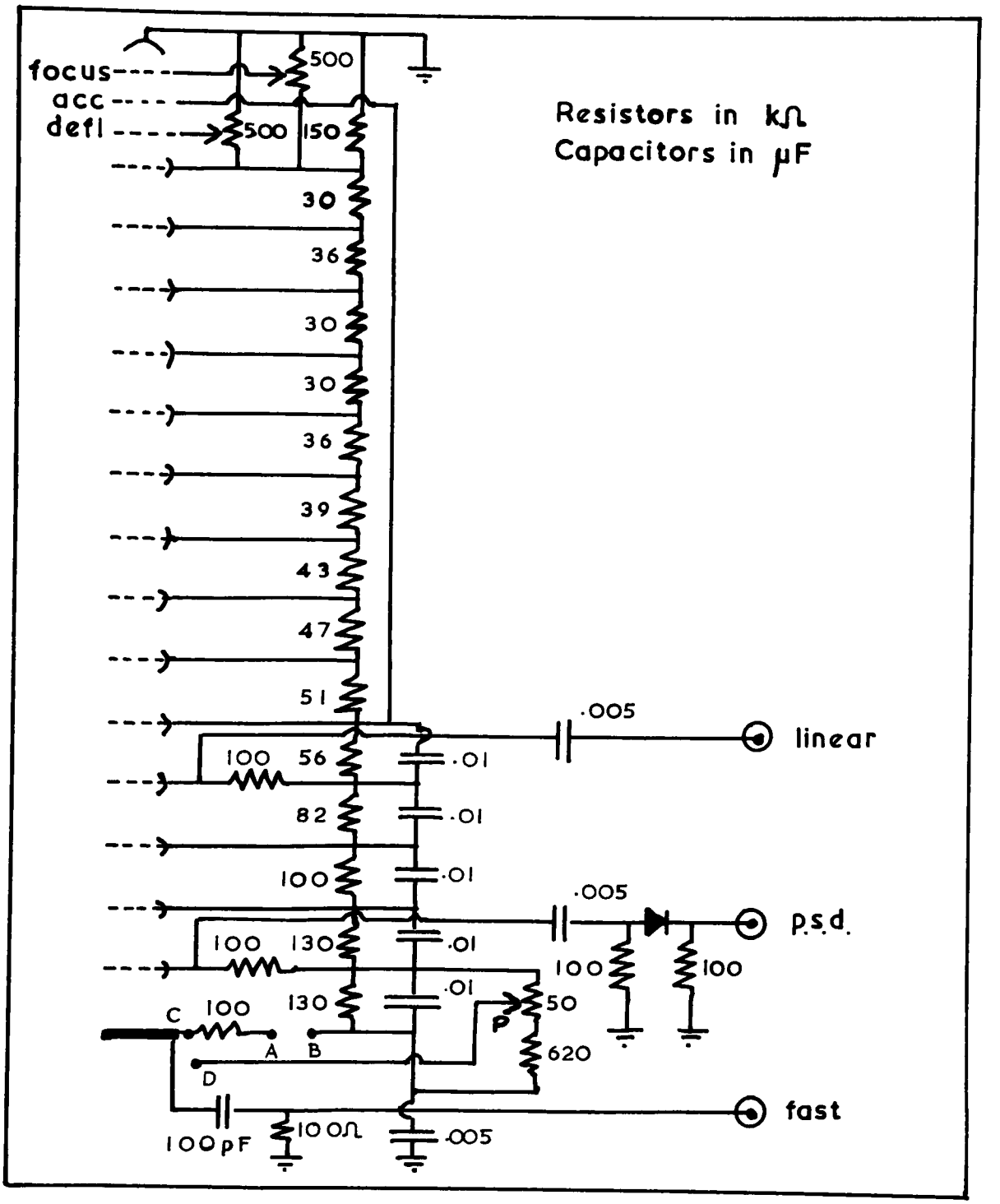

RESISTOR CHAIN FOR XP1040

Fig. (2.8). It consists of two sections, one "fast" and one "slow". In the slow section linear pulses are taken from the eleventh dynodes of the two photomultipliers, added together, amplified by a double delay line amplifier and fed into a discriminator. The reason for taking the sum of the linear pulses is that by setting an amplitude bias on these pulses a much sharper cut off at the low energy end of the detectors response is obtained than would have been obtained if individual biases had been put on the linear pulses. Uneven light distribution between the two photomultipliers makes it impossible to get equal amplitude linear pulses for the same light pulse. By working with the summed pulse we are taking the total light collection into account. From the fourteenth dynode of one of the tubes is taken a pulse which is used for pulse shape discrimination (see next section). This pulse is amplified by an .e.. amplifier before being put into a discriminator. In the fast section a fast pulse is taken from each of the tubes. In the tube from which the discriminator pulse is taken the fast pulse is taken off the twelfth dynode, but in the other tube it is taken off the anode. These pulses are amplified by wide band amplifiers, the one from the dynode being first inverted

FIG 2.8

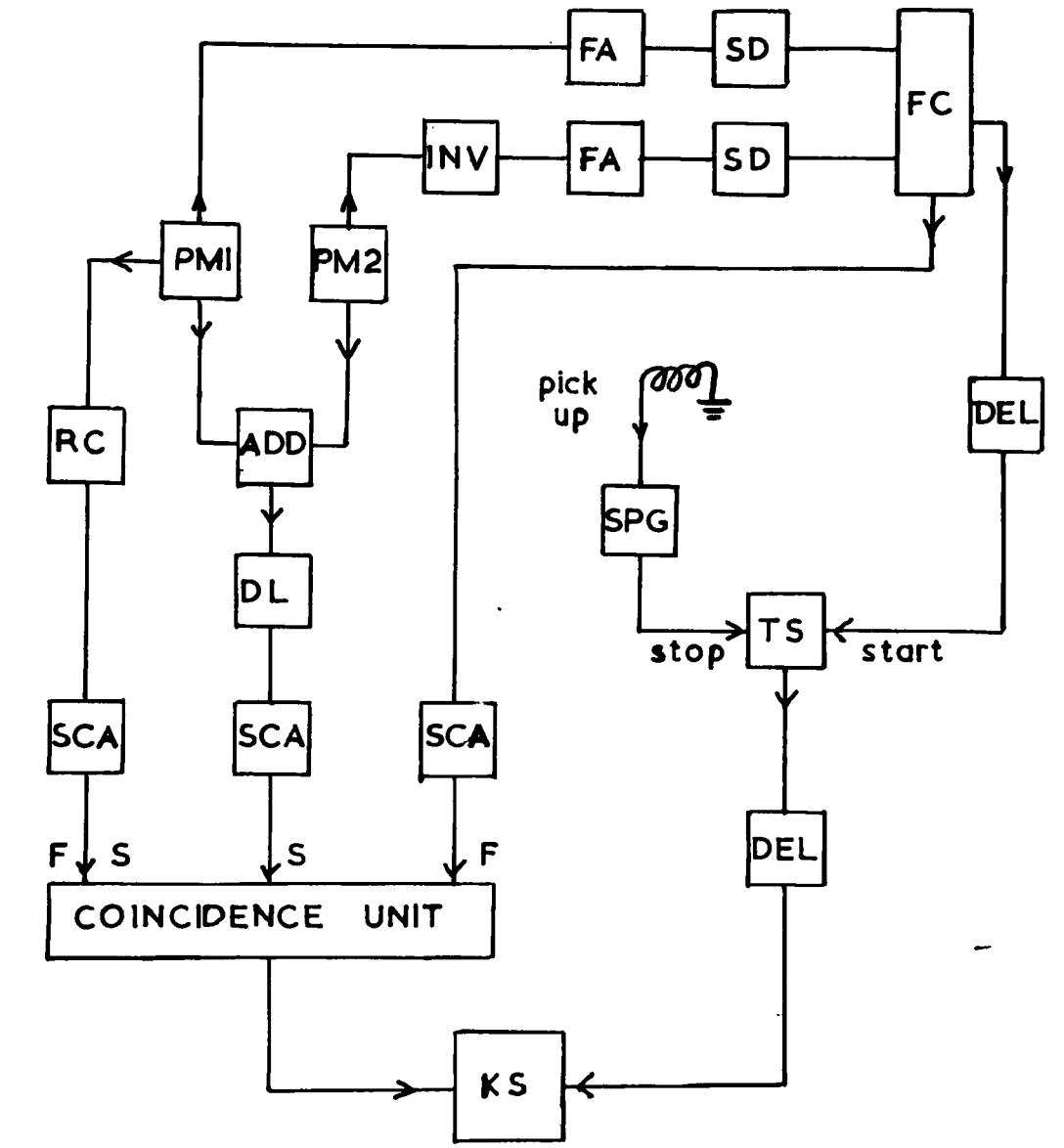

PM photomultiplier. DL delay line amplifier. INV inverter.
SCA single channel analyser. FA fast amplifier.
SD synchronising discriminator. TS time sorter. DEL delay.
FC fast coincidence unit. ADD pulse adder. KS kick sorter.
SPG stop pulse generator. RC R.C. amplifier.

PULSED BEAM T.O.F. ELECTONICS

since it is positive, and then put into synchronising discriminators. The outputs of these discriminators are sent into a fast coincidence unit. By requiring a coincidence between the fast pulses from the two tubes random pulses due to photomultiplier noise are reduced. The fast coincidence unit gives two outputs, a type 1 pulse used for logic and a type 2 pulse. The type 2 pulse is used as the timing signal for the time of flight measurements. This pulse signals the detection of a neutron or gamma ray. The other pulse required for timing is derived from the beam chopper. A small coil placed inside the main chopper amplifier picks up a 10 Mc/sec. signal from this amplifier. The signal so derived is scaled down to 5 Mc/sec. and is then used to operate a trigger circuit known as the stop-pulse generator, (nu 66) which produces fast short pulses with a rise time of less than 5 ns. and duration 10 ns. at a frequency of 5 Mc/sec. Normally the pulses from the stop pulse generator would be used to start the time to pulse height converter, and the pulse from the detector used to stop the time sorter. But since the time sorter we have used will not operate with an input rate of 5 Mc/sec. we have to operate it the other way round. The pulse from the detector starts the time sorter and the pulse from the chopper stops it, so that the time

interval that is measured is that between the triggering of the detector by a neutron and the arrival of the next pulse from the chopper. The output of the time sorter is analysed by a 200 channel Victoreen kicksorter. The kicksorter is gated with a pulse from the slow side of the detector electronics, but before the origin of this pulse can be explained a discussion of the mode of operation of the pulse shape discrimination circuit is needed.

Pulse shape discrimination.

As mentioned before Ne213 is sensitive both to neutrons and gamma rays. Neutrons are detected by means of recoil protons in the scintillator while gamma rays are detected via electrons produced in Compton scattering events. However the response of the scintillator is different for the two types of particle. Any ionizing radiation in the scintillator will excite several modes of light emission the most prolific of which are an intense fast component of about 6 ns. life time due to the decay of excited molecular states, and a much slower component of about 400 ns. decay time due to the recombination of ionized molecules. It is found that for the same total light emission, the percentage of slow component for proton excitation is approximately twice that

for electron excitation, due it is thought to the greater density of ionization along the track. This phenomenon can be used to discriminate against gamma rays. We have adopted the method developed by Batchelor et. al. (Ba 60) which was based on a method originally suggested by Owen (Ow 58). Reference to the dynode resistor chain for the photomultipliers (Fig. 2.7) will show two sets of jumper points AB and CD. Under normal working conditions the jumper points AB are connected together and the potential between the fourteenth dynode and the anode will be of the order of 400V. When the tube is required to produce a discriminating pulse the jumper points CD are connected. The voltage between the fourteenth dynode and the anode can then be varied by means of the potentiometer P. The potential difference is adjusted to be just a few volts. Under these conditions a current pulse coming down the tube space charge saturates the region between the last dynode and the anode while the initial fast component of the light pulse is occurring. This drives the last dynode negative. During the much lower intensity slow component the space charge clears and the dynode behaves normally being left positively charged to a degree depending on the magnitude of the slow component. Since there is a greater proportion of fast

light for electron pulses the dynode is driven more negative than for proton pulses and therefore recovers later. As a result of this the positive swing of the dynode for electron pulses is delayed for the order of a microsecond. Therefore to count just pulses due to neutrons all that is required is an amplitude discriminator to observe the positive part of the pulses and a coincidence circuit to reject those pulses which go positive late. Discriminator pulses of neutrons and gamma rays are shown in Fig. (2.9).

The origin of the gating pulse for the kicksorter can now be explained. The amplified summed linear pulses and the amplified "pulse shape discrimination" (or P.S.D.) pulses are each sent into discriminators. First a slow coincidence is taken between the type 1 pulse from the fast coincidence unit in the fast side of the detector electronics and the output of the discriminator for the summed linear pulses. This sets the lower bias of the detector. The result of this coincidence is put into fast coincidence with the P.S.D. discriminator output with a resolving time of 0.5 μ sec., to eliminate high energy gamma rays which produce P.S.D. pulses with a positive swing. Finally an amplitude bias is set on the P.S.D. pulses to reject the low energy gamma ray pulses which are not intense enough to cause

FIG 2.9

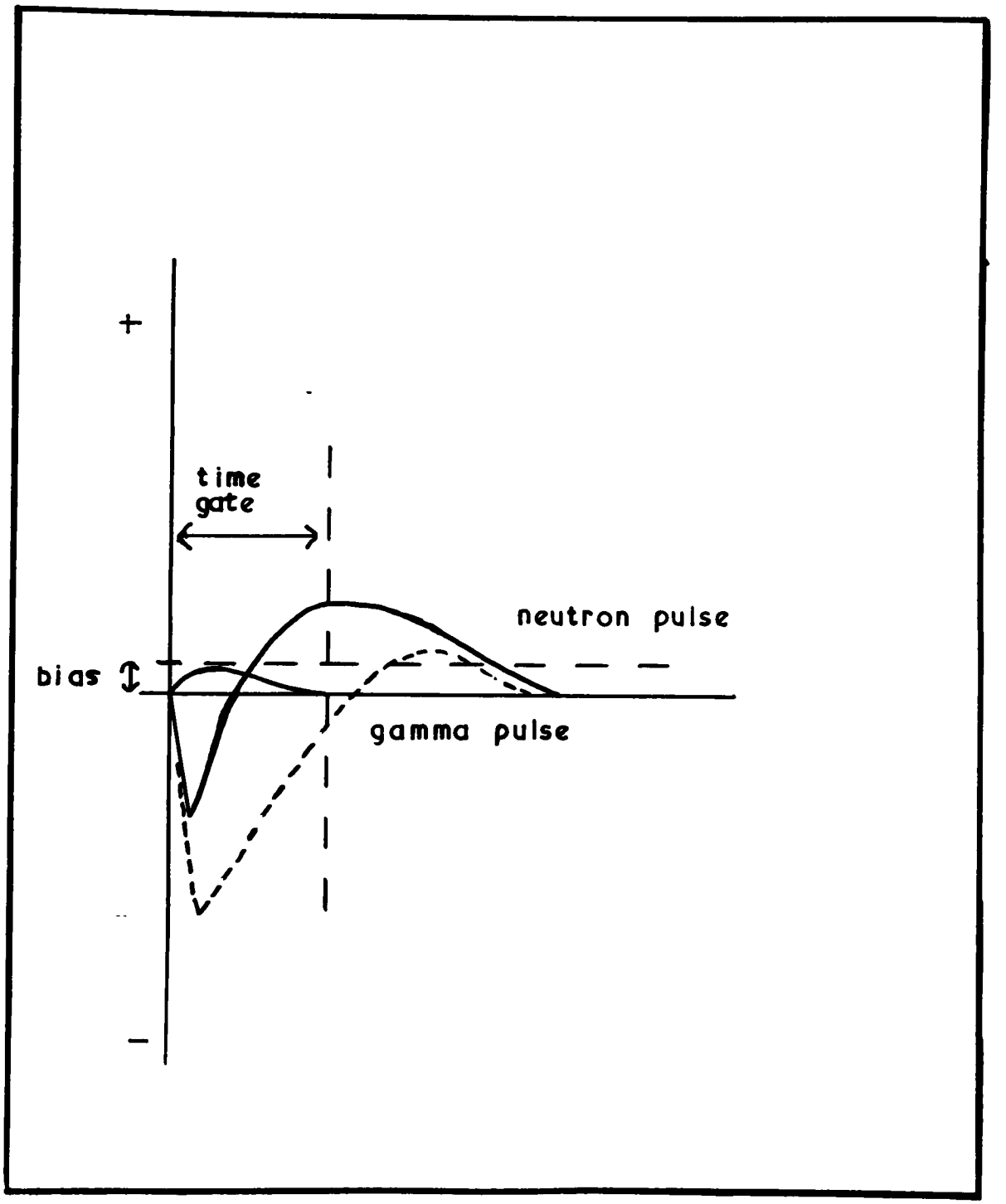

P. S. D. PULSE SHAPES

saturation of the dynode. This bias will also reject low energy neutrons but these in general will be below the linear bias of the detector and will already have been removed. The pulse resulting from this logic is used to gate the kicksorter recording the time of flight spectrum.

Performance of the detector

Two factors which determine the merit of a time of flight spectrometer are its resolution and its efficiency. The resolution of the system depends on several factors, namely the duration of the incident burst of particles, the thickness of the target, the energy spread in the incident beam, the thickness of the detector and the response time of the detector and its associated electronics. The duration of the incident burst ΔT_p causes an uncertainty in the time of release of the neutron from the target. The finite thickness of the target will produce a spread in the energy of the incident beam. This leads to an uncertainty in the energy of the liberated neutron and hence a spread ΔT_T in its time offlight. The energy spread in the incident beam causes a similar effect but with Van der Graaff accelerators this latter effect is negligible. The thickness of the detector will cause an uncertainty ΔT_D in the

$$\frac{\Delta E}{E} = 2\frac{\Delta T}{T}$$

where T is the flight time of a neutron with energy E.

A useful way of measuring the time resolution of the system is to bombard a target with pulses of charged particles from the accelerator and without pulse shape discrimination observe the peak in the time spectrum due to the gamma rays from the target. Since all gamma rays from the target have the same flight time the width of this peak will measure the time resolution of the spectrometer. This peak is also useful as it can be used to fix the time zero of the spectrum. Increasing the amplitude of the r.f. on the chopper plates will at first cause the width of this peak to decrease, but eventually a voltage will be reached above which an increase in voltage will not cause a decrease in the peak width. At this point the resolution is no longer dependent on the pulse length from the chopper but is being determined solely by the electronics. In practice the chopper is normally operated at the lowest voltage for which an increase in voltage does not cause a decrease in the time resolution. The typical time resolution of the system is between 2.5 and 3.0 ns., although occasionally a resolution as low as 2.0 ns. has been achieved.

The efficiency of the detector is defined as the ratio of the number of recoil protons detected to the number of incident neutrons. A theoretical expression for the efficiency of the type of detector we have used is given by (Sw 60)

$$\eta(E) = 1 - \exp [- n_H \sigma_E d]$$

where n_H = number of H atoms per cc. of scintillator

σ_H = n - p scattering cross section

d = thickness of the scintillator.

This expression is derived under the assumptions that :-

1) Carbon does not contribute to the detection
2) the thickness of the scintillator is small compared to $1/n_H \sigma_E$, i.e., only single scattering occurs.
3) All recoil protons are detected.

In practice only proton recoils, or more precisely light pulses above a certain amplitude are detected. So for low energy neutrons a large proportion of the proton recoils will not be detected. For high energy neutrons the proportion not observed will be smaller and the observed efficiency will approach the theoretical value. Calculations by Batchelor

et. al. (Ba 61) on the response of organic scintillators to neutrons have shown that for low energy incident neutrons the proportion of multiple scattering events is relatively high. At high energies multiple scattering is not so important. The calculations also show that carbon does contribute considerably to the detection mechanism but as the carbon recoils produce only very low intensity light pulses they will not in general be recorded and so their effect on the overall efficiency of the detector may be neglected.

We have measured the relative efficiency of our detector as a function of energy using the neutron producing reactions

$$D(d, n)\ He^3$$

and

$$Li^7(p, n)\ Be^7$$

The first reaction can be used to measure the efficiency of the detector for neutrons above 2 MeV. For a bombarding energy of 8.15 MeV the neutron energy varies from 11.37 MeV at 0° to 1.87 MeV at 160°. The differential reaction cross section for this reaction is accurately known (Br 50), and so by measuring the neutron yield at various angles the detector efficiency as a function of neutron energy can be

determined. We therefore bombarded a deuterium gas target with a pulsed beam of 8.15 MeV deuterons and observed the neutron spectra at 10° intervals from 10° to 160° with a flight path of 2 metres. For these experiments the target thickness was 200 µg (approx. 50 keV for 8 MeV deuterons).

For neutron energies below 2 MeV we used the $Li^{7}(p, n)Be^{7}$ reaction. The differential cross section at 0° has been measured for proton energies between 1.9 MeV and 3.3 MeV by Gabbard et. al. (Ga 59) and between 3.0 and 10.0 MeV by Borchers (Bo 63). The reaction is endoergic and has a threshold of 1.88 MeV. Consequently at 0° neutrons can be produced with energies of 120 keV and above. Using a pulsed beam to separate the ground state neutron group from the first excited state group the neutron yield at 0° was measured for proton energies from threshold up to 5 MeV. This produced neutrons with energies up to 3.3 MeV. As the energy ranges covered by the two reactions overlap one set of measurements could be normalized against the other. Figure (2.1.) shows the efficiency curve so obtained.

The associated particle method

Measuring neutron times of flight by the associated particle method requires that another particle be released

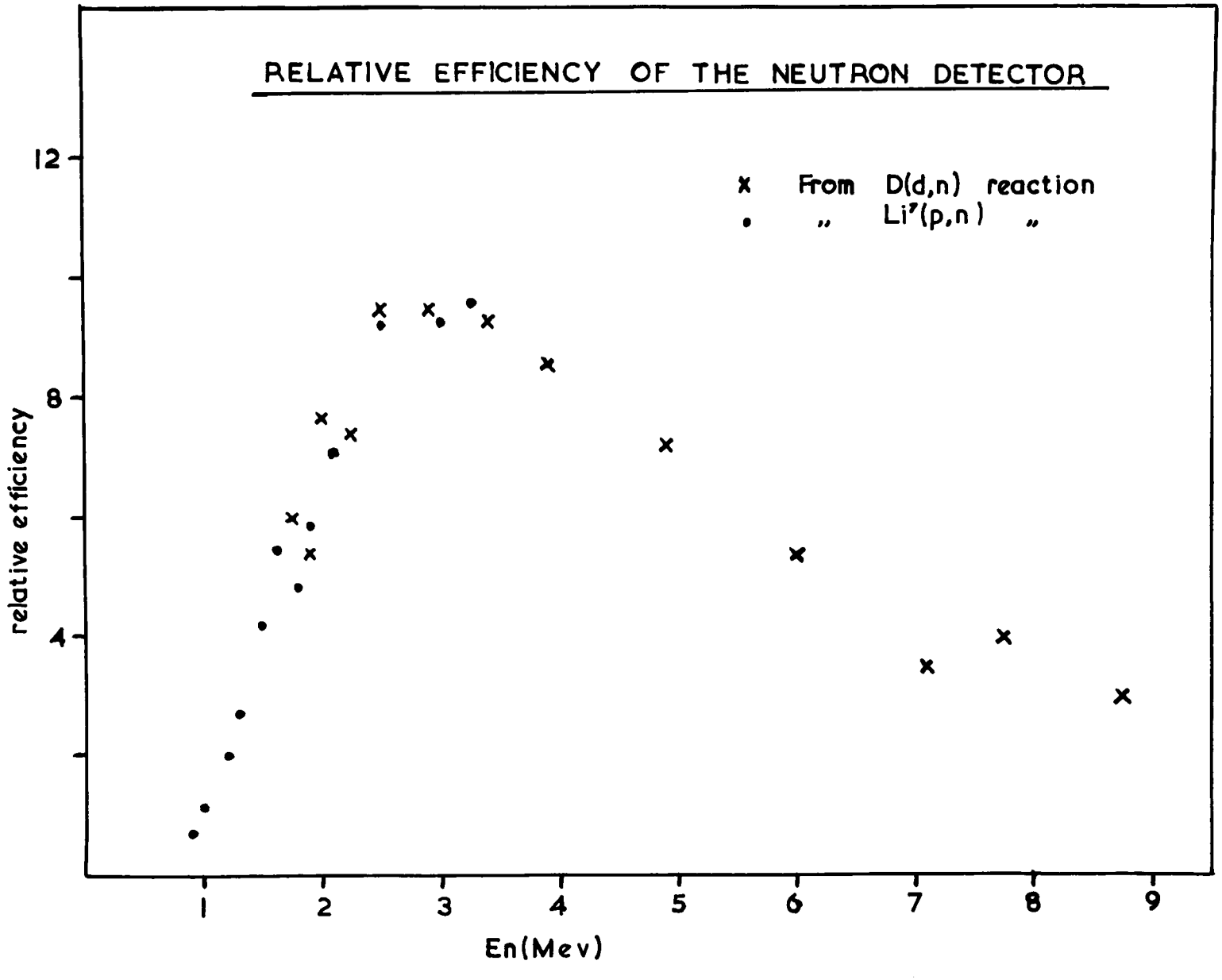
RELATIVE EFFICIENCY OF THE NEUTRON DETECTOR
× From D(d,n) reaction
• „ Li⁷(p,n) „
relative efficiency
12
8
4
1
2
3
4
5
6
7
8
9
En(Mev)

FIG 2·10

from the target in coincidence with the neutron. The time of flight of the neutron is then found from the difference in time between the detection of the neutron and of the associated particle, allowance having been made for the time of flight of the associated particle. If the associated particle is a gamma ray, then the correction is independent of the energy of the associated particle. However since for most applications of this technique the associated particle detector is placed only a few centimeters at most from the target this correction can be neglected. The requirements of the associated particle detector are that it should have a fast response in order to give an accurate time zero signal, and it should have a high efficiency. For some applications it may also be required to have energy discrimination properties so that energy measurements on the particle may be made. Time of flight measurements by this method have the advantage that a pulsed accelerator is not required, but in order that the true coincident rate is not swamped by the random coincidence rate, the count rate in the detector must be kept very much less than $\frac{1}{2\tau}$ where τ is the resolving time of the circuit. One type of experiment in which the associated particle method is preferable to the pulsed beam method is an angular correlation experiment.

In fact beam pulsing is undesirable for such an experiment for while the real coincidence rate is proportional to the average yield from the target, the random rate is proportional to the average of the square of the instantaneous yield. With a 1 per cent duty cycle the instantaneous yield is 100 times greater than the average yield.

We have used the associated particle method to study the neutrons emitted following the beta decay of Li^9. In this experiment the associated particles were the beta particles. In brief the experiment consisted of activating a Li^7 target by bombarding it with tritons for 1 sec., and then stopping the beam for 1 sec. during which time the activity was studied. By the nature of the experiment the pulsed beam method was inapplicable. The experiment involved looking for neutrons from the decay of Be^9 which was formed from the beta decay of Li^9. By requiring that a beta particle and a neutron be observed in coincidence we can select the required activity. The neutron energies were determined by their time of flight which was in turn found from the difference in time between the detection of the neutron and the beta particle. The beta particles were detected in a block of plastic scintillator Nel02 with dimensions 9" x 9" x 3" placed ½" from the target. With this arrangement the detector subtended

a solid angle at the target of almost 2π, and its thickness (3") was thick enough to stop the highest energy beta particles expected from the reaction (13.5 MeV). It therefore should detect approximately 50 per cent of the betas emitted from the target. Coupled to this scintillator by means of a light pipe was a 56 AVP photomultiplier which was wired to give a fast timing pulse from its anode and a linear pulse from its eleventh dynode. The neutrons were detected in the detector previously described except that discrimination against gamma rays was not used. This was because the energies of the neutrons expected from the reaction were in some cases less than 1 MeV, and the P.S.D. method we use is not very efficient for neutrons of these energies. Conventionally the beta counter should provide the start pulse for the time to pulse height converter and the neutron counter the stop pulse. But because of the high counting rate expected in the beta channel we used the neutron pulse as the start pulse and the beta pulse as the stop pulse. This is possible if the beta pulse is delayed sufficiently by a length of delay cable. A block diagram of the electronics is shown in Fig. (2.11). As well as an analogue pulse, the time sorter gives a pulse whenever a start and stop pulse are received within the time range of the time sorter. This pulse was therefore used to provide the gating pulse for the kicksorter. This pulse was

FIG 2·11

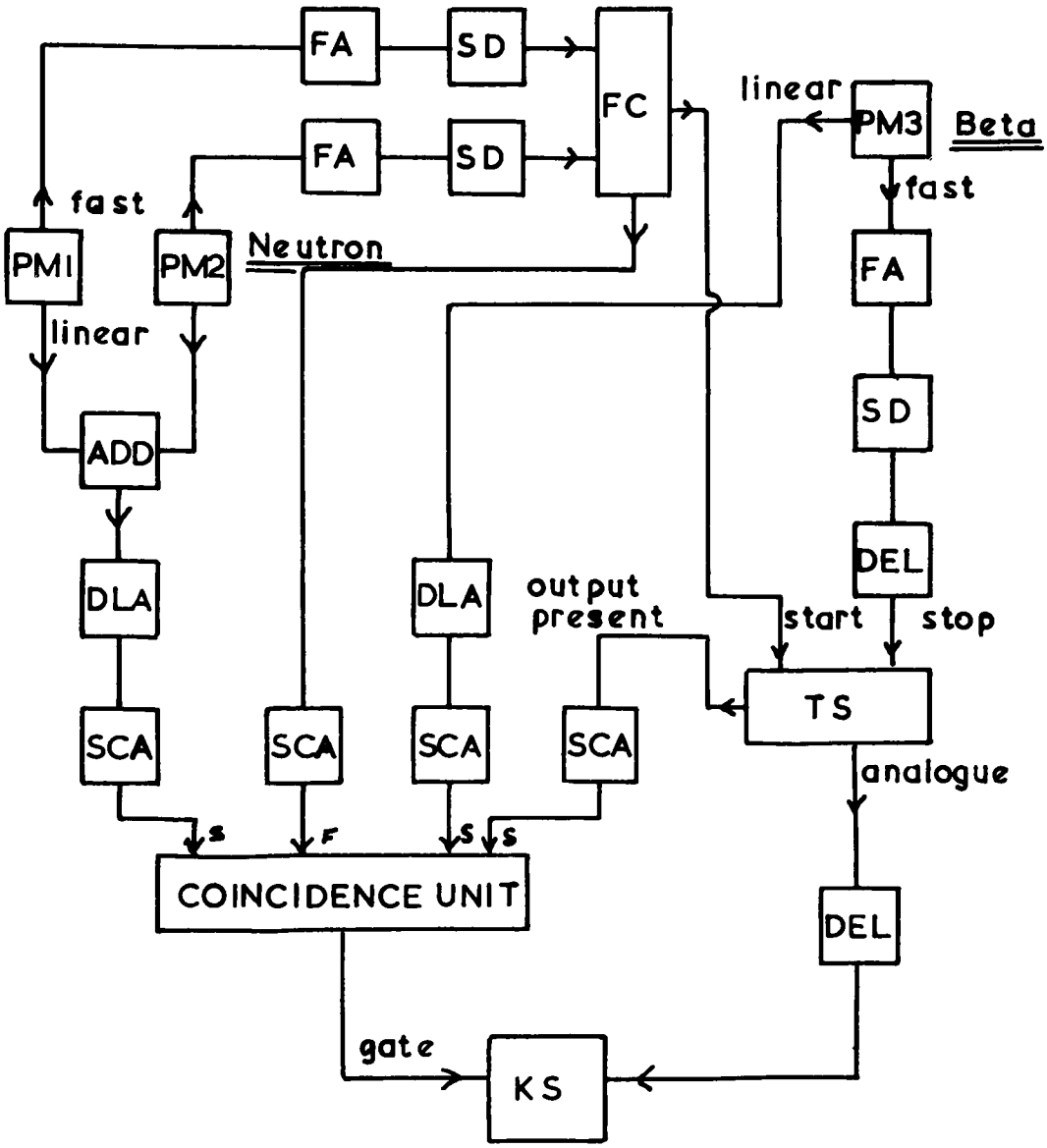

PM1&2 XP1040, PM3 56AVP, FA fast amplifier.
SD synchronising discriminator. ADD pulse adder.
SCA single channel analyser. DLA delay line amplifier.
FC fast coincidence unit. TS time sorter.
DEL delay. KS kick sorter.

ASSOCIATED PARTICLE T.O.F. ELECTRONICS

taken in slow coincidence with the pulses from the discriminators for the linear pulses from the two detectors. These discriminators determined the lower biases of the detectors. The time resolution of the system was measured by placing a Na^{22} source between the two detectors and measuring the width of the γ-γ coincidence peak on the time sorter spectrum. The width of this peak is a measure of the time resolution. With the neutron counter biased to accept neutrons with energies above 1 MeV the resolving time obtained was 2.5 ns. But when biased so as to count neutrons with energies down to about 100 keV the resolution was found to be only 4 ns. However this was adequate for the experiment.

C H A P T E R III

THE $Li^6(p, n)Be^6$ REACTION

Introduction

This experiment was performed primarily to investigate the structure of the Be^6 nucleus. At the commencement of the work only the ground state had been definitely identified. The reaction had been reported by Bogdanov (Bo 58), Ajzenberg-Selove and Osgood (Aj 59) and by Gulyamov et. al. (Gu 63). Bogdanov, using 9.6 MeV protons observed the ground state and measured the angular distribution of the neutrons. He found that the five points of his angular distribution could be fitted to the equation

$$\sigma(\theta) = [0.19 - 0.23 \cos\theta + 0.70 \cos^2\theta] \text{ mb/sterad.}$$

The angular distribution has a fairly deep minimum at 90^o indicating a large p wave contribution to the cross section consistent with the probable assignment of $J^\pi = 0^+$ for the ground state of Be^6. The width of the ground state which is unbound to decay into He^4 + 2p is less than 300 keV, and the Q for the reaction is - 5.2 MeV $\pm$ 0.2 MeV. No indication of any excited state was found.

The work of Ajzenberg-Selove and Osgood was performed with 10.5 MeV protons onto a 150 keV thick Li^6 target. They observed the ground state at 30°, 60°, 90° and 135° with a width of $\leq$ 150 keV. At 90° they saw a neutron group with a width of $<$ 100 keV which they assumed to have arisen from a state in Be^6 at 1.5 MeV. This group was superimposed on a large neutron continuum from the 3 and 4 body breakup reactions :-

$$Li^6 + p \rightarrow Li^5 + p + n - 5.66 \text{ MeV}$$

$$Li^6 + p \rightarrow He^4 + 2p + n - 3.70 \text{ MeV}$$

They suggest that the small width of the ground state, considering it is unbound to breakup into He^4 + 2p, and the small neutron continuum between the ground state neutron group and the limit of the 4-body break-up reaction, indicates that this break-up mode is inhibited. The 1.5 MeV state can decay freely into Li^5 + p (Q = 0.9 MeV) but its small width could be explained if its $J^{\pi} = 2^+$ since then p-wave proton emission would be necessary for its decay.

Gulyamov et. al. measured the α_0 of the reaction and the width of the ground state using 9.96 MeV protons onto a 65 keV thick Li^6 target. Their results were :-

$$Q = -5.08 \pm 0.04 \text{ MeV}$$

$$\Gamma = 0.14 \pm 0.04 \text{ MeV}$$

Be^6 is the T_z =-1 member of the T = 1 triad at mass 6, the other members being He^6 (T_z = +1) and Li^6 (T_z = 0). One is often able to predict the position of excited states in a nucleus by looking at the structure of its isobars. Be^6 should therefore have the same level structure as He^6 and also as the T = 1 states in Li^6. In He^6, apart from the ground state the only other state definitely identified is at 1.79 MeV (Al 60; Le 55; Aj 65), with a width of 100 KeV. Allen also reported a level at 3.4 MeV but this was not confirmed by Ajzenberg-Selove. Information on the T = 1 levels in Li^6 is equally sparse. Two such levels have been identified, one at 3.56 MeV and the other at 5.35 MeV corresponding to the ground state and 1.79 MeV state in the He^6. Other narrow states in Li^6 at 6.63 and 8.37 MeV are possibly T = 1. Their analogues in He^6 and Be^6 would be at 3.07 and 4.81 MeV. States in Li^6 identified as T = 0 are at E_x = 0.0, 2.18, 4.52 and 5.6 MeV. The level structure of the mass 6 triad is summarized in Fig. (3.1).

The properties of the levels of Li^6 are well accounted for by the intermediate coupling calculations of Inglis

FIG 3·1

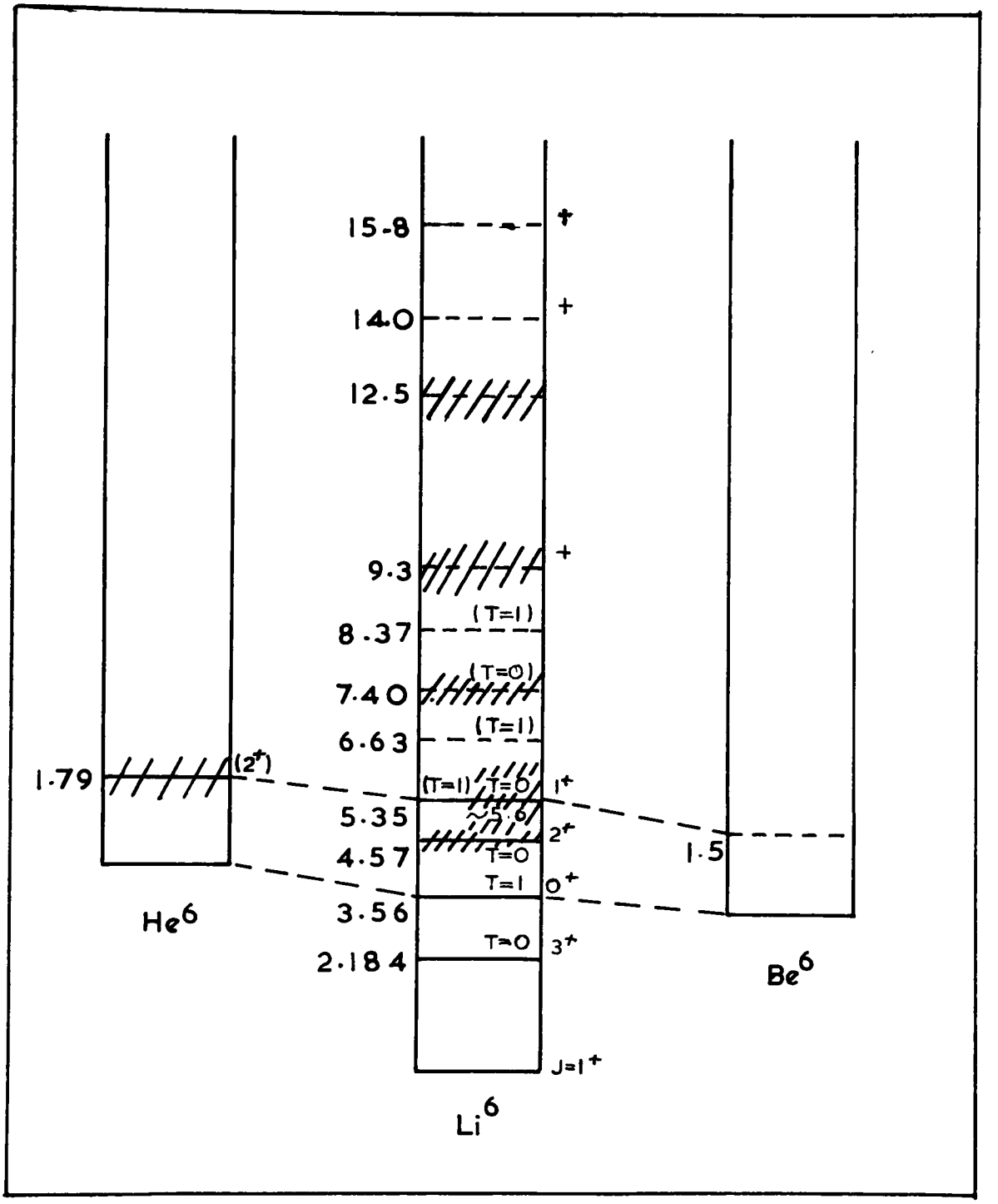

MASS 6 ENERGY LEVELS

(In 53). The states evidently arise from the p^2 configuration and the value of the parameter $a/K = 1.3$ indicates that L.S. coupling is a good approximation. The properties of the first six states in Li^6 are summarized in Table (3.1). On the Inglis model the ^1P and ^3P components are expected at $E_x \geqslant 10$ MeV. Experimental levels are however observed at 6.63, 7.4, 8.37 and 9.3 MeV (La 66), but their properties and origin have yet to be found. In the T = 1 nuclei only the components $^1S_0$, $^1D_2$ and $^3P_{2,1,0}$ can occur. The ground states of Be^6 and He^6 can be identified as the $^1S_0$ component with spin and parity of 0^+. Likewise the 1.79 MeV level in He^6 can be identified as the $^1D_2$ component with $J^\pi = 2^+$, but this assignment has yet to be confirmed.

Since the commencement of this work there have been several other reports of work on the Be^6 nucleus. Honsaker (Ho 64) gives a value of 5.910 ± 0.020 MeV for the threshold of the $Li^6(p, n)Be^6$ reaction, which gives a Q value of - 5.060 ± 0.017 MeV. He also gives the width of the Be^6 ground state as 81 ± 17 keV. Batty et. al. (Ba 65) using 30 and 50 MeV protons reported seeing several states in Be^6 at excitations of 0.0, 1.82, 2.38, 3.65, 5.95, 7.82, 9.33, 11.5, 14.35 and 16.3 MeV. Eccles, Wong and Anderson (Ec 66) approached the problem in two ways. They studied the reaction

TABLE 3.1

Levels in Li^6

E_x	T	J^π	Configuration
0.0	0	1^+	$^3S_1$
2.18	0	3^+	$^3D_3$
3.56	1	0^+	$^1S_0$
4.52	0	2^+	$^3D_2$
5.35	1	2^+	$^1D_2$
5.6	0	1^+	$^3P_1$

$He^4(He^3, n)Be^6$

and

$Li^6(p, n)Be^6$

Using 26 MeV He^3 ions they bombarded a He^4 target and observed the neutron spectra at 3°, 15°, 30° and 45°. At each angle could be seen the ground state neutron group and a broad group consistent with an excited state in Be^6 at an excitation of 1.6 ± 0.1 MeV with a width of 1.1 ± 0.2 MeV. Also seen was a large neutron continuum due to many-body break-up. There was no evidence for other excited states up to an excitation of 5.5 MeV. The angular distribution of the ground state group was more or less isotropic with $\sigma(\theta) \approx$ 0.3 mb/sterad. The $Li^6(p,n)Be^6$ reaction confirmed these results. With 11.6 and 12.6 MeV protons just the ground state and a broad excited state at 1.6 MeV were seen, and again no evidence for the other states reported by Batty. In both reactions the 1.6 MeV state was excited more strongly than the ground state.

The $He^4(He^3,n)Be^6$ reaction was also performed by Gulyamov et. al. (Gu 67) using 30 MeV He^3 ions. They report seeing the ground state and a broad excited state at 1.73 ± 0.1 MeV with a width of 1.7 ± 0.3 MeV. They measured the

angular distributions for both the ground state and first excited state and found that both could be well fitted by squares of Bessel's functions of order 0, which on the Newns theory of double stripping (Ne 60a) indicates an L = 0 angular momentum transfer. According to this both states should have $J^{\pi} = 0^{+}$. This is in agreement for the expected spin of the ground state but in conflict with the expected spin of 2^{+} for the first excited state. The work is also in conflict with that of Eccles et. al. who found an isotropic angular distribution for the ground state. The Russian paper does not explicitly mention the neutron continuum expected from the many body break-up reactions and it seems quite likely that their angular distribution for the excited state contains large contributions from the continuum. They do however point out that anomalous L = 2 double stripping patterns have been observed in the case of $B^{10}(t,p)B^{12}$ (Mi 64).

Another approach to the problem was made by Rogers and Wegner (Ro 66) and also by Mangelson et. al. (Ma 66) using the reaction $Li^{6}(He^{3},t)Be^{6}$. The results of both experiments are in agreement with the (p,n) and (He^{3},n) data except for that of Batty. Rogers observed the ground state and an excited state at 1.63 ± 0.10 MeV, Γ = 1.2 ± 0.1 MeV, but no other significant structure up to an excitation of 10 MeV.

electrostatic generators. For the experiments with protons below 11 MeV the tandem alone was used but for the runs between 15 and 18 MeV the accelerators were used in the coupled mode. Using the tandem alone we were able to obtain a mean current on target of 0.015 μa after chopping, but in the coupled mode the maximum that could be obtained was only 4 na. In the latter case the limit was set by the injector which was able only to produce a D.C. current of 1 μa. Because the currents which could be obtained on target were small, thick targets were required in order to produce a reasonable neutron yield. The targets were made from Li^6 metal of 95 per cent purity supplied by A.E.R.E. Harwell. Various forms of target were tried before a satisfactory one was found. Firstly targets made by evaporating the metal directly onto tantalum backings 0.01" thick were tried but at the proton energies used the neutron background from the tantalum completely masked any yield from the lithium. The same was true for Li^7 targets made in the same way. This indicated that a transmission target was needed, so next the lithium metal was evaporated onto gold foil 0.0001" thick. The maximum thickness of lithium which could be evaporated onto such a backing was only 200 $\mu g/cm^2$. This type of target too proved unsuccessful. Although the background had been reduced the yield from the lithium was still too small to

make measurements possible. Much thicker targets were needed and since the levels in Be^6 were expected to be well separated targets as thick as 2 or 3 mg/cm^2 ($\approx$ 100 keV) could be used. Such targets could not be made by evaporation techniques but it was found to be possible to produce lithium foils of this thickness. The foils were made by placing a small piece of lithium metal between two pieces of polythene and rolling it out in a pack roller. The foils were prevented from oxidizing by pouring oil over them during the rolling process. They were then mounted on tantalum target holders which were discs with a $\frac{1}{2}$" hole punched in the centre, and were kept immersed in oil until required. Before they were mounted in the target chamber they were first washed in benzene to remove the oil, and then rapidly transferred to the target chamber which was then quickly evacuated so as to minimize the oxidation of the foils.

The target chamber is made from thin walled brass with a hole either side to allow the entry and exit of the beam, and can be coupled to the beam line by means of two brass tubes 2" in diameter. It can also be insulated from the rest of the beam line so that the current stopped by the target assembly can be measured. The end section of the flight line is also insulated from earth to enable the

transmitted current to be measured. The targets are mounted in the target chamber on an aluminium disc which has five holes in it to take five targets. The disc can be rotated about its centre to enable any of the five targets to be exposed to the beam. It can also be tilted so that the target may be set either at 90° or 45° to the beam. One of the five target positions has a quartz plate permanently fixed to it. The quartz is used as a guide when focussing the beam before an experiment. To do this a television camera is focussed onto the quartz through a porthole in the side of the target chamber. The picture can be watched on a screen in the control room. With the beam brought to a good focus on the quartz, the target is put into position. Fine adjustments are then made to the beam deflectors to make the current stopped by the target assembly a minimum. This ensures good transmission through the target. The experimental layout is shown in Fig. (3.2).

After passing through the target the beam is stopped in the end section of the line on a lead stop. Ideally the flight line should be extended so that the beam stop can be located in a hole in the wall at the back of the target room, but the divergence of the beam is such that it would strike the walls of the flight line before reaching the

FIG 3.2

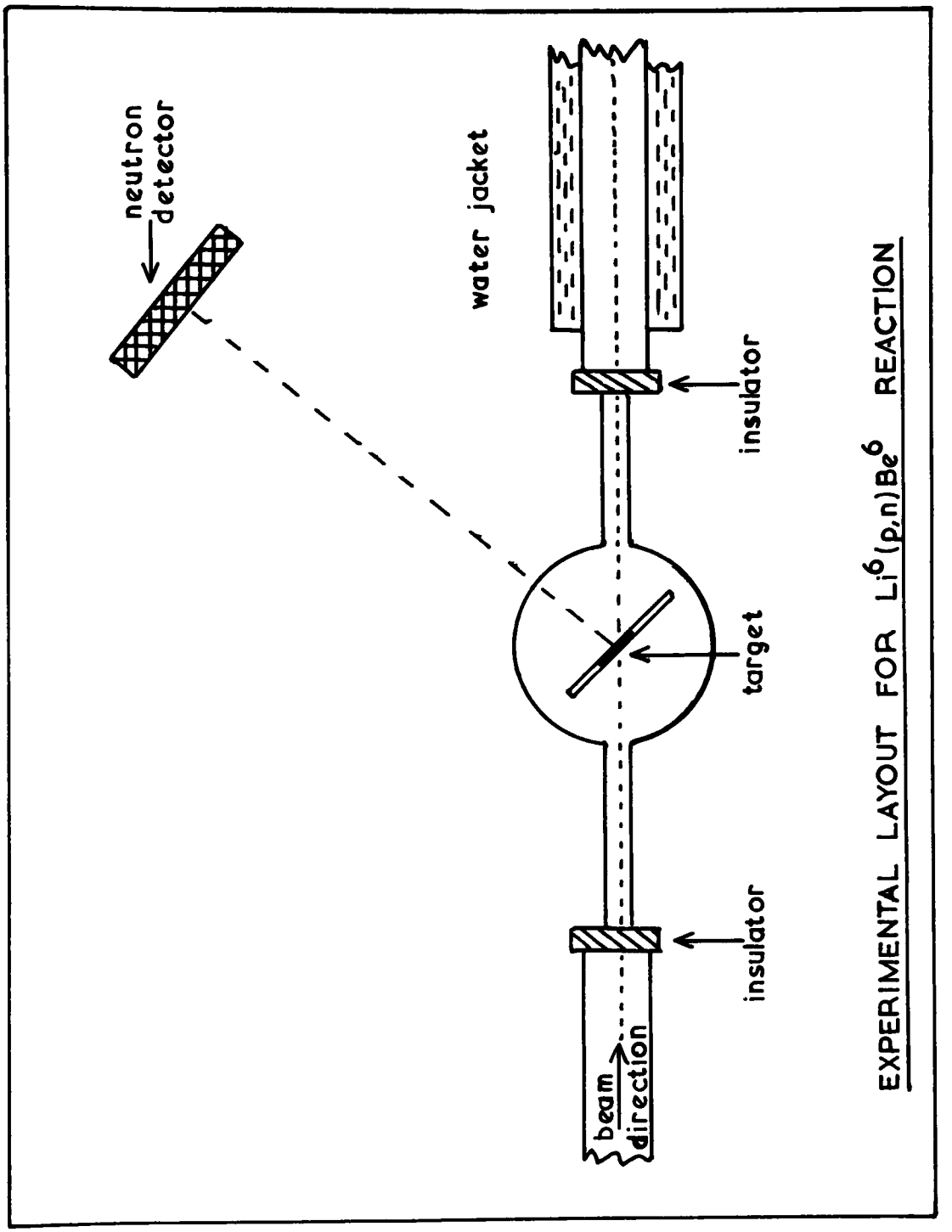
neutron detector
water jacket
insulator
target
insulator
beam direction
EXPERIMENTAL LAYOUT FOR $Li^6(p,n)Be^6$ REACTION

stop. The stop is therefore located about five metres from the target. At the proton energies used there is a considerable neutron background produced by the beam hitting the lead stop. In order to reduce this, and also to remove any neutron background caused by the beam being scattered into the walls of the flight line by the target, the end section of the flight line is surrounded by a 3" thick water jacket. This amount of water is sufficient to slow the neutrons down so that the bias on the detector cuts them out. When a carbon foil was used as a target in order to simulate the scattering expected from the lithium foils the neutron background was found to have been reduced to a negligible level. One disadvantage of the shielding was that the smallest angle at which the neutron detector could be placed was 15^{o} for a 2 metre flight path.

Excitation functions for the $Li^{6}(p,n)$ reaction were measured at 30^{o}, 90^{o} and 150^{o} for proton energies between 7 MeV and 11 MeV with 200 keV intervals. In addition angular distributions were measured at 8.3, 9.0, 9.6, 10.0, 10.5, 15.0, 16.55 and 18.0 MeV proton energies. For the measurements below 11 MeV a flight path of 2 metres was used but at the three highest energies flight paths varied between 3 and 4 metres depending on the angle of observation, the forward angles requiring a longer flight path in order to

resolve the neutron groups. The angular distributions were measured at 15° and at 10° intervals between 20° and 160°.

Results and discussion

The results of the experiments can conveniently be divided into two sections. The first section deals with measurements taken with incident proton energies below 11 MeV, and the second with measurements for proton energies above 15 MeV.

a) Experiments below 11 MeV

In this region an excitation function, and angular distributions at 8.3, 9.0, 9.6, 10.0 and 10.5 MeV were measured. On every spectrum the neutron group corresponding to the ground state of Be^6 was seen. Typical time of flight spectra are shown in Figs. (3.3), (3.4). The striking feature of the spectra especially at forward angles is the intense neutron continuum caused by the multiple break-up reactions

$$Li^6 + p \rightarrow Li^5 + p + n$$

$$\rightarrow He^4 + p + p + n$$

The intensity of the continuum falls off rapidly with

FIG 3.3

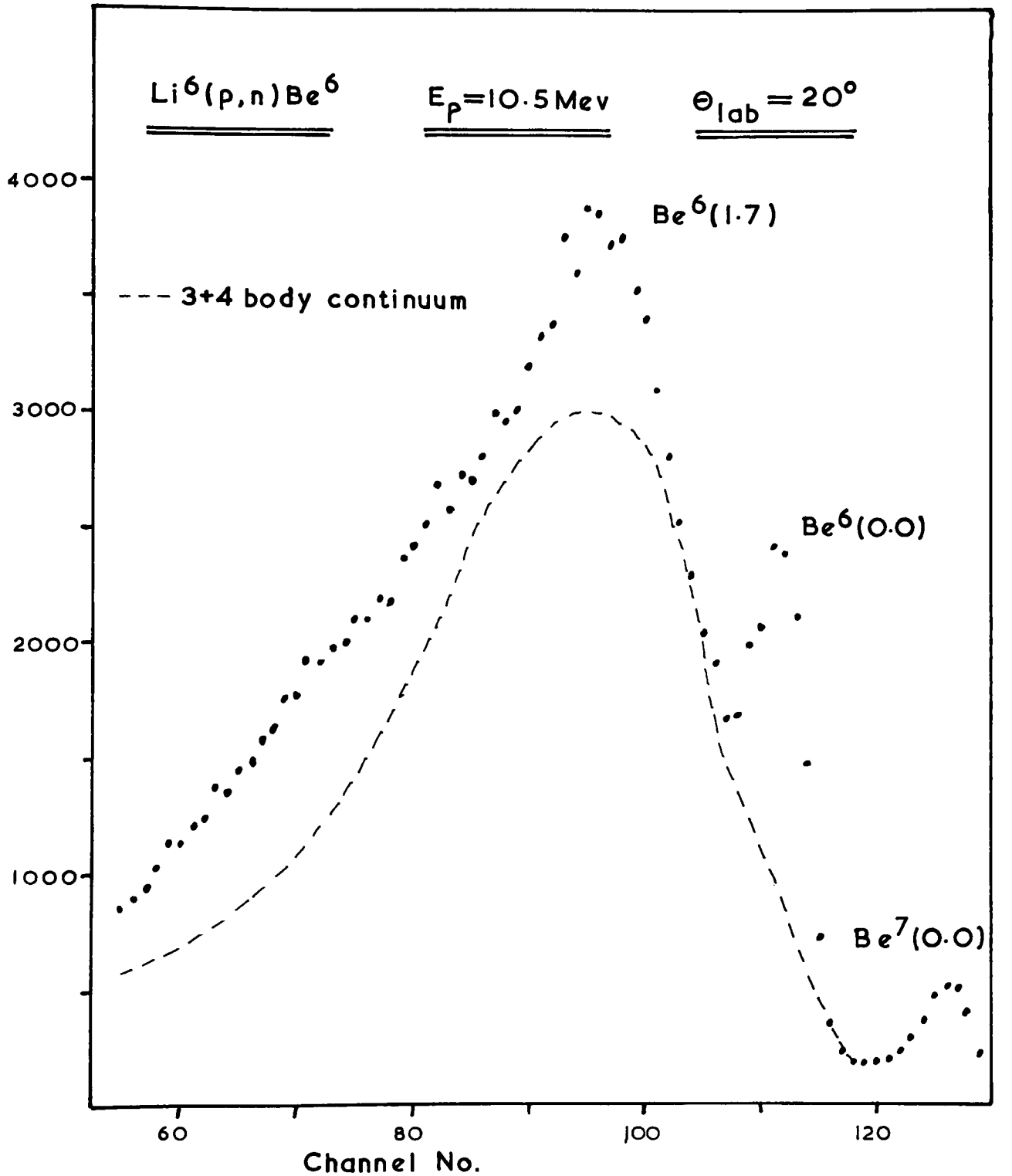
Li⁶(p,n)Be⁶
Eₚ=10.5 Mev
θlab = 20°
4000
3000
2000
1000
Be⁶(1.7)
--- 3+4 body continuum
Be⁶(0.0)
Be⁷(0.0)
60
80
100
120
Channel No.

FIG 3.4

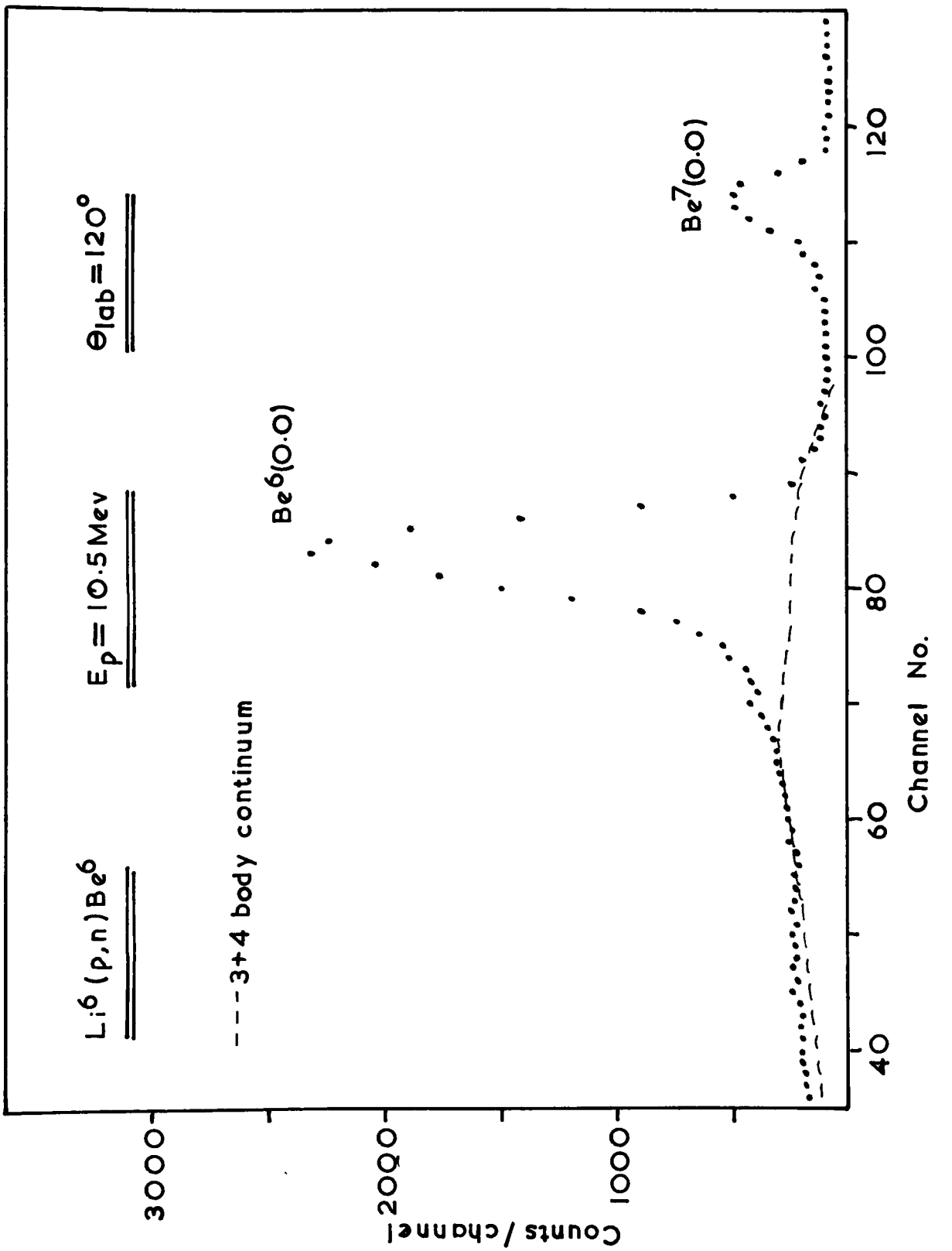
$Li^6(p,n)Be^6$
$E_p = 10.5$ Mev
$\theta_{lab} = 120°$
$Be^6(0.0)$
$Be^7(0.0)$
---3+4 body continuum
Counts / channel
Channel No.
3000
2000
1000
40
60
80
100
120

increasing angle of observation and is scarcely detectable at backward angles. The continuum in general shows little or no structure although at a few angles and energies especially above 10.0 MeV there appears to be discontinuities in an otherwise smooth neutron distribution. Over the range of energies covered by the excitation function the peak of the continuum always fell in that portion of the spectra where an excited state of Be^6 at about 1.6 MeV would be expected to be seen thus making the observation of a broad state difficult. For bombarding energies below 10.0 MeV there was no definite indication of any excited states in Be^6, but above this energy the continuum did develop a broad peak which could be explained by the existence of a broad state in Be^6 at about 1.7 MeV. There is no obvious indication of any other excited states and definitely no sharp states other than the ground state up to an excitation of 4.0 MeV. The small neutron group at higher neutron energies than the $Be^6_{g.s.}$ group is that from the ground state and first excited state of Be^7 formed by the (p, n) reaction on the small amount of Li^7 impurity in the target.

Before the angular distributions and the excitation functions for the Be^6 ground state group could be extracted an estimate of the shape of the neutron continuum beneath

the ground state group was needed. From pure phase space considerations the probability of observing a particle with energy E_c in the centre of mass from a three body break-up reaction is given by

$$P_3(E_c)dE_c = C_3 E_c^{\frac{1}{2}}(E_{max} - E_c)^{\frac{1}{2}} dE_c$$

where E_{max} is the maximum allowed energy for the particle. (Ba 54). Similarly for a four body break-up reaction the probability is

$$P_4(E_c)dE_c = C_4 E_c^{\frac{1}{2}}(E_{max} - E_c)^2 dE_c$$

C_3 and C_4 are constants.

Converted to the lab. system these expressions have the form

$$P_3(E_\ell,\theta)dE_\ell d\Omega_\ell = C_3' E_\ell^{\frac{1}{2}} \left[\frac{(M_3-m_n)}{M_3} E_{Tot}-E_\ell + 2aE_\ell^{\frac{1}{2}}\cos\theta-a^2\right]^{\frac{1}{2}} dE_\ell d\Omega_\ell$$

$$P_4(E_\ell,\theta)dE_\ell d\Omega_\ell = C_4' E_\ell^{\frac{1}{2}} \left[\frac{(M_4-m_n)}{M_4} E_{Tot}-E_\ell + 2aE_\ell^{\frac{1}{2}}\cos\theta-a^2\right]^2 dE_\ell d\Omega_\ell$$

where

M_3 = sum of final masses for 3 body reaction

M_4 = sum of final masses for 4 body reaction

m_n = mass of observed particle

m_p = mass of incident particle

m_t = mass of target

$$a = \frac{(m_n\, m_p\, E_p)^{\frac{1}{2}}}{m_p + m_t}$$

E_p = lab. energy of incident particle

θ = lab. angle of observation

E_{Tot} = total energy of system

$$= \left[a + \frac{m_t}{m_p + m_t} E_p \right]$$

These distributions can be converted from an energy scale to a time of flight scale by the relations

$$E \propto \frac{1}{t^2}$$

and $$dE \propto \frac{1}{t^3}\, dt$$

and finally corrected for the variation of the detector's efficiency $\eta(E)$ to give the expected shape of the neutron continuum on a time of flight spectrum.

$$P_3(t,\theta)dt \propto \eta(E)\, P_3(E,\theta) \cdot \frac{1}{t^3}\, dt$$

and $$P_4(t,\theta)dt \propto \eta(E)\, P_4(E,\theta) \cdot \frac{1}{t^3}\, dt$$

Spectra based on these distributions were calculated using a IBM-7 computer for the reactions

$$Li^6 + p \rightarrow Li^5 + p + n \qquad 1)$$
$$Li^6 + p \rightarrow He^4 + p + p + n \qquad 2)$$
$$Li^6 + p \rightarrow He^4 + 2p + n \qquad 3)$$

The latter reaction assumes that the two protons are emitted as a diproton.

An attempt was then made to fit the observed spectra to suitable mixtures of these three theoretical spectra. It was found that the experimental spectra could be well represented by mixtures of reactions 1) and 2) especially for high neutron energies. The fit was less good at the low energy end of the spectra. Also the higher the bombarding energy the better the fit. There was however no indication of a contribution from reaction 3). Figure (3.5) shows the experimental neutron spectrum for E_p = 11.3 MeV at 30° together with the calculated neutron continuum and the result of subtracting the continuum from the observed spectrum. Assuming the shape of the calculated continuum to be correct, the subtracted spectrum clearly shows the ground state group together with a broad neutron group which can be identified as being due to an excited state in Be^6 at an excitation of 1.7 ± 0.1 MeV with a width of 0.7 ± 0.1 MeV. The broad distribution at the low energy end of the subtracted spectrum could possibly be due to a broad state in Be^6 at

FIG 3.5

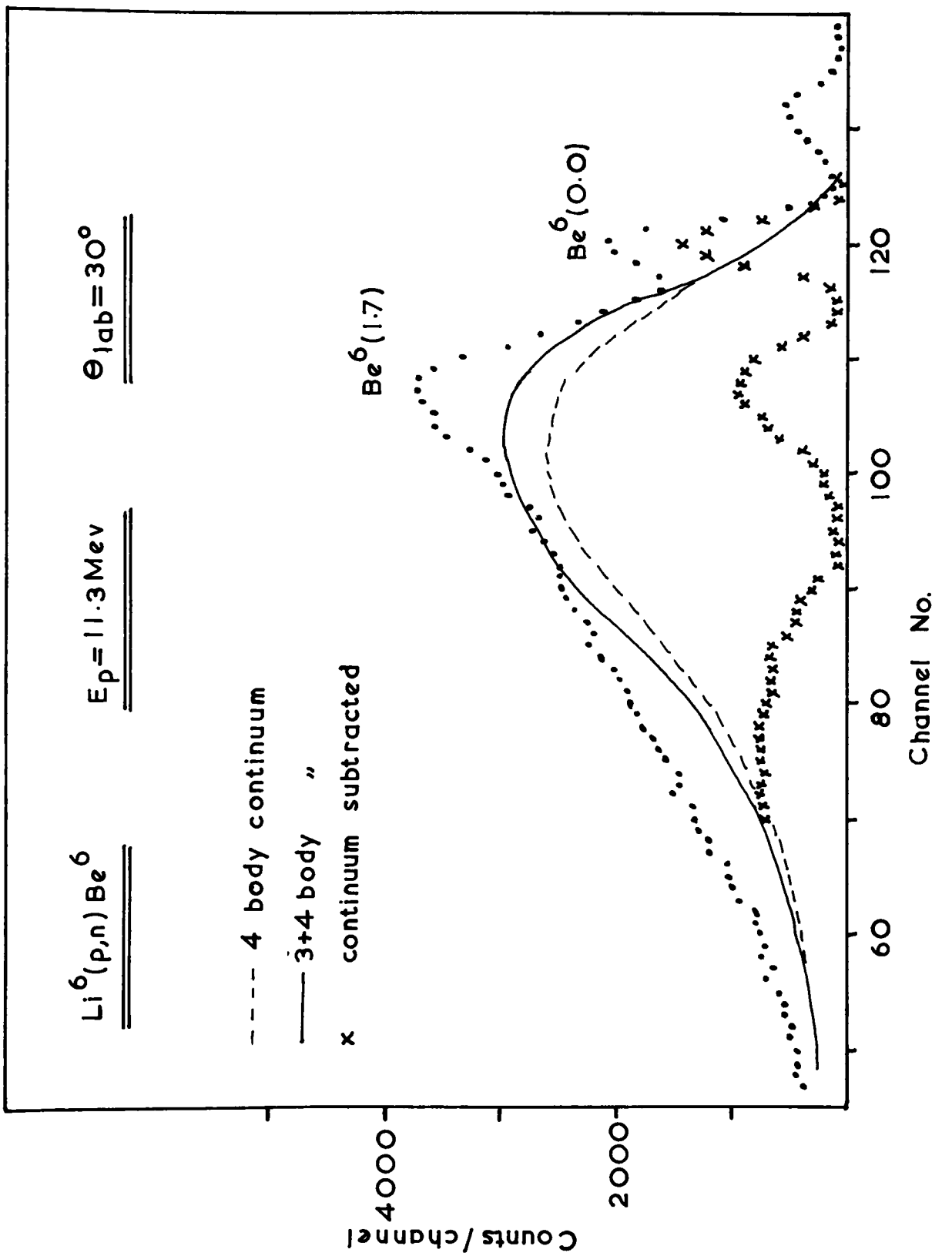
$Li^6(p,n)Be^6$
E_p=11.3 Mev
θ_{lab}=30°
---- 4 body continuum
—— 3+4 body "
x continuum subtracted
Be^6(1.7)
Be^6(0.0)
Counts/channel
2000
4000
60
80
100
120
Channel No.

about 3 MeV, but is more likely to be due to a departure of the continuum from a pure phase space distribution. A possible cause of distortion could be the Coulomb interaction between the residual nucleus and the protons from the break-up similar to the Coulomb distortion of β ray spectra. The repulsion between the protons and the residual nucleus will increase the number of fast protons. The effect of this will be to increase the number of slow neutrons. This is just the observed effect. The phase space calculations consistently underestimate the magnitude of the experimental continuum at low neutron energies. As can be seen from Fig. (3.5) most of the neutrons in the continuum arise from the four body break-up reaction. This is contrary to the conclusions of Ajzenberg-Selove (Aj 59) who suggested that this break-up mode was inhibited. It is now seen to be the most probable mode of decay. The variation with angle of the four body contribution to the continuum followed closely that calculated from phase space considerations. It also showed the same variation with bombarding energy.

The calculated continuum always could be fitted to the experimental continuum in the region of the Be^6 ground state neutron group. This was then subtracted to give the number of counts in the ground state group thus enabling the

excitation functions and angular distributions to be plotted. Figure (3.6) shows the excitation functions thus obtained at 30° for E_p = 7 to 11.3 MeV and at 90° for E_p = 8.0 to 11.0 MeV. In each case the cross section remained approximately constant and showed no significant structure over the entire energy range covered. Small fluctuations were not reproduceable and can be explained by non-uniformity in the target thickness. In any case the fluctuations were no more than 10 per cent of the total cross section, only just outside the uncertainty produced by the subtraction of the background and in the measurement of the relative efficiency of the detector.

Figures (3.7) to (3.11) show the angular distributions obtained for the ground state neutrons at incident proton energies of 8.3, 9.0, 9.6, 10.0, 10.5 MeV. These energies were chosen as they were once believed to be points of maxima and minima on the excitation function. The solid lines are least squares fits to the experimental points of a series of Legendre polynomials. The characteristics of the angular distributions are :-

1) they are not symmetrical about 90°

2) they are strongly peaked in the backward direction.

FIG 3.6

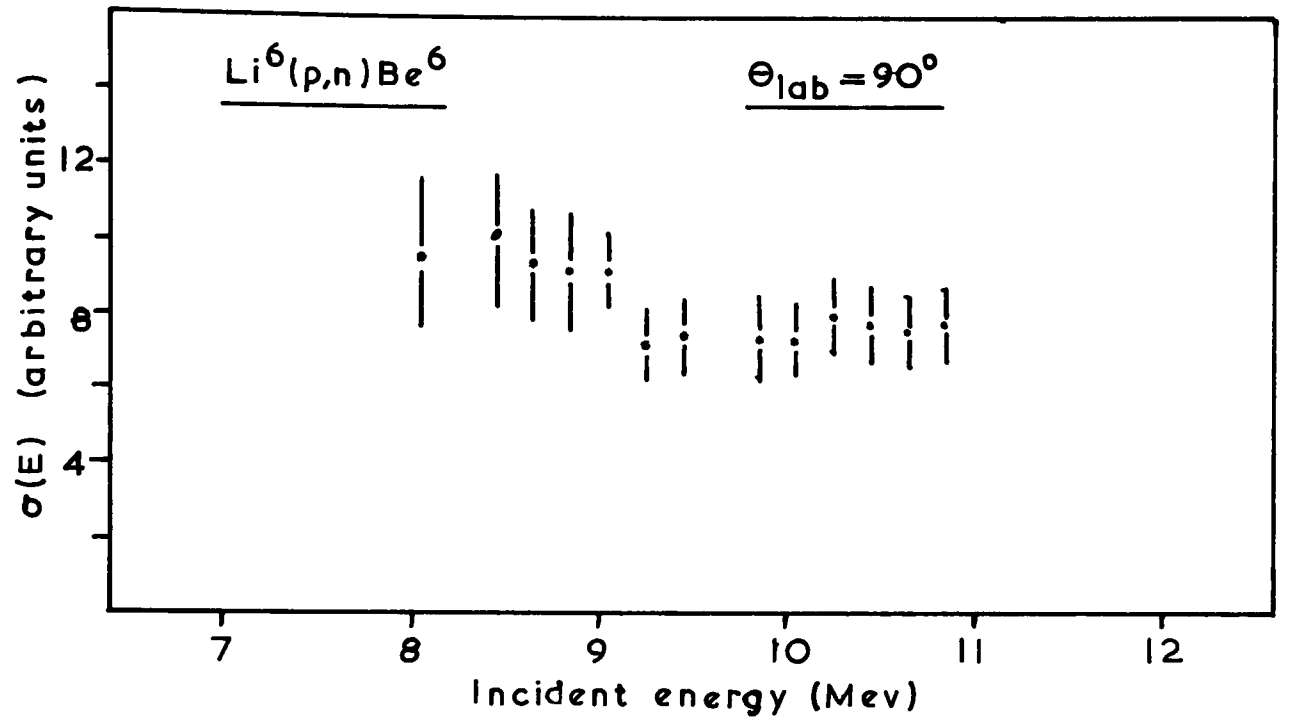

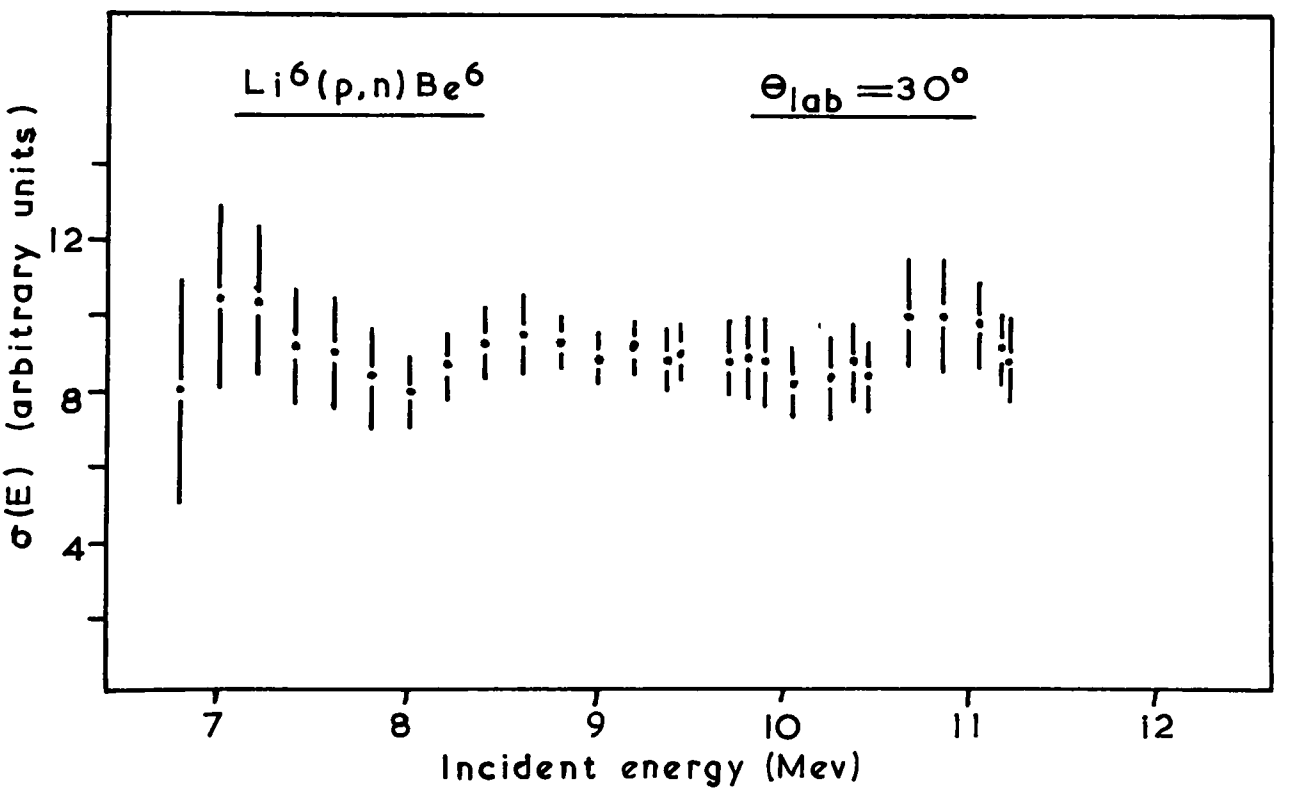

EXCITATION FUNCTIONS

FIG 3.7

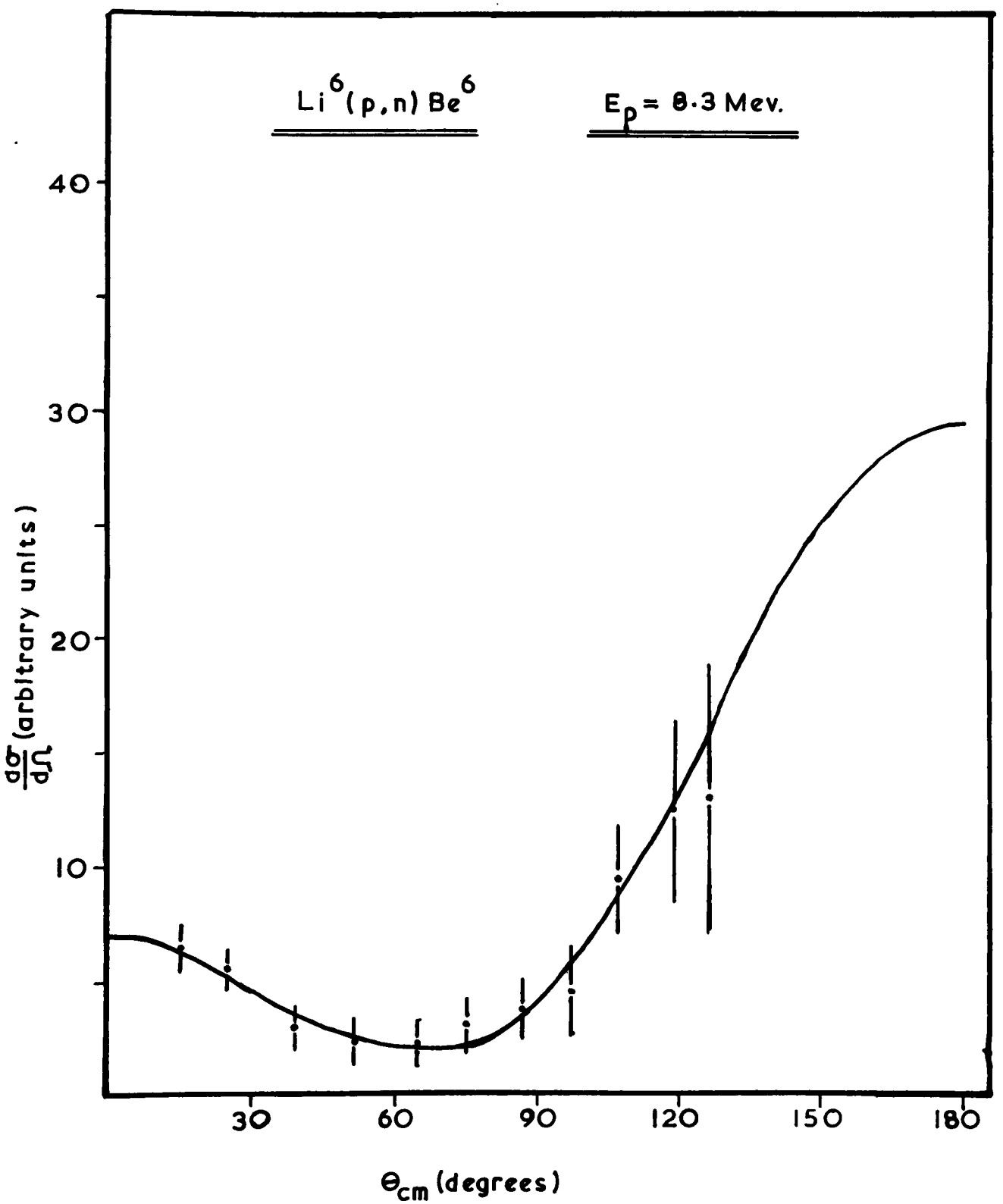
$Li^6(p,n)Be^6$
$E_p = 8.3$ Mev.
40
30
20
10
$\frac{d\sigma}{d\Omega}$ (arbitrary units)
30
60
90
120
150
180
θ_{cm} (degrees)

FIG 3·8

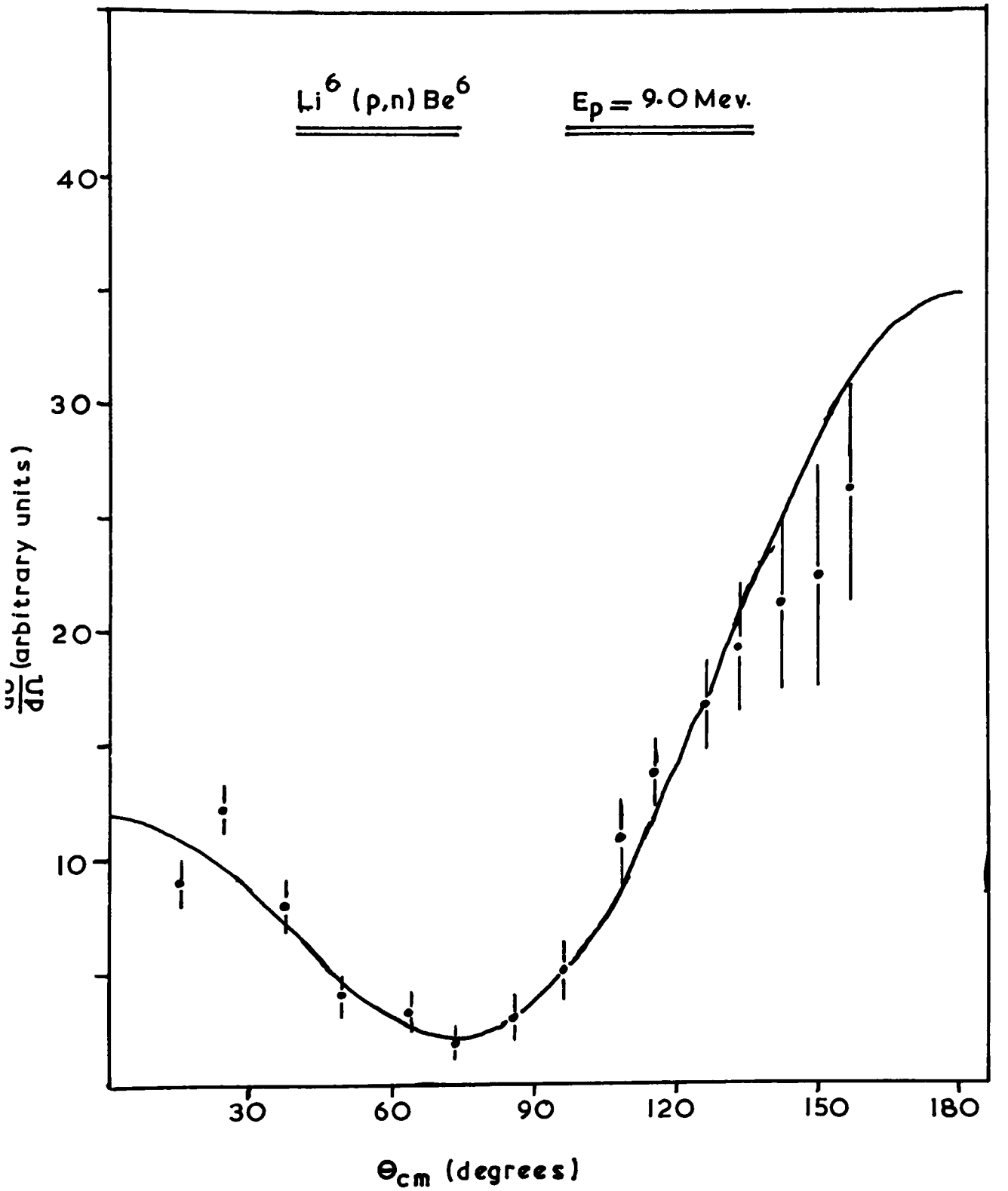
$Li^6(p,n)Be^6$
$E_p = 9.0$ Mev.
40
30
20
10
$\frac{d\sigma}{d\Omega}$ (arbitrary units)
30
60
90
120
150
180
Θ_{cm} (degrees)

FIG 3.9

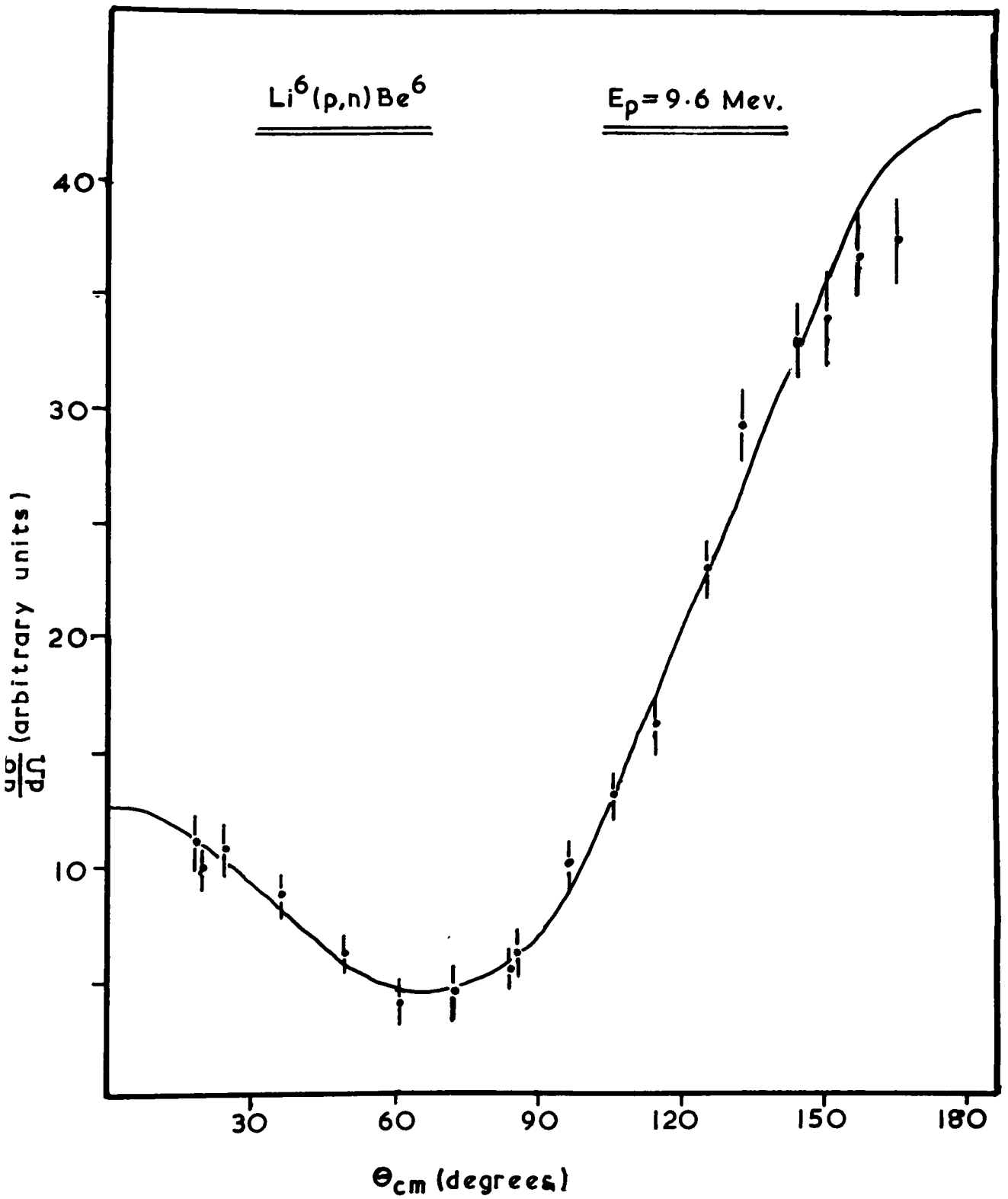
Li⁶(p,n)Be⁶
Ep = 9.6 Mev.
40
30
20
10
dσ/dΩ (arbitrary units)
30
60
90
120
150
180
θcm (degrees)

FIG 3·10

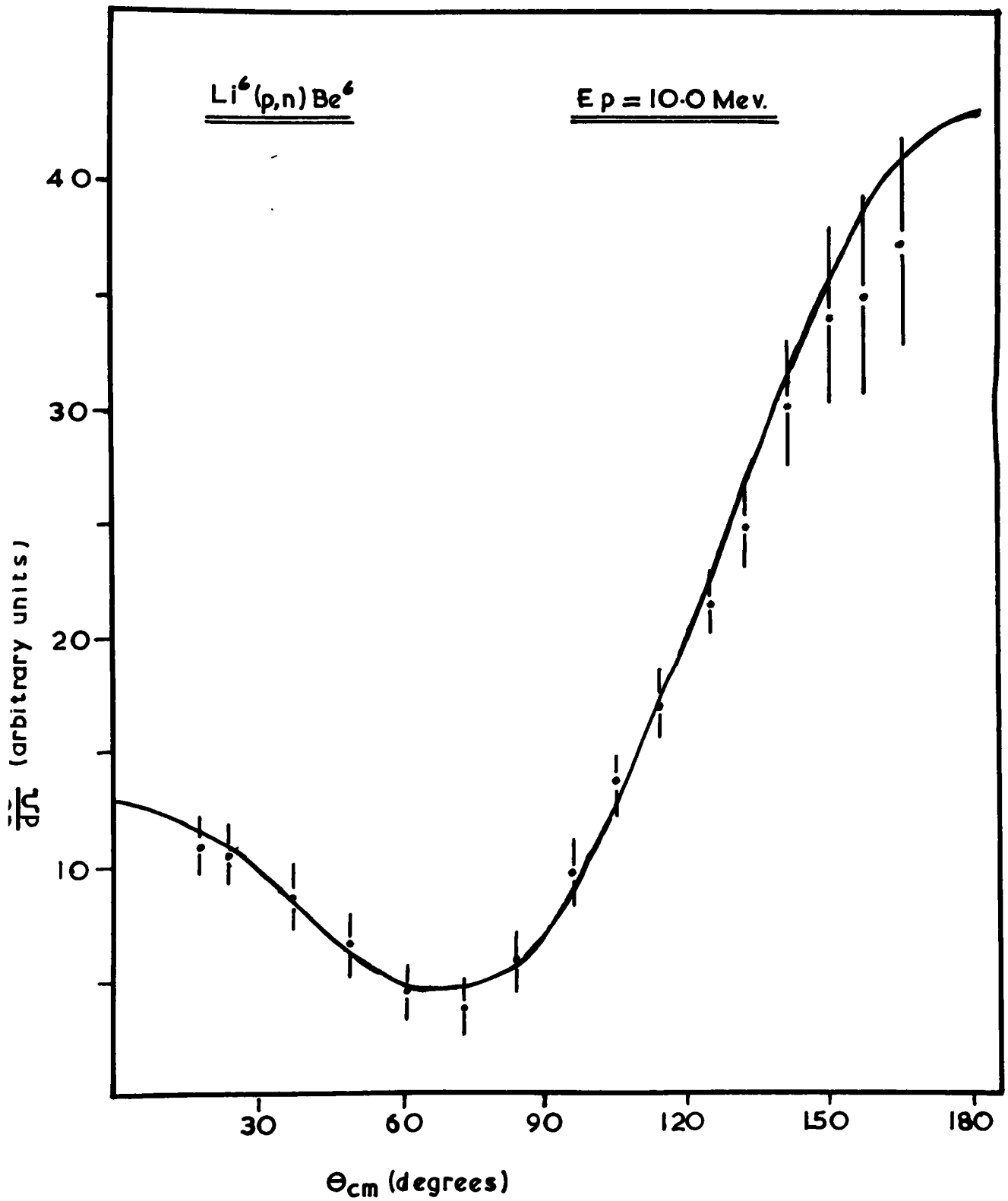
Li⁶(p,n)Be⁶
Ep = 10·0 Mev.
40
30
20
10
dσ/dΩ (arbitrary units)
30
60
90
120
150
180
θcm (degrees)

FIG 3.11

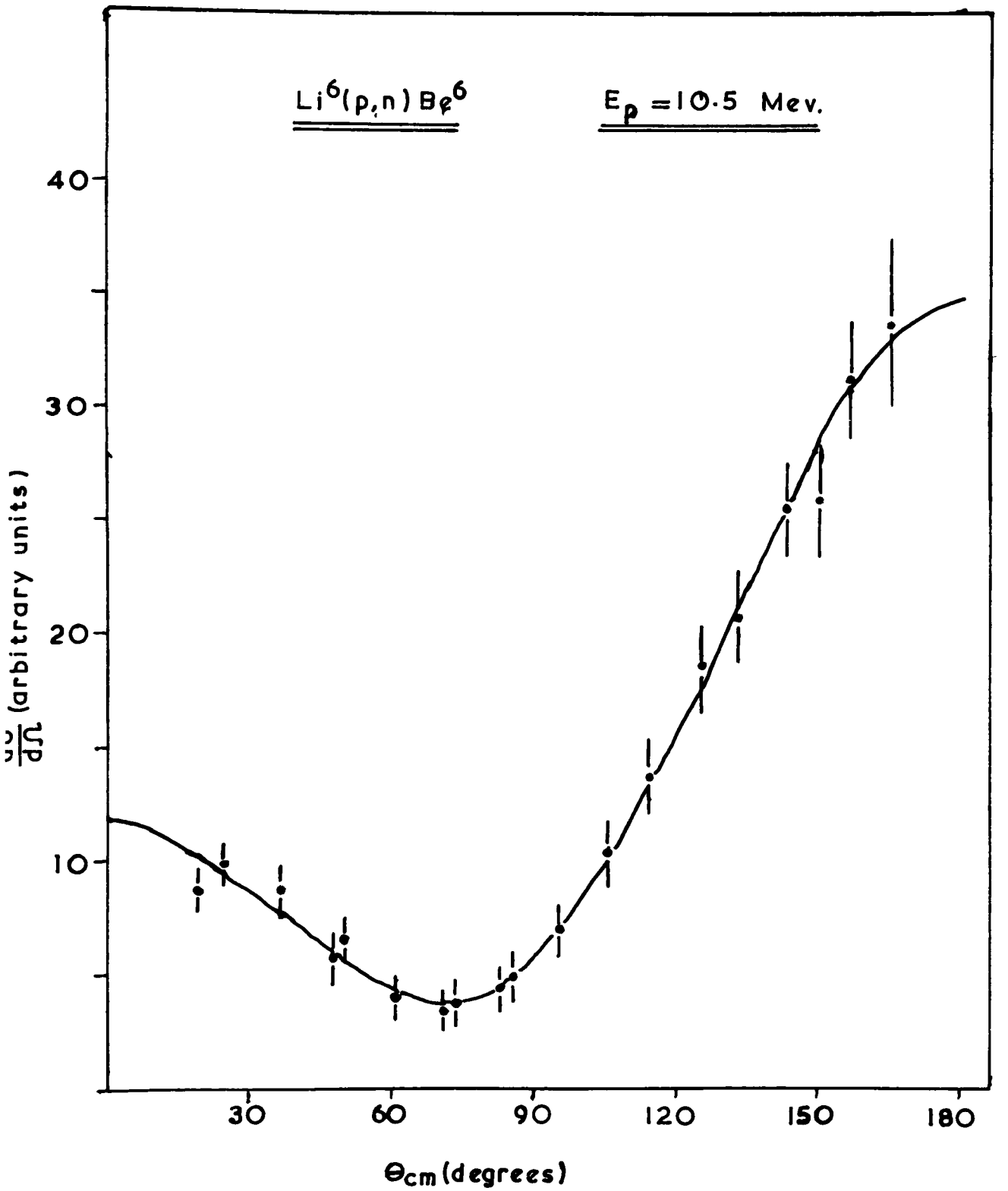
$Li^6(p,n)Be^6$
$E_p = 10.5$ Mev.
40
30
20
10
$\frac{d\sigma}{d\Omega}$ (arbitrary units)
30
60
90
120
150
180
θ_{cm} (degrees)

In each case the cross section at 180° is three to four times that at 0°.

A series of Legendre polynomials of the form

$$a_o (P_o + a_1 P_1 + a_2 P_2 + \ldots a_n P_n)$$

was fitted to the experimental angular distributions by the method of least squares using a PDP-7 computer. In each case the first three polynomials were sufficient to obtain a good fit. The coefficients of higher order polynomials were an order of magnitude smaller than those of the first three, and the same magnitude as the calculated variances of the coefficients and were so not significant. The values of the coefficients of the first three polynomials together with the computed errors are given in Table (3.2).

If the absolute differential cross section had been measured then the total cross section for the reaction would be equal to $4\pi a_o$. However in this case since the absolute cross sections are not known the coefficient a_o is just a normalization constant. The shape of the angular distribution is seen to be independent of energy indicating that there are no resonances in the cross section over the range of energies used, in agreement with the excitation function. The general shape of the angular distributions agrees with

TABLE 3.2

Results of "Least Squares" calculations

E_p (keV)	a_o	Δa_o	a_1	Δa_1	a_2	Δa_2
8.3	8.37	0.87	-1.278	0.076	1.047	0.061
9.0	10.33	0.59	-1.106	0.059	1.258	0.051
9.6	10.20	0.28	-1.085	0.030	0.960	0.030
10.0	7.46	0.28	-1.107	0.050	0.844	0.056
10.0	10.17	0.32	-1.047	0.029	0.951	0.027
10.5	11.59	.23	-0.987	0.028	1.000	0.030

that obtained by Bogdanov et. al. at 9.6 MeV (Bo 58) but differs in the ratio of the cross section at 0^{o} to that at 180^{o}.

Assuming that the reaction proceeds through the compound nucleus Be^{7*} the following conclusions may be drawn. Since the excitation function shows no resonances there are no well defined states in Be^{7} between excitations of 12 and 15 MeV. This is not surprising at this excitation where resonances are expected to be broad. Also as the cross section is constant over this range of energies, the region of excitation in the compound nucleus must be well away from any state in Be^{7}. The highest known state in Be^{7} is at 9.9 MeV with a width of 2 MeV (Ha 63). The reaction could proceed through the tail of such a broad state. Since both odd and even order polynomials are required to fit the angular distributions there must be a contribution to the reaction from states with both odd and even parity. If the reaction proceeded through an isolated state in the compound nucleus only even order polynomials would be required to fit the angular distribution. From compound nucleus theory (Bl 52) if a reaction proceeds through an isolated resonance the highest order Legendre polynomial appearing in the angular distribution is $P_{\ell}(\cos\theta)$ where $\ell \leq$ 2L or 2J-1,

which ever is the smaller, where L is the angular momentum of the highest partial wave in the transition and J is the total spin of the compound state. If there are two or more interfering levels then both odd and even order polynomials can appear. In the present case the highest order polynomial appearing is P_2 so that the highest partial wave taking part in the reaction is the p wave. But since both odd and even order polynomials appear there must be interference between s wave and p wave neutrons.

Using the method of analysis adopted by Tasckek (Pa 48) the amplitude of the neutron wave can be written as

$$f(\theta) = c_o P_o(\cos\theta) + c_1 P_1(\cos\theta)$$

$$\text{where } c_j = a_j \exp(i \beta_j)$$

Hence the intensity observed at an angle θ in the centre of mass is

$$I(\theta) = \left| f(\theta) \right|^2$$

$$= \left| c_o P_o(\cos\theta) + c_1 P_1(\cos\theta) \right|^2$$

This can be written as

$$I(\theta) = a_0 P_0 + a_1 P_1 + a_2 P_2$$

where $a_o = a_o^2 + \frac{a_1^2}{3}$

$a_1 = 2a_o a_1 \cos(\beta_1 - \beta_o)$

$a_2 = \frac{2}{3} a_1^2$

From the experimental data the parameters a_o, a_1 and $\cos(\beta_1 - \beta_o)$ may be determined. The results are given in Table (3.3).

The amplitude of the neutron wave for the 14.5 MeV data can therefore be written as

$$f(\theta) = 0.71 P_o + 1.23 \exp(0.49 i\pi) P_1$$

This shows clearly the large contribution from the p wave neutrons to the reaction.

The final nucleus ^{56}Fe is expected to have spin 0^+. Assuming this, the selection rules severely limit the spins of any compound state which might be excited by the reaction. These are given by the relations

$$\underline{J}_c = \underline{J}_f + \underline{\ell}_n + \underline{s}_n$$

$$\pi_c = (-)^{\ell_n} \pi_f$$

where $J_c\ \pi_c$ is the spin and parity of the compound state

TABLE 3.3

E_p (keV)	a_0	a_1	$\cos(\beta_1-\beta_0)$
8.3	0.69	1.25	-0.74
9.0	0.61	1.37	-0.46
9.6	0.72	1.20	-0.62
10.0	0.77	1.13	-0.64
10.0	0.68	1.28	-0.72
10.5	0.71	1.23	-0.57

$J_f\ \pi_f$ is the spin and parity of the final nucleus

S_n is the spin of the neutron = $\frac{1}{2}$

ℓ_n is the angular momentum of the outgoing neutrons.

Since $J_f = 0$ and $\pi_f = +1$, the allowed spins of the compound states are :-

$J_c^{\pi_c} = \frac{1}{2}^+$ for the s wave contribution

and

$J_c^{\pi_c} = \frac{1}{2}^-$ or $3/2^-$ for the p wave contribution.

The spin $\frac{1}{2}^-$ can be eliminated since the angular distribution of particles from the decay of such a state is limited to a P_0 term and hence would be isotropic. Therefore the two states in the compound nucleus contributing to the reaction have $J^\pi = \frac{1}{2}^+$ and $3/2^-$. Since the ratio of the amplitudes of the p wave to s wave neutrons does not vary systematically with energy it can be argued that the two interfering levels are probably close together. The level in Be^7 at 9.9 MeV has been tentatively assigned $J^\pi = 3/2^-$ (Ha 63) and could be the negative parity state contributing to the reaction. No positive states in Be^7 are known but Lane (La 60) predicts the existence of such states. He considers them to be single

particle states produced by a particle in the $2s_{\frac{1}{2}}$, $1d_{5/2}$ or $1d_{3/2}$ shells outside a Li^6 core. The energy of these states is calculated assuming that the binding energy of these particles to the core is the same as in C^{13}, i.e., 1.87, 1.06 and - 1.92 MeV respectively. Since we are looking for a positive parity state which breaks up into Be^6 plus a neutron we can assume the core to be the Be^6 nucleus. The excitation energies of the states so predicted would be 8.80, 9.61, 12.59 MeV with spins $\frac{1}{2}^+$, $5/2^+$, $3/2^+$. We are also looking for a positive parity state with spin $\frac{1}{2}^+$ which decays by s wave neutron emission and therefore this points to the state predicted at 8.8 MeV. It also satisfies the requirement of being near to the negative parity state assumed to be at 9.9 MeV. A similar argument can be applied to the $3/2^-$ state. If it is pictured as a Be^6 core plus a $1p_{3/2}$ neutron, and assuming that the binding energy of a $p_{3/2}$ neutron is the same as in C^{13}, i.e., 1.27 MeV, it would have an excitation energy of 9.4 MeV. This compares favourably with the energy of the known $3/2^-$ level at 9.9 MeV.

b) <u>Experiments above 15 MeV</u>

The appearance of the first excited state of Be^6 at the highest bombarding energy available from the tandem

prompted the investigation of the Li^6(p,n) reaction at the much higher energies obtainable using the accelerators in the coupled mode. This move was immediately rewarded. Figure (3.12) is the spectrum obtained at 80° using a beam energy of 15.0 MeV and shows clearly the ground state of Be^6 together with a strong broad neutron group which can be identified with a state in Be^6 at 1.67 MeV. This excited state could be identified on every spectrum recorded and mean values for its excitation and width obtained from measurements at 14 different angles with an incident energy of 15.0 MeV are :-

$$E_x = 1.67 \pm 0.05 \text{ MeV}$$

$$\Gamma = 1.18 \pm 0.07 \text{ MeV}.$$

With a bombarding energy of 16.55 MeV we found evidence for a second excited state in Be^6. Several spectra taken at this energy, in particular those for 50°, 60°, 105° and 130° showed bumps on the high excitation side of the 1.67 MeV group which can be explained by the existence of a state at about 3.0 MeV. This state if it exists is much narrower than the 1.67 MeV state. Figures (3.13) and (3.14) show the spectra taken at 60° and 105°. Also shown is the

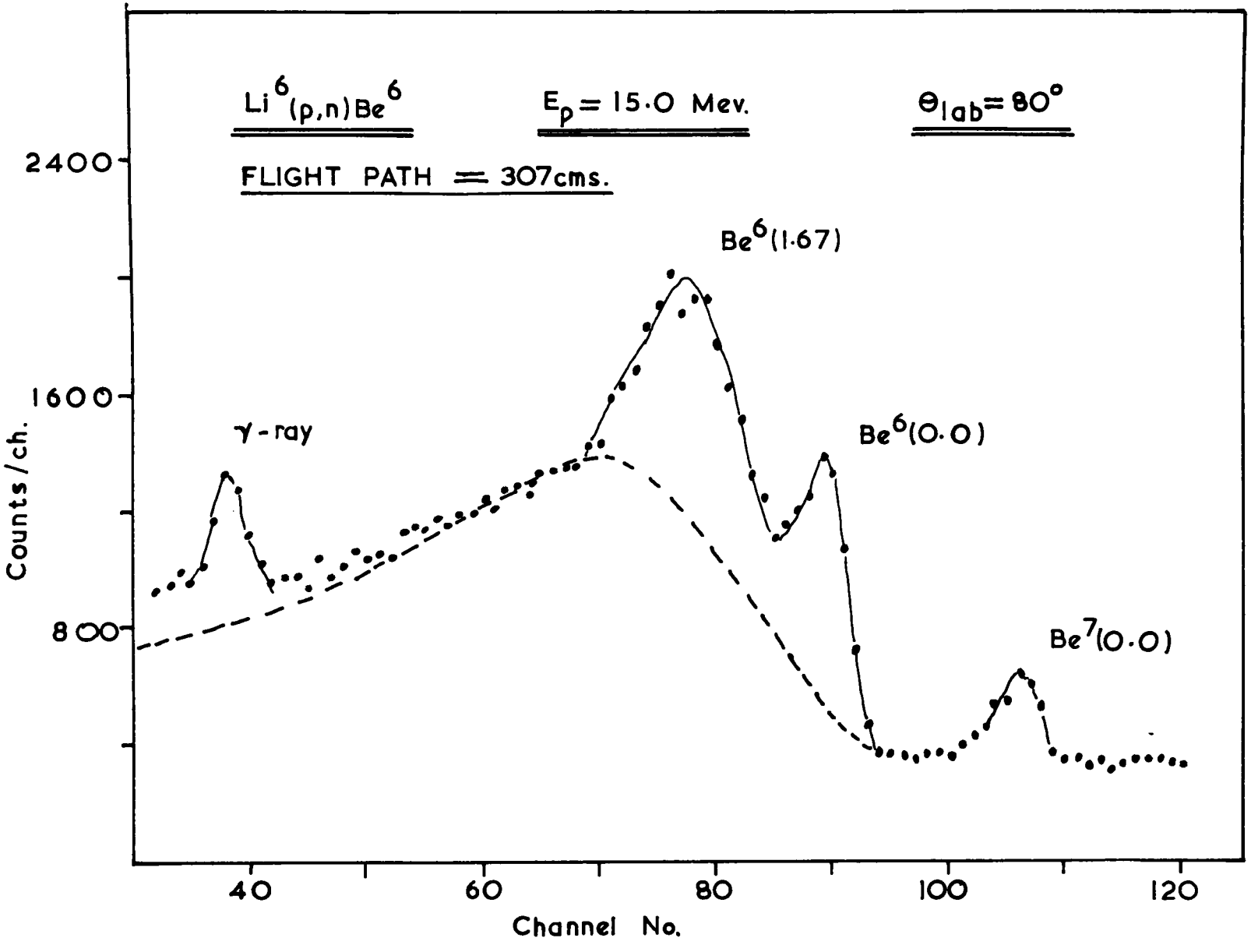
$Li^6(p,n)Be^6$
$E_p = 15.0$ Mev.
$\theta_{lab} = 80°$
FLIGHT PATH = 307cms.
$Be^6(1.67)$
$Be^6(0.0)$
$Be^7(0.0)$
γ-ray
2400
1600
800
Counts/ch.
40
60
80
100
120
Channel No.

FIG 3.12

FIG 3.13

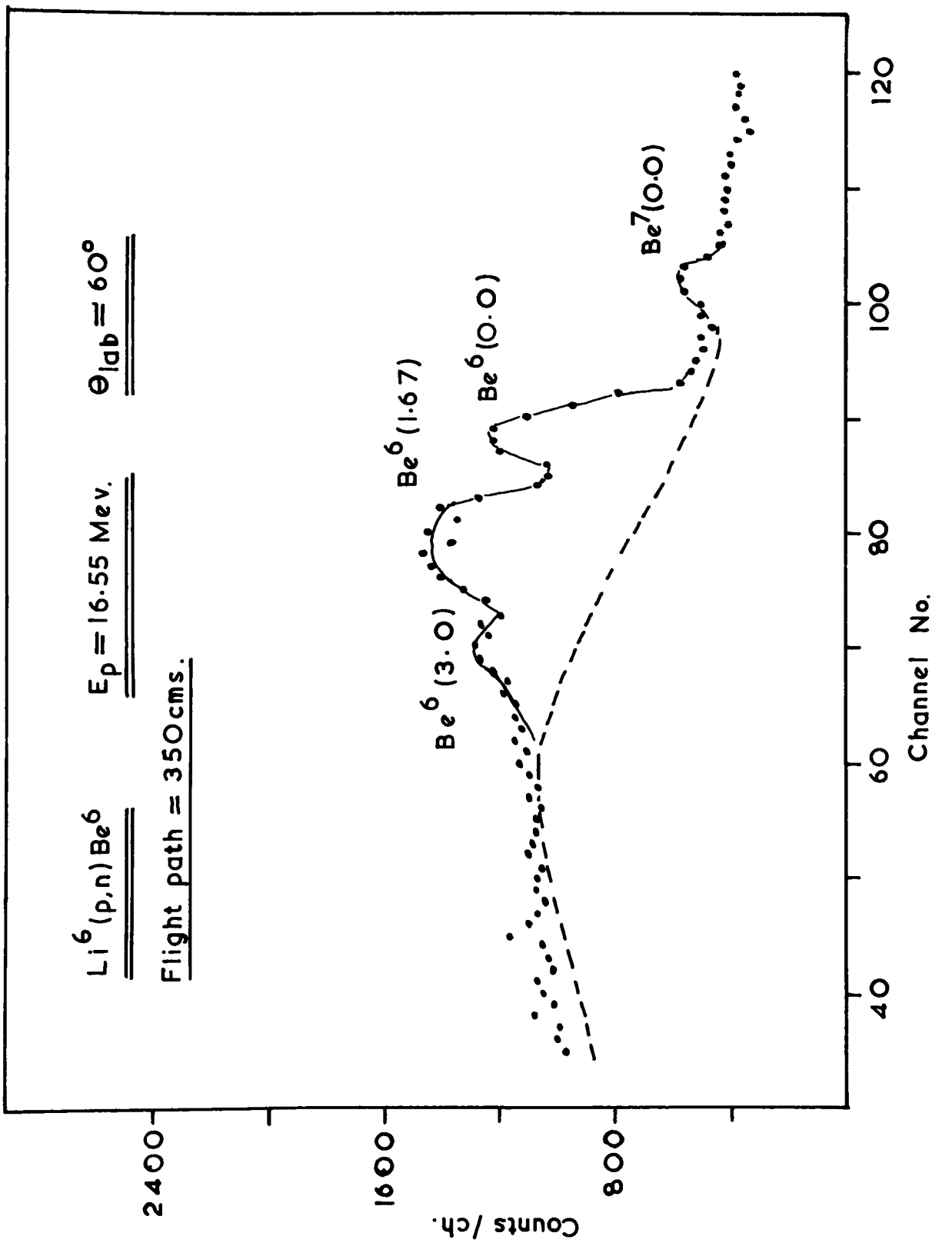
$Li^6(p,n)Be^6$
$E_p = 16.55$ Mev.
$\theta_{lab} = 60°$
Flight path = 350cms.
Be^6 (3.0)
Be^6 (1.67)
Be^6 (0.0)
Be^7 (0.0)
Counts /ch.
2400
1600
800
40
60
80
100
120
Channel No.

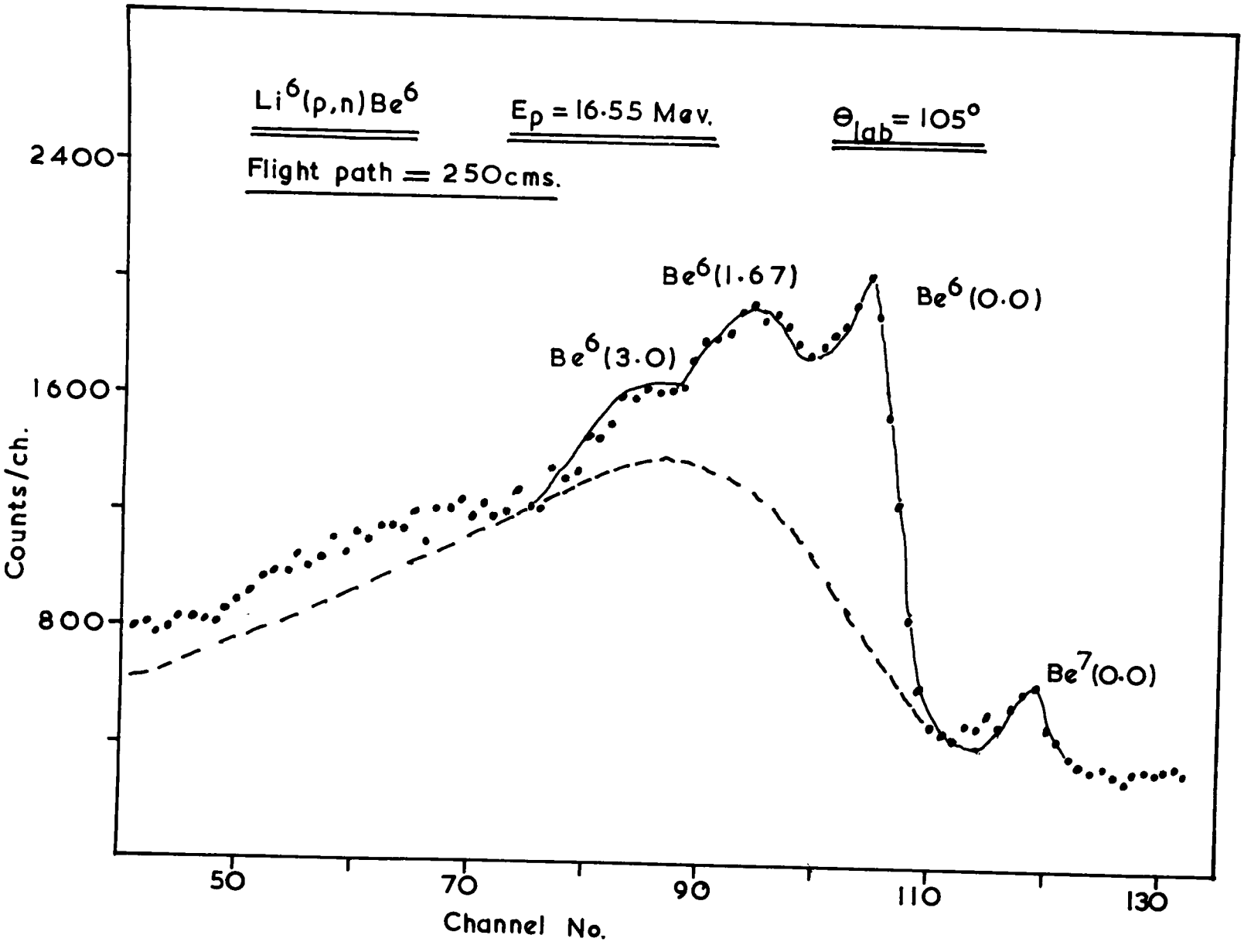
$Li^6(p,n)Be^6$
E_p = 16.55 Mev.
θ_{lab} = 105°
Flight path = 250cms.
Be^6(1.67)
Be^6(0.0)
Be^6(3.0)
Be^7(0.0)
2400
1600
800
Counts/ch.
50
70
90
110
130
Channel No.

FIG 3.14

calculated four body break-up continuum. Further evidence was found for a possible second excited state on the spectra recorded for a bombarding energy of 18.0 MeV. At this energy the 1.67 MeV neutron group appeared broader than its previously determined width of 1.2 MeV suggesting that there was a contribution from a weak unresolved level at a higher excitation.

We obtained angular distributions for the ground state neutrons at 15.0, 16.55 and 18.0 MeV, and these are shown in Figs. (3.15) to (3.17). At 15.0 MeV we also obtained the angular distribution for the neutrons from the first excited state of Be^6, and this is shown in Fig. (3.18). To obtain these angular distributions, a four body break-up continuum, calculated as described in the previous section, was first subtracted. At these higher energies it was not found necessary to include a three body component in order to fit the experimental spectra. The solid lines in Figs. (3.15) to (3.18) are the result of fitting a series of Legendre polynomials to the angular distributions, by the method of least squares.

A state at 3.0 MeV in Be^6 could be the lowest member of the ^3P multiplet. The calculations of Inglis [In 53] put this level at approximately 6 MeV excitation, but a more recent calculation by Barker [Ba 66] predicts the $^3P_2$

FIG 3·15

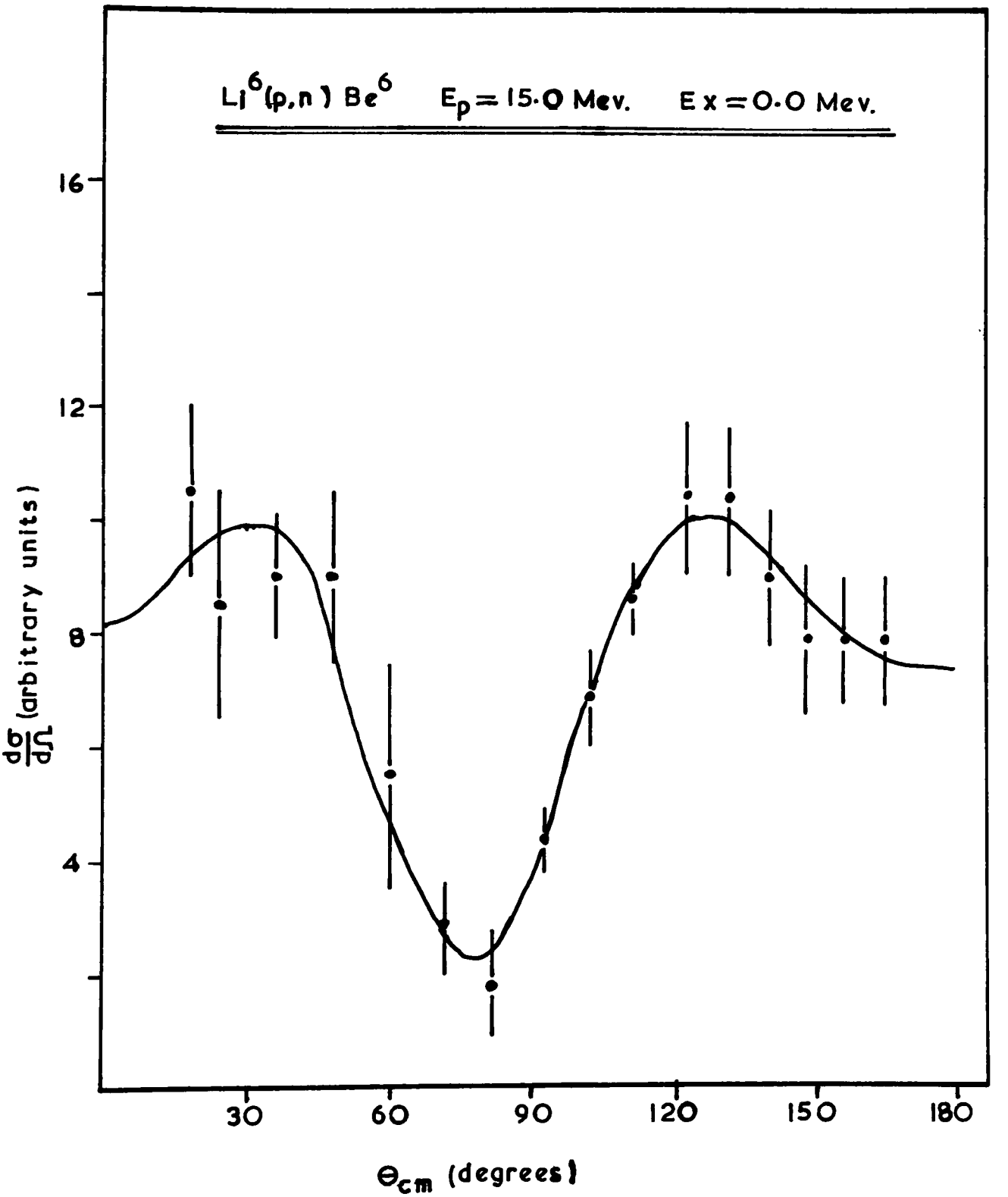
$Li^6(p,n)\,Be^6$ $E_p = 15.0$ Mev. $E_x = 0.0$ Mev.
16
12
8
4
$\frac{d\sigma}{d\Omega}$ (arbitrary units)
30
60
90
120
150
180
θ_{cm} (degrees)

FIG 3·16

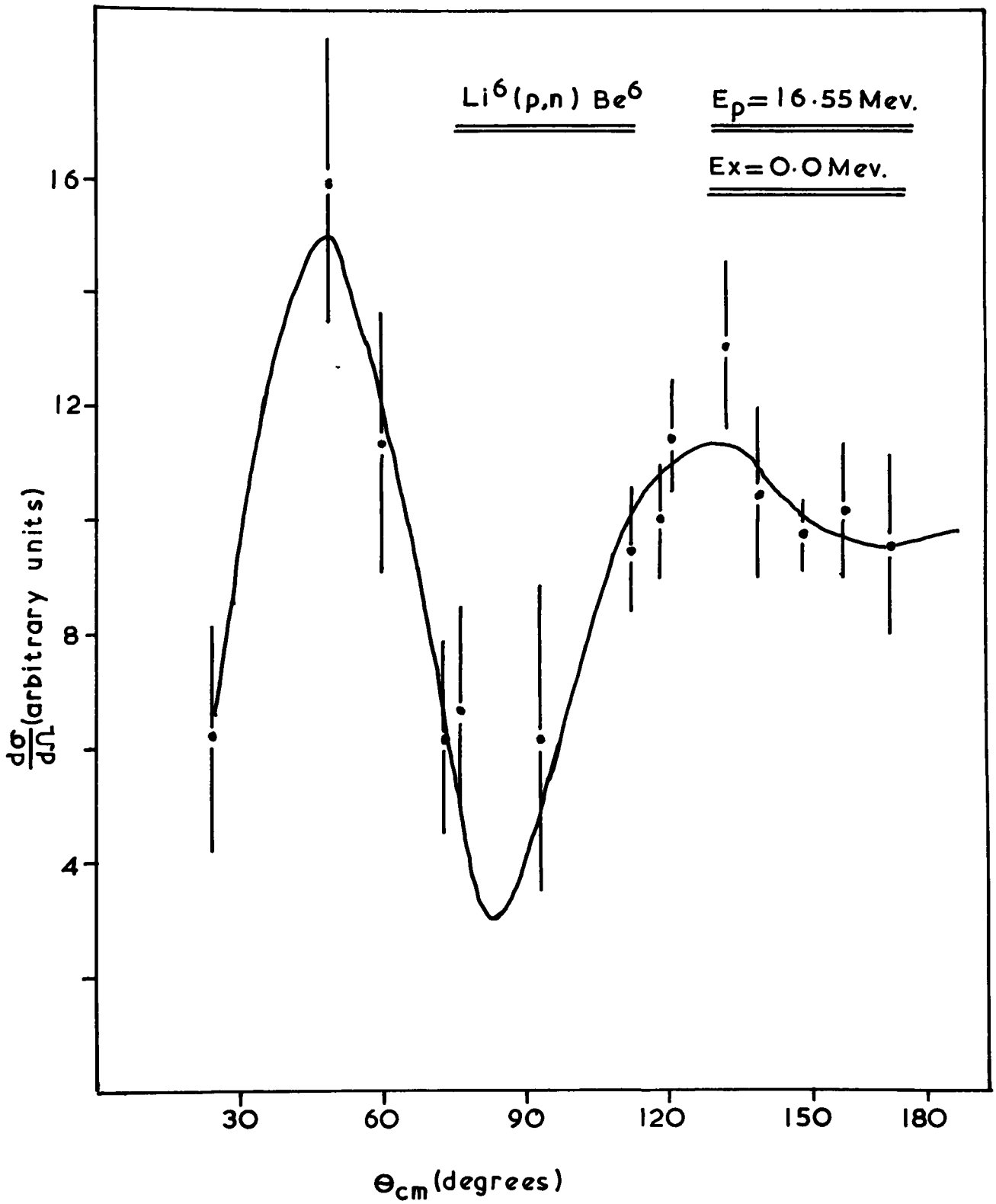
Li⁶(p,n) Be⁶
Ep = 16·55 Mev.
Ex = 0·0 Mev.
16
12
8
4
dσ/dΩ (arbitrary units)
30
60
90
120
150
180
θcm (degrees)

FIG 3·17

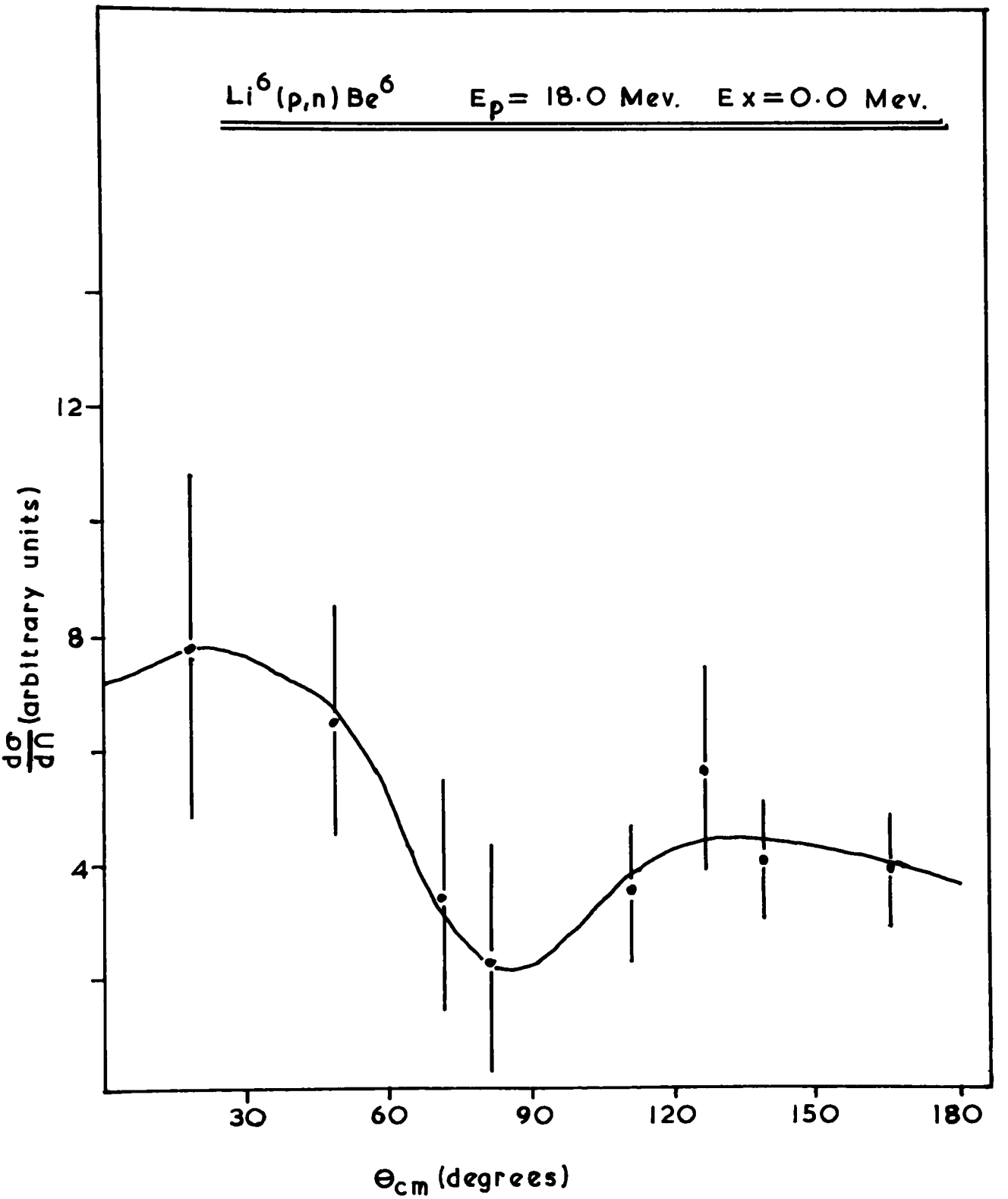
$Li^6(p,n)Be^6$ E_p= 18·0 Mev. Ex=0·0 Mev.
12
8
4
$\frac{d\sigma}{d\Omega}$ (arbitrary units)
30
60
90
120
150
180
θ_{cm} (degrees)

FIG 3.18

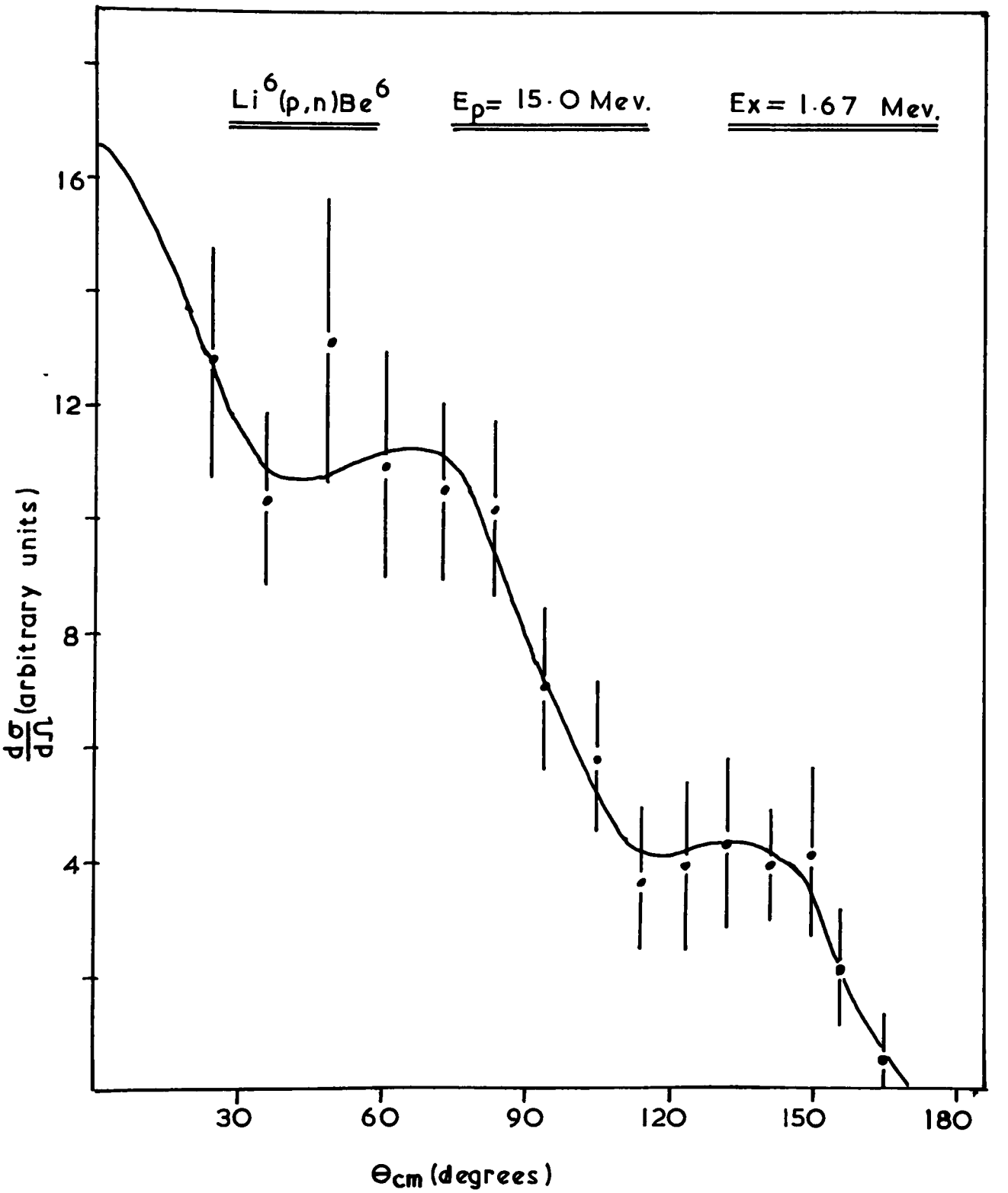
Li⁶(p,n)Be⁶
Ep= 15.0 Mev.
Ex= 1.67 Mev.
16
12
8
4
dσ/dΩ (arbitrary units)
30
60
90
120
150
180
Θcm (degrees)

level to be at 4.2 MeV in Be^6. The position however varied with the choice of parameters used in the calculation and because of insufficient data on the mass 6 nuclei, the parameters could not be determined uniquely. If the above interpretation is correct then the spin of this state would be 2^+. As mentioned in the introduction Rogers [Ro 66] found evidence for an excited state at 3 MeV from the reaction $Li^6(He^3,t)Be^6$, and a narrow state has been seen in Li^6 at an excitation of 3.67 MeV above the lowest T = 1 state [Al 60]. Allen et. al. also reported a level in He^6 at 3.4 MeV.

The ground state angular distributions obtained at 15.0, 16.55 and 18.0 MeV are quite different from those obtained at the lower energies. There is no longer a strong backward peak. Although they are more symmetric about 90^o they are not so readily interpreted by compound nucleus theory as were the lower energy angular distributions. The simplest series of Legendre polynomials which fitted the experimental points, required large contributions from all polynomials up to and including P_5. The angular distribution for the 1.67 MeV state (Fig. 3.18) is completely different in shape from the ground state one. The simplest series of Legendre polynomials which fitted this angular distribution was :-

$$\sigma(\theta) = (7.79 \pm 0.21)\,[P_0 + (0.77 \pm 0.04)P_1 + (0.43 \pm 0.09)\,P_5]$$

Incident proton energies of 15 MeV and above would reach excitation energies in the compound nucleus system above 20 MeV, and it is questionable whether it is valid to talk in terms of a compound nucleus. We have therefore attempted to interpret the data in terms of a direct reaction theory. The direct interaction model we have used is one of inelastic scattering with charge exchange [see Chapter I]. Calculations were made on the Atlas computer using a D.W.B.A. programme written by Dr. A.D. Hill. The initial state was taken to have spin 1^+ and the configuration in LS coupling of $^{13}S_1$. The ground state of Be^6 was assumed to have spin 0^+ and the configuration $^{31}S_0$, while the 1.67 MeV state was taken to have spin 2^+ with the configuration $^{31}D_2$. The optical model parameters used in the calculations were Perey-Buck parameters calculated for mass 6 nuclei. The results of the calculations are shown in Figs. (3.19) to (3.22). In no case is there any semblance of a fit. The calculations predict a backward peak for both L = 0 and L = 2 transfer, and this is not observed experimentally. The theory predicts oscillatory structure for L = 0 angular momentum transfer and little structure for L = 2 transfer. Experimentally

FIG 3·19

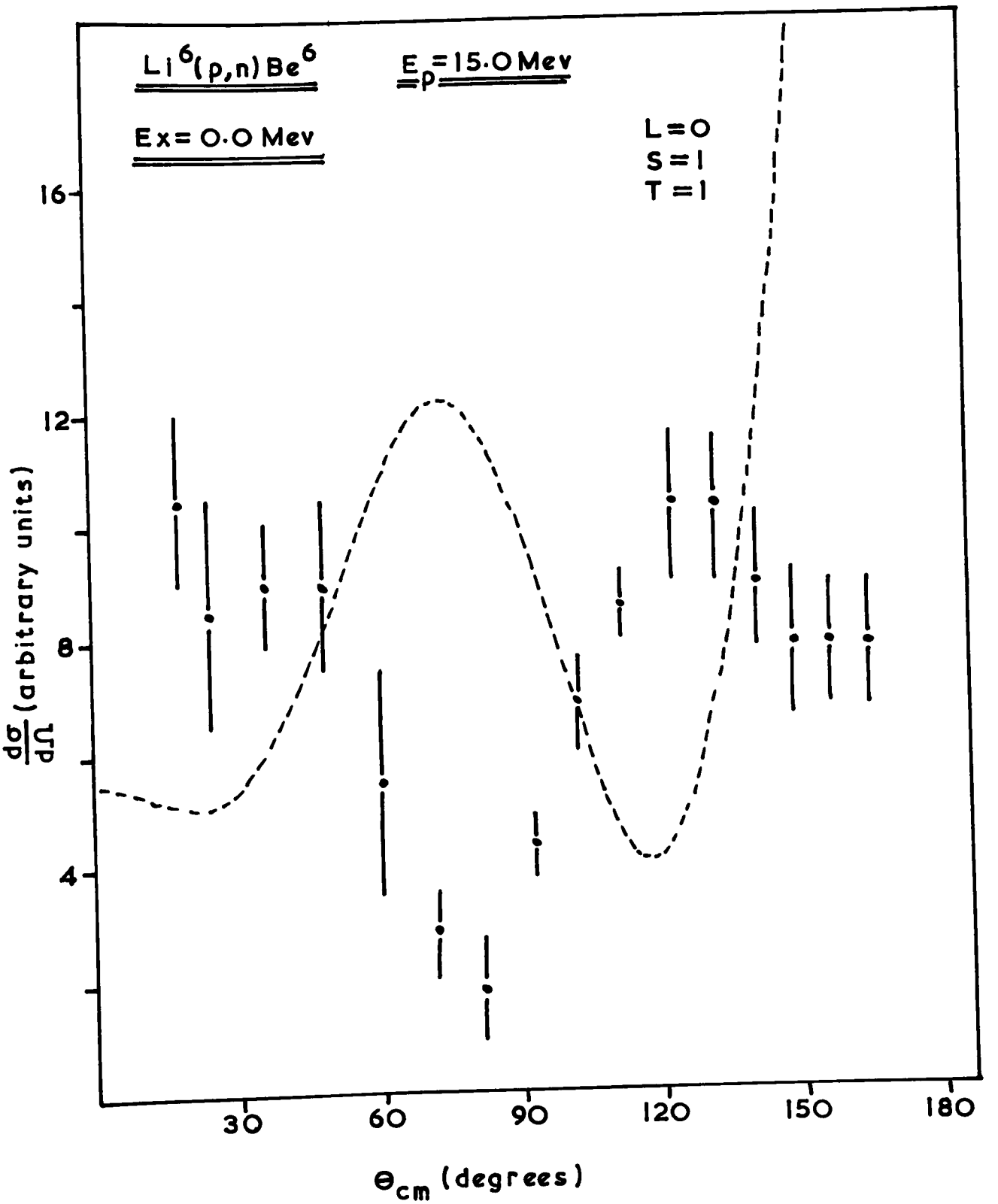
Li⁶(p,n)Be⁶
Ep=15.0 Mev
Ex= 0.0 Mev
L=0
S=1
T=1
16
12
8
4
dσ/dΩ (arbitrary units)
30
60
90
120
150
180
θcm (degrees)

FIG 3·20

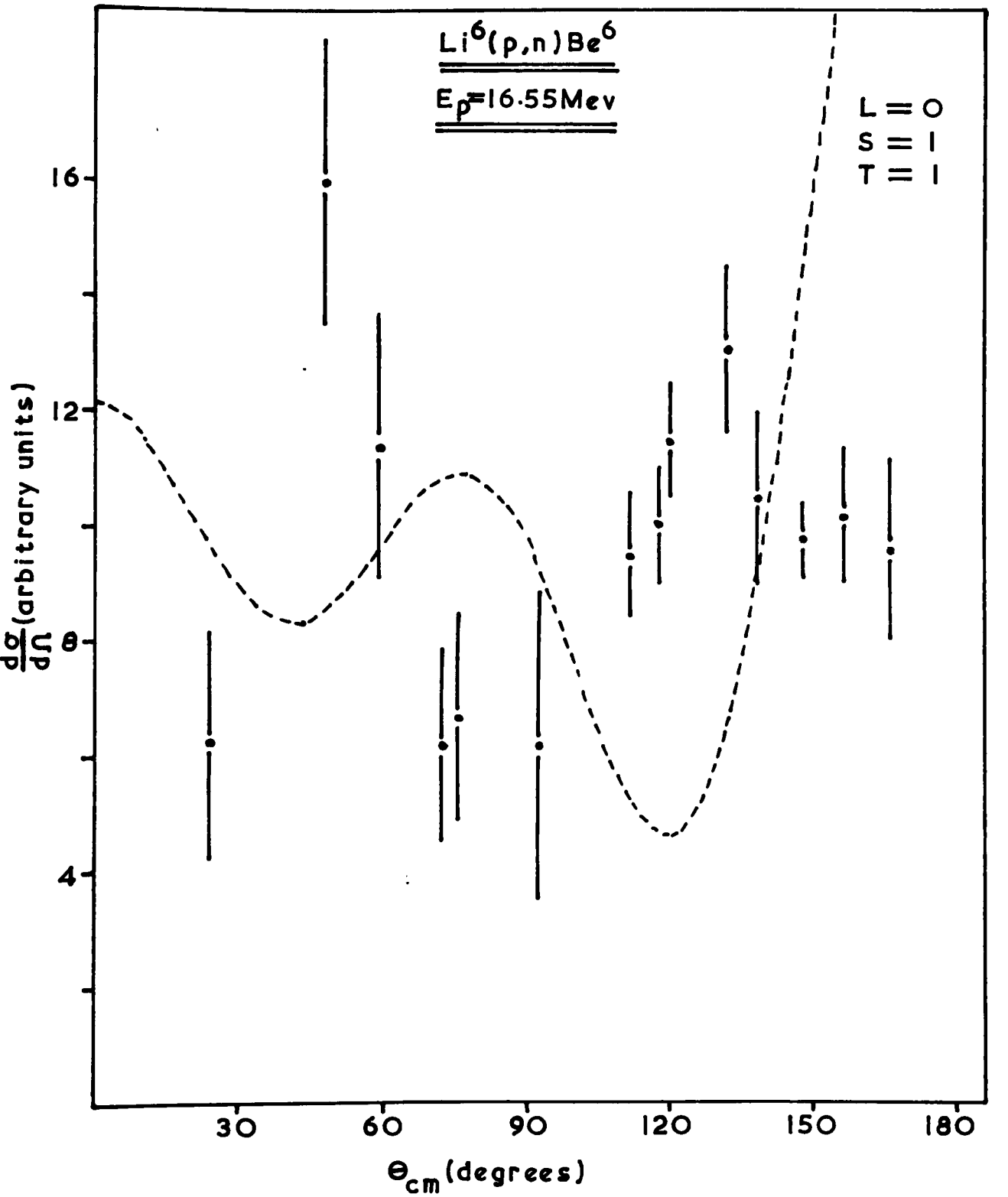
$Li^6(p,n)Be^6$
E_p=16·55Mev
L = 0
S = 1
T = 1
16
12
8
4
$\frac{d\sigma}{d\Omega}$(arbitrary units)
30
60
90
120
150
180
θ_{cm}(degrees)

FIG 3·21

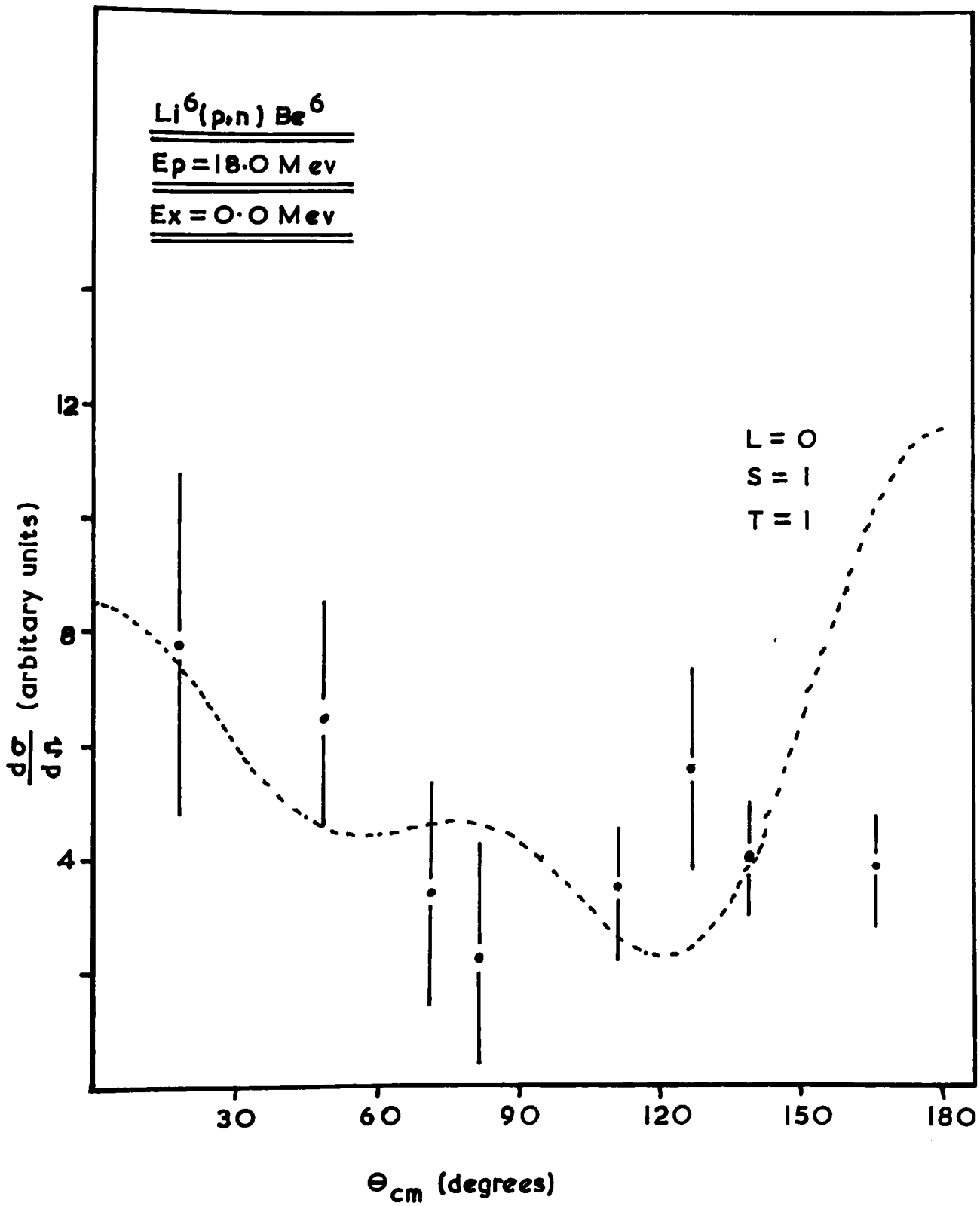
Li⁶(p,n) Be⁶
Ep = 18·0 Mev
Ex = 0·0 Mev
L = 0
S = 1
T = 1
12
8
4
dσ/dΩ (arbitary units)
30
60
90
120
150
180
θcm (degrees)

FIG 3·22

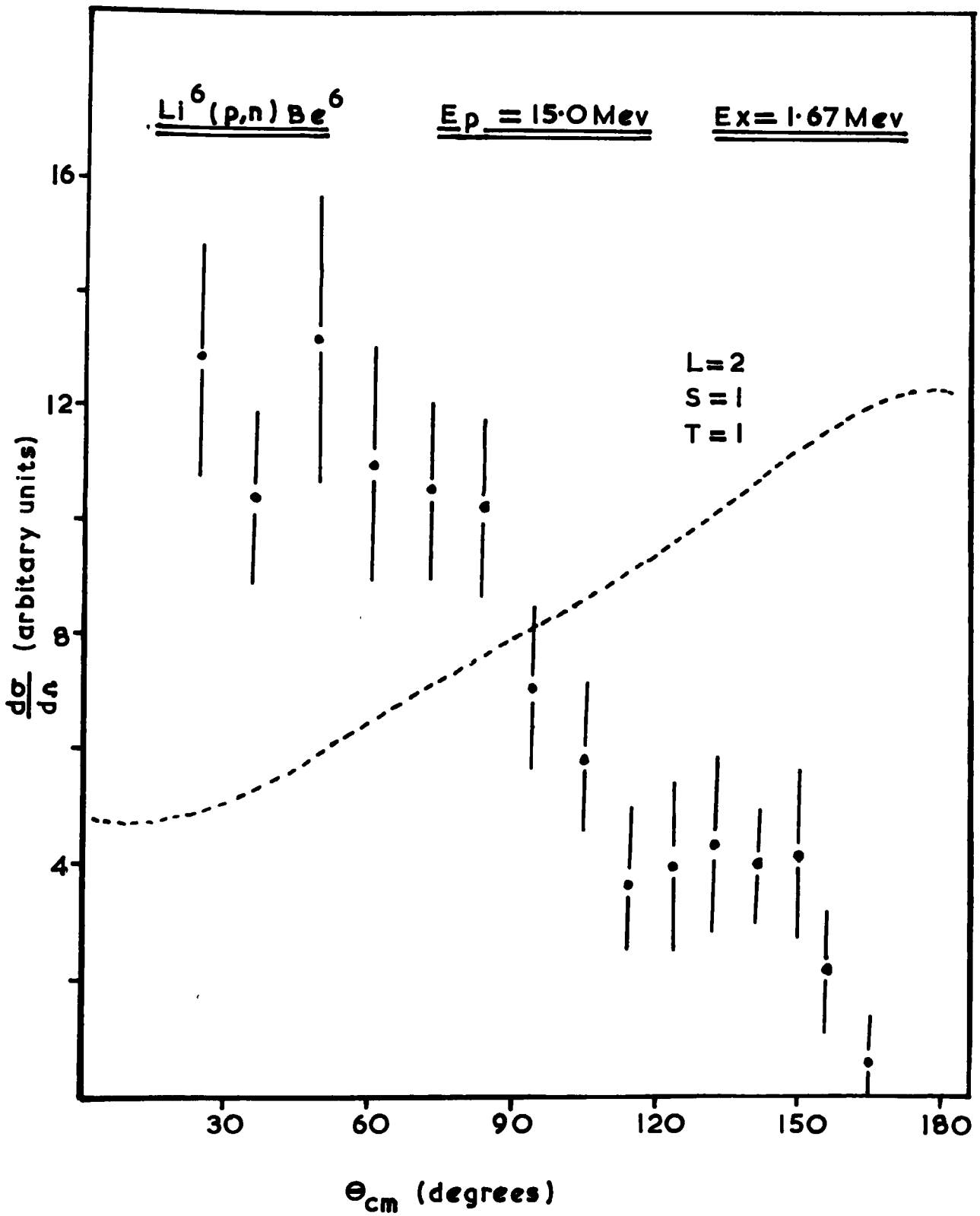
Li⁶(p,n)Be⁶
Ep = 15·0 Mev
Ex = 1·67 Mev
L = 2
S = 1
T = 1
16
12
8
4
dσ/dΩ (arbitary units)
30
60
90
120
150
180
θcm (degrees)

the ground state angular distributions exhibit oscillatory behaviour while the first excited state shows little structure, but they both have the opposite phase to that predicted. In view of this no definite conclusions can be drawn from these results about the spins of the Be^6 states. All that can be said is that either the D.W.B.A. is not valid for a target as light as Li^6, or else the reaction mechanism is not one that can be described as charge exchange inelastic scattering. A second type of direct reaction mechanism which can be used to describe (p,n) reactions is a "knock-out" process. However, we have no predictions from this model with which to compare our experimental data.

Summary

This experiment has verified the existence of an excited state in Be^6 at an excitation of 1.67 ± 0.05 MeV and its width has been found to be 1.18 ± 0.07 MeV. This state is only weakly excited by the $Li^6(p,n)Be^6$ reaction for bombarding energies below 11 MeV, but at 15 MeV and above it is excited more strongly than the ground state. There is also evidence for a second excited state at an excitation of about 3 MeV. If this state exists it is not as broad as the 1.67 MeV state and is only excited with reasonable

strength at angles near 90°.

The angular distributions of the ground state neutrons measured for incident energies below 11 MeV are independent of energy. They can be well represented by a series of the first three Legendre polynomials and as a result they have been interpreted in terms of compound nucleus theory. On the basis of this we have concluded that for incident energies below 11 MeV the reaction proceeds through two interfering states in Be^{7} at about 10 MeV excitation with spins of $\frac{1}{2}^{+}$ and $3/2^{-}$.

For energies above 15 MeV the angular distributions cannot be interpreted so simply. The first six Legendre polynomials are required to fit the experimental points for the ground state. These angular distributions are quite different in shape from the lower energy ones. The angular distribution for the first excited state differs considerably from that of the ground state suggesting that the spins of the two states are different. The experimental data was compared with the predictions of a direct interaction theory which assumed that the reaction mechanism was one of charge exchange inelastic scattering, but no agreement was found.

Our results have also shown that the $Li^{6}(p,n)Be^{6}$ reaction has to compete strongly with multiple break-up

reactions. A comparison between experiment and pure phase space calculations has shown that the most probable break up reaction is

$$Li^6 + p \rightarrow He^4 + p + p + n \qquad (1)$$

Below 11 MeV there is a small contribution from the reaction

$$Li^6 + p \rightarrow Li^5 + p + n \qquad (2)$$

but at 15 MeV and above the break up appears to be entirely via mode (1). At no energy was there evidence for di-proton emission.

C H A P T E R IV

THE DECAY OF Be^9 AND Li^9

Introduction

There has recently been interest in the mode of decay of the mass 9 nuclei, and in particular the decay of the 2.43 MeV level in Be^9 and of its analogue at 2.34 MeV in B^9 (Wi 66; Ch 66). The question asked is "to what extent is the configuration $(1s)^4(1p)^{n-4}$ an adequate description of the low lying states of nuclei in the 1p shell, and are mixtures of other configurations such as $(1s)^4(1p)^{n-5}(1f)$ and $(1s)^3(1p)^{n-4}(2s)$ necessary to get a realistic description of these states". Shell mouel calculations have been performed in terms of the basic configuration $(1s)^4(1p)^{n-4}$ [see for example Ba 66; Go 65] and these have had considerable success in predicting level spacings, spins, parities, β decay matrix elements, magnetic moments and E1 transition rates for the low lying nuclear states in the 1p shell. This is therefore a good indication that the basic configuration makes up the bulk of the wavefunctions. However the measured quadrupole moments and E2 transition rates are frequently much larger than those predicted by the same shell

model wavefunctions implying that there is a sufficient mixture of other configurations to affect these nuclear properties.

Such a situation occurs with the state in Be^9 at 2.43 MeV or with its analogue in B^9 at 2.34 MeV. Its properties are well described by the shell model. It is predicted to lie at an excitation of 2.4 MeV, its M1 radiative width is (0.12 ± 0.02) eV compared to the calculated value of 0.06 eV, and the log. ft value for the beta decay of Li^9 to the 2.43 MeV state of Be^9 is 4.7 ± 0.2 compared to the predicted value of 5.0 (Wi 66). However its E2 transition rate to the ground state is extremely strong, thus implying that configuration mixing is present. Energetically this state can decay in the following ways.

$$Be^9(2.43\ MeV) \rightarrow Be^8(g.s.) + n \rightarrow 2\alpha + n \qquad 1)$$
$$\rightarrow Be^8(2^+) + n \rightarrow 2\alpha + n \qquad 2)$$
$$\rightarrow He^5 + \alpha \rightarrow 2\alpha + n \qquad 3)$$
$$\rightarrow Be^9(g.s.) + \gamma \qquad 4)$$

Although it lies below the nominal energies of $Be^8(2^+) + n$ and $He^5 + \alpha$, it can still decay via modes 2) and 3) since $Be^8(2^+)$ and He^5 are broad states. The spin and parity of

$Be^9(2.43)$ is $5/2^-$ and so decay by mode 1) requires emission of an $\ell = 3$ neutron. Therefore by looking for the decay of this state via mode 1), one can discover whether the wave function of this state contains an admixture of the configuration $(1s)^4(1p)^4(1f)$ and if such an admixture is found to exist, then a measurement of the branching ratio for decay mode 1) will determine the amount of the admixture in the wavefunction.

The neutron decay of the 2.43 MeV level in Be^9 to the ground state of Be^8 has been observed by Christensen and Cocke (Ch 66), while the proton decay of the mirror state in B^9 to the ground state of Be^8 has been investigated by Wilkinson, Sample and Alburger (Wi 66). Using the reaction $Li^7(He^3,p)Be^9$ Christensen populated the low lying states in Be^9 and then looked for neutrons from the decay of these states. Their method was to look for coincidences between protons and neutrons and to measure the neutron energies by the associated particle time of flight technique. By setting windows on different parts of the proton spectrum they were able to investigate the mode of decay of the low lying, neutron unbound states in Be^9. Their results showed that the majority of the decays of the 2.43 MeV state were via modes 2) and 3), but in addition (7.5 ± 1.5) per cent of

the decays were indeed by $\ell = 3$ neutron emission to the Be^8 ground state. This indicated an admixture of the configuration $(1s)^4(1p)^4(1f)$ in the wave function of (2.1 ± 0.6) per cent. On the other hand Wilkinson in his study of the mirror decay, populating B^9 by the reaction $B^{10}(He^3,\alpha)B^9$ failed to observe any proton decays from the 2.34 MeV level to the Be^8 ground state. He concluded therefore that the 2.34 MeV state in B^9 decays by less than 0.5 per cent by this mode, which puts an upper limit on the percentage admixture of the configuration $(1s)^4(1p)^4(1f)$ of 0.55 per cent.

A difficulty common to both these experiments is the possible confusion of the real Be^8 ground state decays of the $5/2^-$ state with the Be^8 ground state decays of the nearby broad $5/2^+$ state at 3.03 MeV in Be^9 and 2.03 MeV in B^9. In fact the main mode of decay of the $5/2^+$ state is by nucleon decay to the Be^8 ground state. One would therefore like a way of preferentially populating the $5/2^-$ state. Such a mechanism is available in the case of Be^9. This is the beta decay of Li^9 which populates chiefly the ground state and 2.43 MeV state in Be^9 (Al 63). The broad even parity state at 3.03 MeV will not be populated significantly in this way since it would be a forbidden transition. A neutron time

of flight experiment in which neutrons are looked for in coincidence with beta particles could then be used to observe the required decay mode free from contamination by the even parity state. Also one would hope to be able to sort out the ground state decays of the 2.43 MeV state from the continuum of neutrons which will arise from decay modes 2) and 3).

An interesting feature of the A = 9 level scheme is the non-appearance so far of the $J^{\pi} = \frac{1}{2}^-$ state predicted to lie in the region of the $5/2^-$ state (Co 65; Er 64; Ba 66). It is predicted as having the same log. ft value for population by the Li^9 decay as the $J^{\pi} = 5/2^-$ state. This state could be responsible for the observation of beta transitions to the region above the $5/2^-$ level (Al 63). The $\frac{1}{2}^-$ level could well be broad since it would be able to decay to the ground state of Be^8 by $l = 1$ neutron emission and this could well have inhibited its discovery especially with the proximity of the broad $5/2^+$ level. In addition the shell model calculations of Eramjian (Er 64) and Barker (Ba 66) predict a level in the region of 4.4 MeV excitation with spin $3/2^-$ which should have a log. ft value for population by the beta decay of Li^9 comparable with that for the $5/2^-$ level. A neutron time of flight experiment might also prove useful

in detecting these higher states. Delayed neutrons have been observed from Li^9 (Al 63; Se 65) but they were not studied by time of flight, and in neither case were precise energy measurements possible. Alburger used a plastic scintillator to detect the neutrons and based his deductions on the shape of the proton recoil spectrum, while Schönebarg used as a neutron detector a Li^6 I crystal, which has only modest energy discriminating properties. Both however did observe neutrons which they attribute to the decay of the 2.43 MeV state in Be^9. In addition Alburger detected neutrons up to a maximum energy of between 3 and 4.5 MeV.

In order to clarify the situation we have performed the necessary time of flight experiment. Li^9 was formed by means of the reaction $Li^7(t,p)Li^9$. The formation of an excited state in Be^9 by the beta decay of Li^9 was signalled by the detection of a beta particle and a neutron in coincidence. The neutron energies were measured by the associated particle time of flight technique, the associated particle in this instance being the beta particle.

Experimental Procedure

Li^9 was produced by means of the reaction $Li^7(t,p)Li^9$. A piece of Li^7 metal 2 cms. square and 0.5 mm. thick was

bombarded with 7 MeV tritons from the A.W.R.E. Aldermaston tandem accelerator. A rotating shutter placed between the accelerator and the target allowed the target to be irradiated for a period of approximately 1 sec., and then interrupted the beam for 1 sec. Thus during the "beam on" period, which is about six lifetimes of Li^9 ($t_{\frac{1}{2}}$ = 169 m sec.) Li^9 was produced and in the "beam off" period the subsequent decay of Li^9 was studied by looking for beta-neutron coincidences. The highest energy beta particle expected from the decay of Li^9 is 13.5 MeV, and the beta detector was chosen so as to be able to stop the highest energy beta particle from Li^9. The detector was therefore a block of plastic scintillator Nel02, supplied by Nuclear Enterprises Limited, Edinburgh, 9 inches square and 3 inches thick. It was placed $\frac{1}{2}$ inch from the target at an angle of 45° to the beam direction [see Fig. 4.1]. With this arrangement the detector subtended a solid angle at the target of approximately 2π. Coupled to this scintillator by means of a light pipe was a 56AVP photomultiplier wired so as to give a fast timing pulse from its anode and a linear pulse from its eleventh dynode. The resistor chain used for this photomultiplier was the same as that used for the XP 1040 [Fig 2.7]. The neutron detector was the one described previously in Chapter 2,

except that pulse shape discrimination against gamma rays was not used. The reason for this was that it was necessary to operate the detector with a bias of below 100 keV in order to detect efficiently the neutrons from the decay of the 2.43 MeV State in Be^9, which should have an energy of 680 keV, and with this low bias the P.S.D. technique we have used is not very efficient. The bias was set by requiring that the detector should record the 60 keV gamma rays from an Am^{241} source. The gain of the detector's amplifier was then increased still further by a factor of two in order to make the bias as low as possible, without getting too far into noise, and to thus ensure that the efficiency of the detector for neutrons between 0.5 MeV and 3 MeV was approximately constant, since we were not able to calibrate the detector during this experiment. It was also checked that all the light pulses which triggered the linear signal discriminator also triggered the fast signal discriminator. There was one further modification to the neutron detector and also to the beta detector. In order that the photomultipliers and associated electronics should not be overloaded during the period that the beam was on the target, it was arranged that the photomultipliers were gated out during the beam on period. This could not be done by simply switching the EHT

to the tubes off and on because of the relatively long recovery time of the tubes (approx. 0.5 sec.). Neither could it be done by grounding the first dynode of the tube during the beam on period for the same reason. It was found out however that if the first and second dynodes were shorted together during the beam on period, the gain of the photomultipliers was reduced to such an extent that as far as the subsequent electronics was concerned the tube was switched off. When the short circuit was broken the tubes recovered within 1 μsec. A microswitch connected to the drive motor of the rotating shutter operated relays which made and broke the short circuit between the first and second dynodes of the photomultipliers. Another microswitch also operated a relay which switched on the recording equipment during the beam off period. The beam interrupter was driven by a 32 r.p.m. electric motor and was placed immediately after the analysing magnet of the tandem. The target room was shielded from background caused by the beam striking the interrupter by a thick concrete wall.

The experimental layout of the target and detectors is shown in Fig. (4.1). The beta detector and target was enclosed in a light tight thin walled brass target chamber. A quartz viewer could be placed in the target position and could be observed through a port-hole in the side of the

FIG 4·1

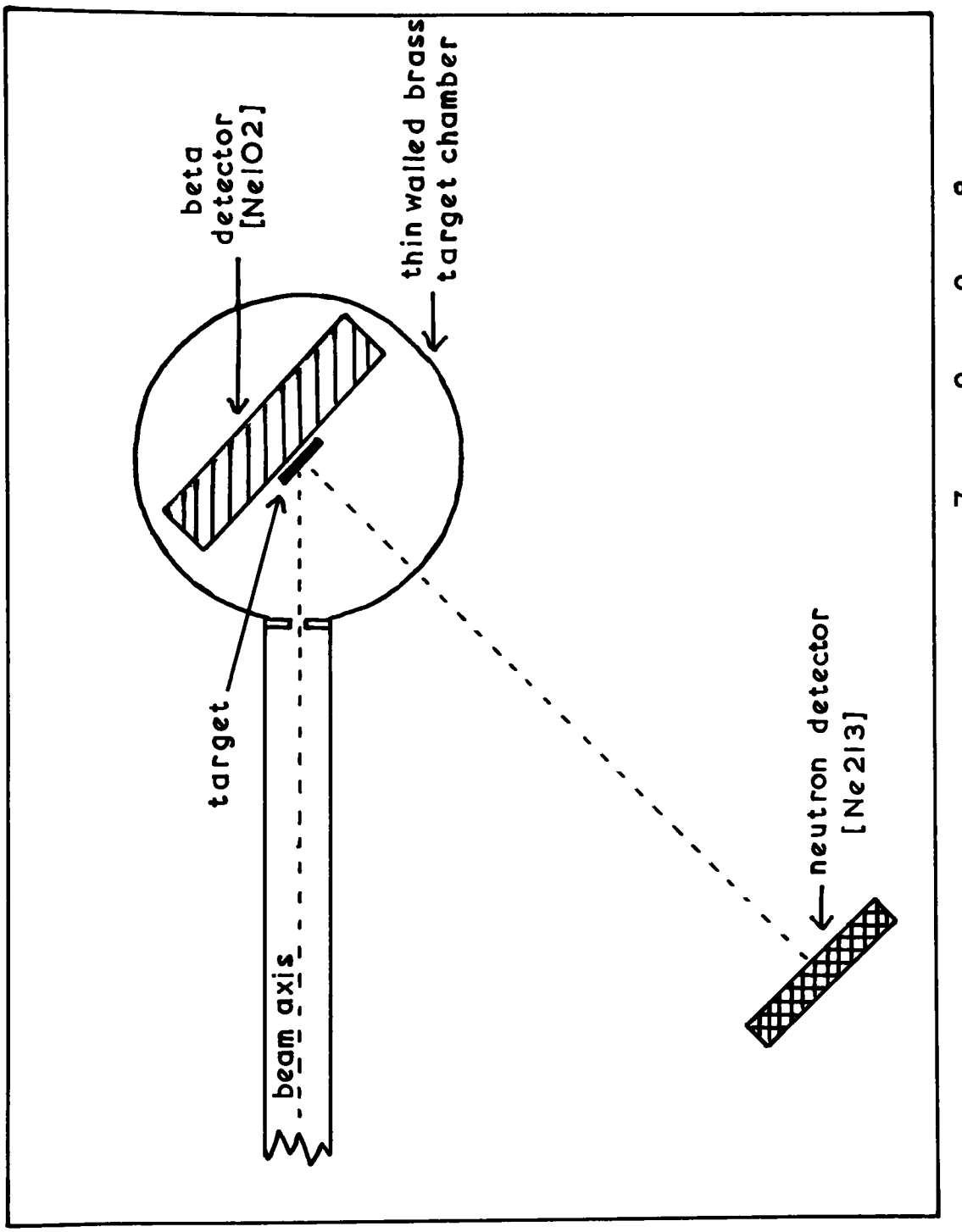

EXPERIMENTAL LAYOUT FOR $Li^{7}(t,p)Li^{9}(\beta)Be^{9}(n)Be^{8}$ REACTION

target chamber. This port-hole was of course covered up before the EHT of the beta counter's phototube was switched on. The quartz viewer was used to make sure that the beam from the accelerator was striking the centre of the target. For this alignment check a 2 MeV proton beam was used and so the viewer could be observed directly. The angular position of the neutron detector for this experiment is irrelevant. Since we are only making measurements during the beam off period there can be no angular correlation between the direction of emission of a neutron and the direction of the incident beam, and any angular correlation that might exist between the direction of emission of a beta particle and that of the associated neutron is lost since we are detecting betas emitted into a solid angle of 2π. For convenience the neutron detector was placed so that it was in line with the target and the centre of the beta counter.

The neutron energies were measured by their time of flight using the associated particle technique, the associated particles being the betas. This technique has been described in Chapter 2. In order to keep the counting rate in the beta channel down to a reasonable level the bias on the beta counter was set on the Compton edge for the 0.51 MeV annihilation gamma rays. This reduced the number of pulses caused by positron activity, induced in the target chiefly

by the impurity reaction $O^{16}(t,n)F^{18}$. In order that the random coincidence rate was not excessive the beam from the accelerator was limited to 10 n.a. Flight paths for the neutrons varying between 60 cms. and 116 cms. were used and time of flight spectra were recorded at each flight path for several hours. The time spectrum was calibrated by introducing known lengths of delay cable into the stop channel and observing the shift of the gamma-gamma coincidence peak. The calibration was found to be 1.28 n.sec. per channel. From the position of the gamma-gamma coincidence peak we could also determine the position of the time zero on the spectrum by making allowance for the known flight time of gamma rays from the target to the detector; i.e., 3.3 n.sec. per metre.

Results

Time of flight spectra recorded with flight paths of 80 cms. and 116 cms. are shown in Figs. (4.2) and (4.3). Clearly visible is an intense peak due to gamma-gamma and beta-gamma coincidences. This peak conveniently fixes the time zero for the spectra. Also visible is a sharp neutron group with an energy of 720 keV, a broad group or groups of neutrons with energies between 1 MeV and 4 MeV, and a

FIG 4.2

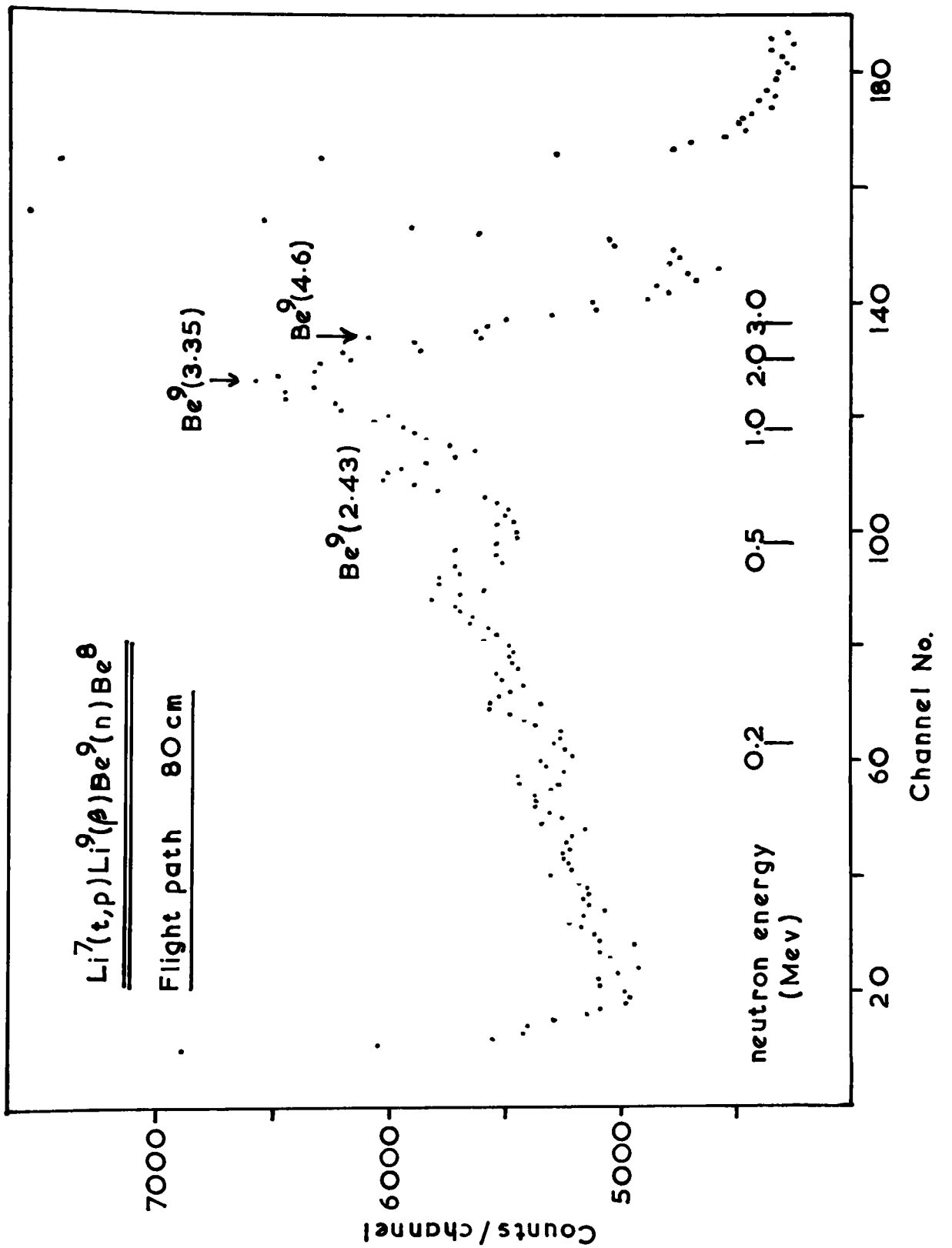
$Li^7(t,p)Li^9(\beta)Be^9(n)Be^8$
Flight path 80 cm
$Be^9(3.35)$
$Be^9(4.6)$
$Be^9(2.43)$
neutron energy (Mev)
0.2
0.5
1.0
2.0
3.0
Counts / channel
7000
6000
5000
20
60
100
140
180
Channel No.

FIG 4·3

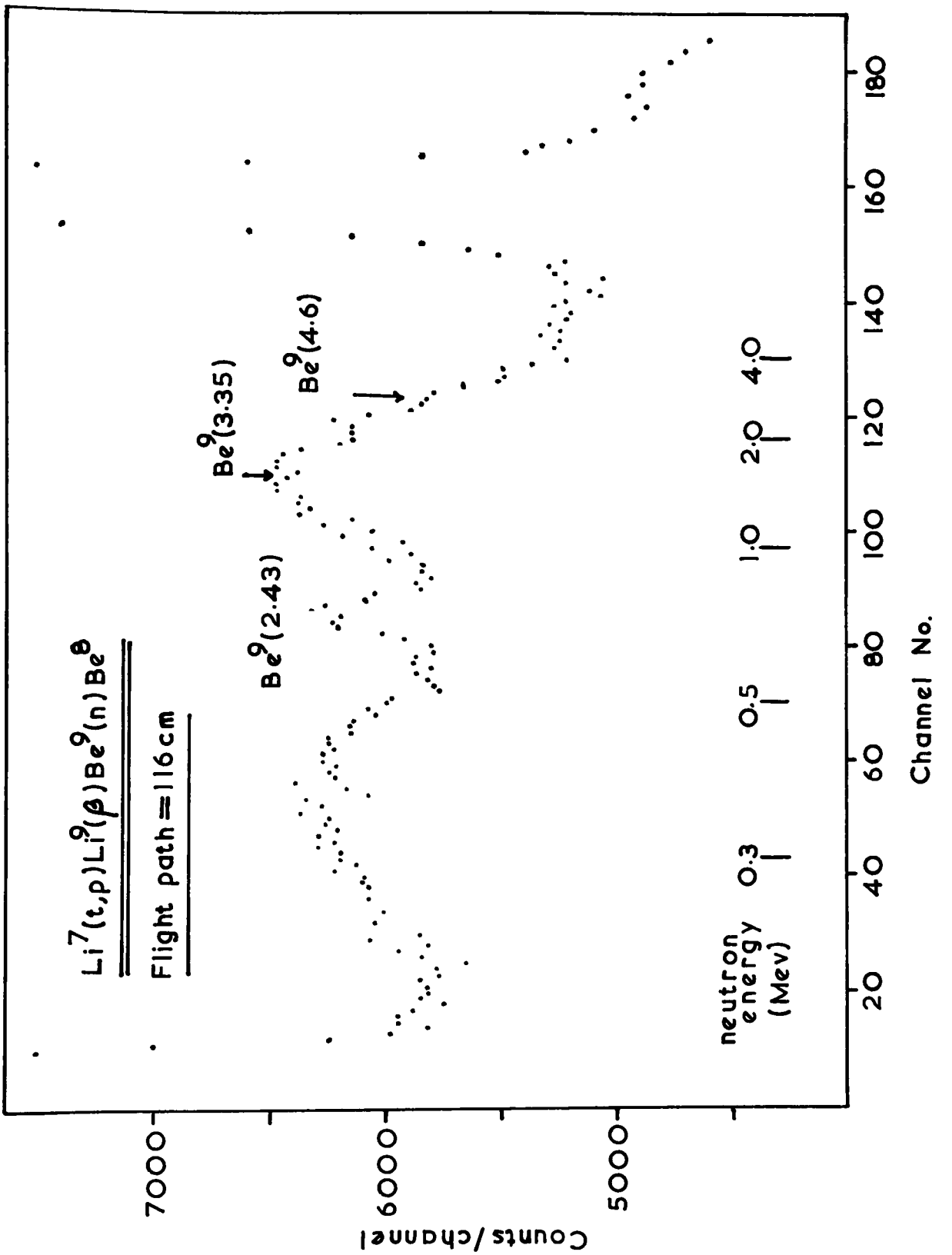
$Li^7(t,p)Li^9(\beta)Be^9(n)Be^8$
Flight path = 116 cm
$Be^9(2.43)$
$Be^9(3.35)$
$Be^9(4.6)$
neutron energy (Mev)
0.3
0.5
1.0
2.0
4.0
Counts/channel
7000
6000
5000
20
40
60
80
100
120
140
160
180
Channel No.

distribution of low energy neutrons ranging from about 500 keV down to below 200 keV. The enormous background underneath the spectra arises solely from random coincidences between the two detectors. The magnitude of this background is consistent with the counting rate in the two channels and a resolving time of 250 n.sec. The resolving time of 250 n.sec. is set by the range of the time to pulse height converter. The time sorter will only produce an output pulse if it receives a stop pulse within 250 n.sec. of receiving a start pulse.

We can immediately identify the sharp neutron group at 720 keV with the neutrons from the decay of the 2.43 MeV state of Be^9 to the ground state of Be^8 which are estimated to have an energy of 680 keV. The continuum of neutrons presumably arises from the decay of Be^{9*} to the broad first excited state in Be^8 and also from the sequential decay mode $Be^{9*} \rightarrow He^4 + He^5 \rightarrow He^4 + He^4 + n$.

Both spectra are consistent with the existence of a broad neutron group with a mean energy of 1.5 MeV and a width of 1.0 MeV together with one or more groups. In Fig. (4.4a) we show the result of subtracting from the 116 cm. spectrum an estimate of the random background and the low energy neutron continuum. We also show in Fig. (4.4a) a Breit-Wigner fit to the broad group for a neutron group with

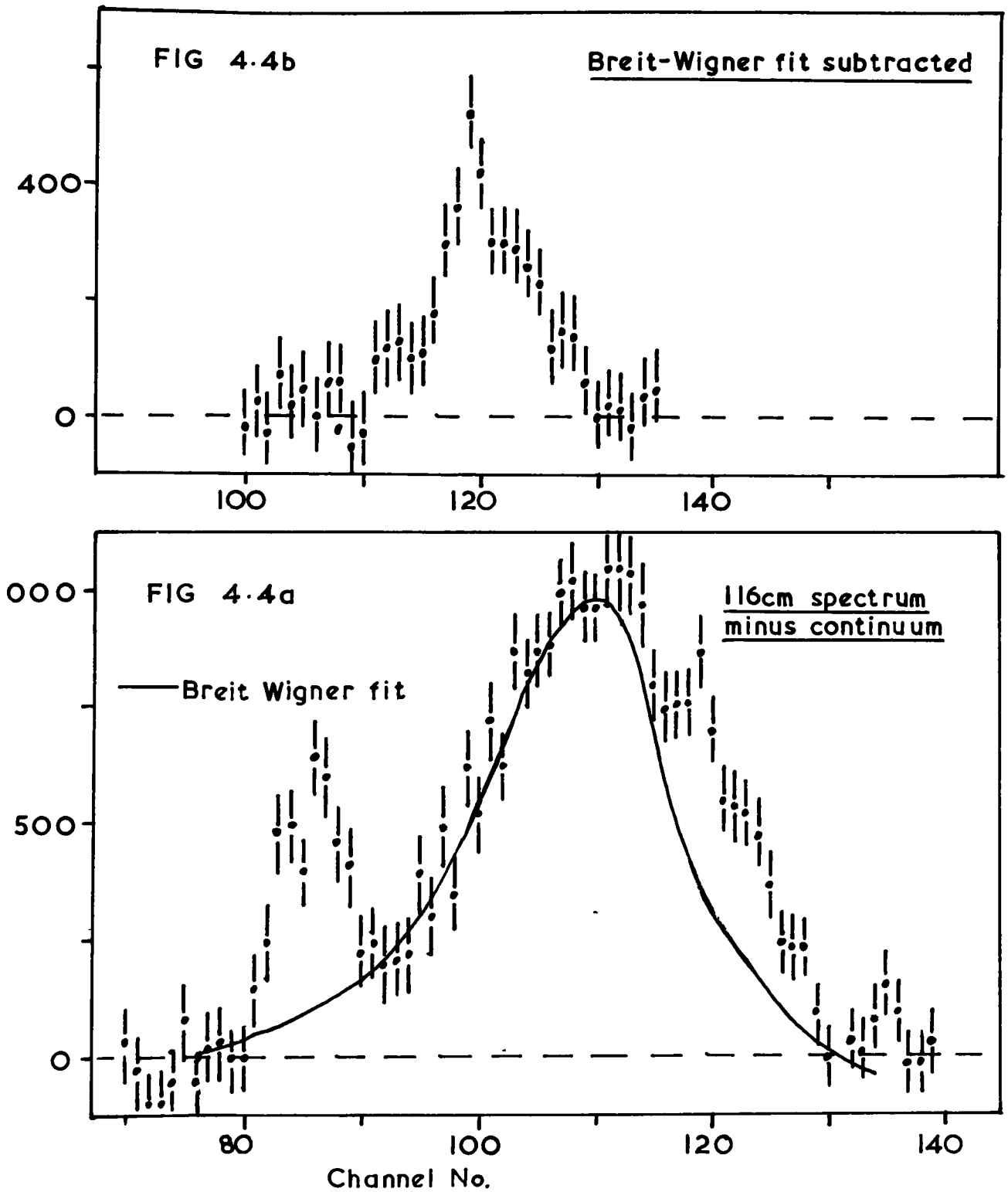
FIG 4·4b
Breit-Wigner fit subtracted
400
0
100
120
140

000
FIG 4·4a
116cm spectrum
minus continuum
Breit Wigner fit
500
0
80
100
120
140
Channel No.

an energy of 1.5 MeV and a width of 1.0 MeV. This clearly shows the existence of a higher energy neutron group. Figure (4.4b) shows the result of subtracting the Breit-Wigner fit from Fig. (4.4a), and this indicates the existence of a neutron group with an energy of 2.6 MeV and a width of approximately 1 MeV. The 80 cm. spectrum is not inconsistent with this interpretation. Assuming that these neutron groups arise from the decay of excited states in Be^9 to the ground state of Be^8, the excitation energy of these states in Be^9 would be 3.35 ± 0.10 MeV and 4.6 ± 0.2 MeV.

These delayed neutrons which we have observed can only have come from the decay of Be^9. They cannot be explained as arising from triton induced reactions on possible impurities in the target such as O^{16}, N^{14} and C^{12}, nor can they be explained as coming from other reactions induced by tritons on Li^7. Most of the reactions energetically possible form final nuclei which are stable against beta decay, and the few beta emitters which can be formed, other than Li^9, such as Li^8, He^6 and F^{18} all decay into nuclei which are stable against neutron decay. Li^9 is the only one which can be formed which beta decays into a neutron unstable final nucleus. In view of this the only possible source of the neutrons which we have observed is from the decay of excited

states in Be^9 populated by the beta decay of Li^9. A measurement of the lifetime of the beta emitter producing each of these groups would settle the matter but unfortunately we were unable to make such a measurement.

Discussion

The results of this experiment clearly show that the decay scheme of Li^9 is not as simple as that proposed by Alburger (Al 63), namely that the beta decay is to the ground state and to the 2.43 MeV state in Be^9. The existence of decays to the state at 2.43 MeV is confirmed, but in addition the beta decay is found to populate higher excited states of Be^9. These states are at excitations of 3.35 ± 0.10 MeV and at 4.6 ± 0.2 MeV, and have not previously been observed. The widths of these states are 1.0 ± 0.2 MeV and approximately 1 MeV respectively.

The observation of neutrons from the ground state decays of the 2.43 MeV state is in agreement with the work of Christensen and Cocke. We are however unable to make an estimate of the branching ratio for the decay of this state by neutron emission to the ground state of Be^9 since such a measurement requires the knowledge of the absolute efficiencies of the neutron and beta detectors, and also

we do not know what fraction of the counts recorded by the beta counter was due to beta particles from Li^9, in particular those populating the 2.43 MeV level of Be^9.

Our results are in conflict with those of Schöneberg (Sc 65). We have found ground state decays from excited states in Be^9 above 2.43 MeV while Schöneberg found no such decays. It seems likely, though, that he could easily have missed detecting these neutrons. He used a Li^6 I crystal to measure the energies of his neutrons and since even a monoenergetic neutron group does not produce a sharp peak in the spectrum from such a crystal, the spectrum of two broad neutron groups representing energies between about 1 MeV and 4 MeV would be spread over many channels thus making the observation of such states above the background difficult. In our spectra, because of the relation between energy and time of flight, these higher energy neutrons are compressed into a small region on the spectrum with the result that the intensity of these groups relative to the background is enhanced. To get an idea of what would happen to our spectra if they were recorded on a linear scale compare Figs. (4.2) and (4.3). Although both spectra are still on a time scale one can see the effect of spreading out the broad groups. The longer flight path used to obtain the spectrum shown

in Fig. (4.3) has caused the broad neutron groups to spread out while the monoenergetic group has remained sharp. But one can see that the apparent relative intensity of the broad groups to the sharp group has dropped considerably. If therefore the spectra had been recorded on a linear scale, as in the case of the spectrum from a Li^6 I crystal, then it is quite possible that these neutrons would be lost in the background. All that Schöneberg did see was a continuum of neutrons with a high energy end point of 760 keV which he attributed to the decay of the 2.43 MeV level into $He^4 + He^4 + n$. He was unable to see the decays of this state to the ground state of Be^8.

Our results do however confirm the suspicions of Alburger who found inconclusive evidence for neutron decays from states in Be^9 above 2.43 MeV. He did see neutrons with energies up to between 3 and 4.5 MeV, though the intensity of these neutrons was much less than those from the decay of the 2.43 MeV state. In the light of our present results these observations can be understood. We have observed neutrons with energies up to about 4 MeV, but these came from the decays of two broad states. The neutron spectrum which Alburger obtained was a proton recoil spectrum. In such a spectrum even a monoenergetic neutron group will

produce a continuous proton recoil spectrum, but it will have a fairly well defined end point which determines the neutron energy. The neutrons from a broad state will also produce a continuous proton recoil spectrum, but in this case the end point will not be well defined. Also since the neutrons from the broad states in Be^9 are more energetic than those from the 2.43 MeV state their proton recoil spectrum will be spread over a much larger portion of the entire spectrum thus making their observation even more difficult. Alburger quotes a ratio of the intensity of these higher neutrons to that of the lower group of 5 to 10 per cent, but he does not seem to have taken account of possible decays into 2α + n, which for the 2.43 MeV state would produce a continuum with an end point of about 760 keV, and as we have seen a large number of neutrons do arise from decays via this mode.

We can readily find an explanation for the existence of the two new states which we have excited from the shell model calculations (Co 65; Er 64: Ba 66). The state at 3.35 MeV could be the $\frac{1}{2}^-$ state predicted to lie in the region of the state at 2.43 MeV, but whose actual position depends on the choice of parameters used in the calculation. The 4.6 MeV state can be identified as the $3/2^-$ state calculated

to be at an excitation of about 4.4 MeV (Er 64; Ba 66). Both states are strongly populated by the beta decay of Li^9 in agreement with the shell model predictions and they are both broad implying decay by $\ell = 1$ neutron emission (rather than $\ell = 3$) which is consistent with the spin assignments.

With the above assumptions for the spins and parities of the two new states we can obtain an estimate of the initial populations of these states by the beta decay compared to that of the 2.43 MeV, $5/2^-$ state. The $\frac{1}{2}^-$ state at 3.35 MeV can decay by $\ell = 1$ neutron emission to the ground state of Be^8. It can also decay to the broad first excited state of Be^8, but since the 3.35 MeV state is 1.2 MeV below the nominal energy of $Be^8(2^+) + n$ this mode of decay is much less probable than the ground state decay. Another decay mode is by $\ell = 2$ alpha emission to He^5. But again this mode of decay is likely to be inhibited. In fact the ratio of the penetrability (defined in the usual way as $(F^2 + G^2)^{-1}$ where F and G are the regular and irregular Coulomb functions (Bl 52)) of the d-wave alpha particle to that of the p-wave neutron emitted from the decay of the 3.35 MeV state is 0.03. The decay by p-wave neutron emission to the ground state is therefore the most likely process and we can assume

that this state decays by 100 per cent via this mode. That this is a reasonable assumption is shown by the work of Christensen and Cocke who found that the $5/2^+$ state in Be^9 at 3.03 MeV, which can decay either by $\ell = 2$ neutron emission to the Be^8 ground state or by $\ell = 1$ alpha emission to He^5, does in fact decay 100 per cent by neutron emission. The observed number of decays from the 3.35 MeV state to the Be^8 ground state for the spectrum taken at 116 cms. is 19000 ± 2500, and assuming that this state decays 100 per cent by this mode the initial population of this state by the beta decay of Li^9 is

$$(1.90 \pm 0.25) \times 10^4 \times \frac{4\pi}{\omega\eta}$$

where ω is the solid angle subtended at the target by the neutron detector, and η is the efficiency of the neutron detector. The branching ratio for ground state decays for the 3.43 MeV state is (7.5 ± 1.5) per cent (Ch 66). The number of such decays which we have observed is 4130 ± 400. Assuming the above branching ratio the initial population of this state is

$$\frac{4130}{0.075} \times \frac{4\pi}{\omega\eta} = (5.51 \pm 1.70) \times 10^4 \times \frac{4\pi}{\omega\eta}$$

We thus see that the beta decay of Li^9 to the 3.35 MeV state of Be^9 accounts for a considerable fraction of the total decays. Within the limits of the above approximations, the ratio of decays to the 3.35 MeV state to that to the 2.43 MeV state is 1 : 3. From the spectrum measured with a flight path of 80 cms. the corresponding numbers for the initial populations of the states are

$$(2.02 \pm 0.25) \times 10^4 \times \frac{4\pi}{\omega\eta} \qquad \text{for the 3.35 MeV state}$$

and

$$(6.10 \pm 1.80) \times 10^4 \times \frac{4\pi}{\omega\eta} \qquad \text{for the 2.43 MeV state.}$$

Again the ratio is 1 : 3.

From the measured width of the 3.35 MeV state we can calculate its reduced width which measures the fraction of the wavefunction which can be represented as the ground state of Be^8 plus an orbiting $\ell = 1$ neutron. The relation between the experimental width and the reduced width is

$$\theta^2_{\ell=1} = \frac{m R^2}{\hbar^2} \cdot \frac{1}{2kR\, P_{\ell=1}} \cdot \Gamma_{\ell=1}$$

where $P_{\ell=1}$ is the penetrability of $\ell = 1$ neutrons with

wave number k, R is the radius of the nucleus and m is the reduced mass. P is given by (Bl 52)

$$P_{\ell=1} = \frac{(kR)^2}{1 + (kR)^2}$$

Using the same values for R and $\frac{\hbar^2}{mR^2}$ as Christensen and Cocke, i.e.,

$$R = 4.35 \text{ fm} \quad \text{and} \quad \frac{\hbar^2}{mR^2} = 2.47 \text{ MeV}$$

and with our measured value of the width of the 3.35 MeV state, $\Gamma_{\ell=1} = 1.0 \pm 0.2$ we obtain for the reduced width

$$\theta^2_{\ell=1} = 0.34 \pm 0.07$$

We can apply the same reasoning to the state at 4.6 MeV. If we assume that the spin of this state is $3/2^-$ then it can decay to the ground state of Be^8 by $\ell = 1$ neutron emission and also to the first excited state of Be^8 by $\ell = 1$ neutron emission. This state is near to the nominal energy of $Be^8(2^+) + n$, which on an energy scale with the ground state of Be^9 as zero lies at an excitation of 4.57 MeV. The decay rate to the first state of Be^8 is now likely to be comparable with that to the ground state. The 4.6 MeV state can also

decay by $\ell = 0$ alpha emission to He^5 and this process too is likely to have an appreciable transition rate. Since we do not know the branching ratio we cannot calculate the initial population of the 4.6 MeV level. We can however obtain an estimate of the lower limit of the initial population of this state by assuming that the branching ratio to the ground state of Be^8 is 100 per cent. The number of ground state decays that we have observed is 4000 ± 1000 and so the lower limit of the population of the 4.6 MeV state by the beta decay of Li^9 is

$$(0.4 \pm 0.1) \times 10^4 \times \frac{4\pi}{\omega\eta}$$

If the branching ratio is B then the population becomes

$$(0.4 \pm 0.1) \times 10^4 \times \frac{1}{B} \times \frac{4\pi}{\omega\eta}$$

The ratio of the beta decay probability to the 4.6 MeV state, assuming it has spin $3/2^-$, to that to the 2.43 MeV state is thus seen to be at least 7 per cent.

The estimates of the above beta decay probabilities are of course made with the assumption that the neutron detector efficiency is constant over the range of neutron energies considered. We were unfortunately unable to calibrate the

detector under the conditions in which it was used during this experiment. But from a knowledge of the response of organic scintillators to fast neutrons (Ba 61) and also of previous calibrations of the detector with higher biases [see Fig. (2.10) and also Mu 66, Fig. (2.10)], it is reasonable to assume that the efficiency is constant to within 10% for neutron energies between 0.7 MeV and 3 MeV.

The decay scheme of Li^9 Fig. (4.5) is thus shown by this experiment to be not as simple as that proposed by Alburger. In addition to beta transitions to the ground state and 2.43 MeV state in Be^9, we have seen that there is a strong branch to a state in Be^9 at an excitation of 3.35 MeV and a weaker branch to a state at 4.6 MeV. Alburger does however admit that a third beta branch to a state in Be^9 above 2.43 MeV would not be inconsistent with his data but he was unable to give an estimate of the end point energy of such a branch. As we have seen, this third branch is probably the one to the 3.35 MeV state. It is however unlikely that his experiment could have detected the weak branch to the state at 4.6 MeV. Using the log. ft values calculated by Barker (Ba 66) for the beta decay to the Be^9 states $3/2^-$, $5/2^-$, $\frac{1}{2}^-$ and $3/2^{-*}$, which we have taken to be at excitations of 0.0, 2.43, 3.35 and 4.6 MeV, and using the extended nomogram for log. ft values of Verrall, Hard, and

FIG 4·5

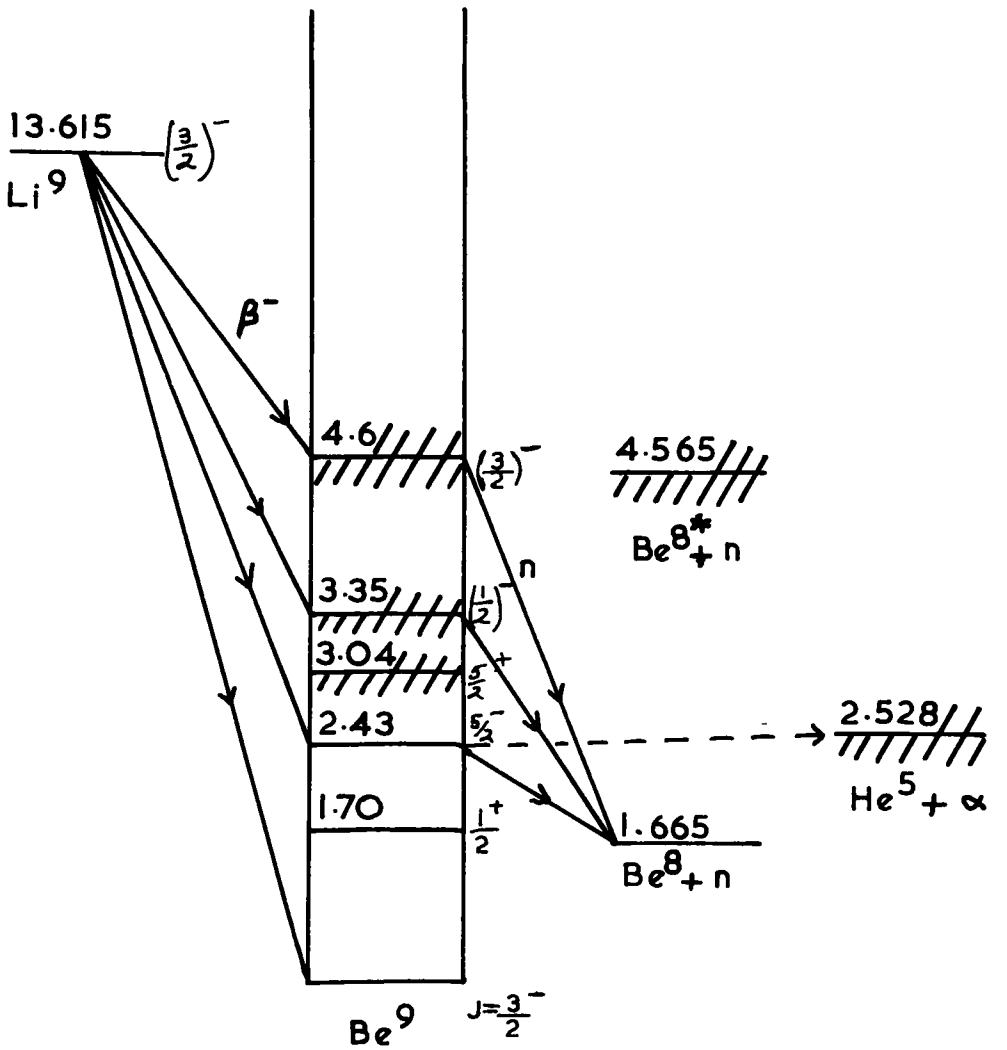

PROPOSED DECAY SCHEME OF Li^9

Bell (Ve 66) we can calculate the beta decay branching ratios to these states expected from the simple shell model. We cannot compare the experimental branching ratios directly with these calculated values since our experiment could not detect the ground state beta transitions. If we normalise our results to the calculated branching ratio for the $5/2^-$ state we can compare the predicted values with the experimental values for the three excited states. The results of these calculations are given in Table 4.1.

The value of 1.5 per cent for the 4.6 MeV state is only a lower limit on the branching ratio since no account has been taken of decays of this by modes other than neutron emission to the ground state of Be^8. However the relative branching ratios for the 2.43 and 3.35 MeV states are in good agreement with those calculated from the simple shell model. One point to notice about the calculations is that the expected branching ratio for the beta decay to the ground state is about 50 per cent whereas Alburger's estimate from experiment of this branching ratio is only (25 $\pm$ 15) per cent.

The mirror decay to the beta decay of Li^9, that is the positron decay of C^9, has been studied by Hardy et. al. (Ha 65a). In their experiment they looked for delayed protons from C^9, and found two proton groups which they

TABLE 4.1

E_x (MeV)	J^π	log(ft) (Ba 66)	$\log(f_o t)$ (Ve 66)	Branching Ratio (calc)	Branching Ratio (expt)
0.0	$3/2^-$	5.32	5.35 ± .05	(54 ± 6) %	-
2.13	$5/2^-$	5.31	4.30 ± .05	(20 ± 3) %	20%
3.35	$\frac{1}{2}^-$	5.38	4.40 ± .05	(10 ± 2) %	(7 ± 4) %
4.6	$3/2^-$	5.07	4.15 ± .10	(12 ± 3) %	> 1.5 %

interpreted as having come from the decay of a state in B^9 at 12.05 MeV to the ground state and first excited state of Be^8. They found no proton groups which could have come from low lying states in B^9. We, on the other hand, found no evidence for beta transitions from Li^9 to a state in Be^9 at 12 MeV, but this is not surprising. The available energy for such a transition is only 1.6 MeV, and even taking a log. ft value as low as 4.0 we find that the expected branching ratio is only a fraction of one per cent.

CHAPTER V

THE ANALOGUE STATE IN Cl^{33}

Introduction

The two nucleon transfer reaction (He^3,n) is an ideal mechanism for populating $T = 3/2$ states in $T_z = -\frac{1}{2}$ nuclei. The reaction can produce a change of isospin of 0 or 1 so that if a target with $T_z = +\frac{1}{2}$ is used, states in the final nucleus with $T = \frac{1}{2}$ or $3/2$ may be excited. Since the reaction may be pictured as one in which two nucleons are dropped into single particle orbits it is reasonable to expect that states in the final nucleus which have a simple shell model configuration will be strongly excited by such a reaction. In particular the state which is the analogue of the ground state of the $T_z = \frac{1}{2}$ $3/2$ member of the isobaric quartet is expected to be preferentially excited. To understand this consider the reactions (He^3,n) and (t,p) on the same target with $T_z = +\frac{1}{2}$. The first reaction will reach states with $T_z = -\frac{1}{2}$ and the second one states with $T_z = +3/2$. In shell model terms the (t,p) reaction will populate the ground state of the $T_z = +3/2$ nucleus by adding two neutrons to the target nucleus in the lowest available orbits. This state will have $T = 3/2$. The (He^3,n) reaction, being the mirror reaction will be expected to populate a state which has the same

configuration as that state populated by the (t,p) reaction except that two protons have been added instead of two neutrons. This state will not be the ground state of the $T_z = -\frac{1}{2}$ nucleus but an excited state which is the analogue of the ground state of the $T_z = 3/2$ nucleus, and as such will have total isospin $T = 3/2$.

Another property of (He^3,n) reactions which make them ideal for exciting analogue states is the large positive Q value. Analogue states in general lie at a fairly high excitation, usually above 5 MeV and so the positive Q value means that these states are easily reached with the He^3 ion energies available from electrostatic generators.

The main interest in locating the higher isospin states in light nuclei is to test the isobaric mass formula (Wi 64a; Wi 64b). If the nuclear force is charge independent and if the Coulomb force is treated as a perturbation then to first order the masses within an isobaric multiplet may be expressed

$$M = a + b T_z + c T_z^2$$

where a, b and c are constants for a given multiplet. If we know the masses of three of the members of a multiplet we can use the formula to calculate the masses of the other

members, and then compare these calculated masses with the experimentally determined ones. For example, denoting the mass of a state by ${}_{T}M_{T_z}$, we have for $T = 3/2$

$$ {}_{3/2}M_{-3/2} - {}_{3/2}M_{+3/2} = 3({}_{3/2}M_{-\frac{1}{2}} - {}_{3/2}M_{+\frac{1}{2}}) $$

Usually, however, either the mass of one of the ${}_{3/2}M_{\pm 3/2}$ states is not known accurately, or else the location of the ${}_{3/2}M_{\pm 1/2}$ states has not been found. For this reason it is desirable to locate these analogue states.

We can make an estimate of the position of the analogue states as follows. The excitation of such a state is given by

$$ E(\text{analogue}) = {}_{3/2}M_{-\frac{1}{2}} - {}_{\frac{1}{2}}M_{-\frac{1}{2}} $$

$$ = {}_{3/2}M_{+\frac{1}{2}} - {}_{\frac{1}{2}}M_{+\frac{1}{2}} $$

If we assume the nuclear force to be charge independent, then the difference in mass between the states ${}_{3/2}M_{+3/2}$ and ${}_{3/2}M_{+\frac{1}{2}}$ is just the difference in Coulomb energy between the two states plus the proton-neutron mass difference.

Hence the excitation of the analogue state is

$$E(\text{analogue}) = ({}_{3/2}M_{+3/2} - {}_{\frac{1}{2}}M_{+\frac{1}{2}}) + \Delta_{\frac{1}{2},3/2} + \delta(p,n)$$

where $\Delta_{\frac{1}{2},3/2}$ is the Coulomb energy difference between nuclei with T_z components $\frac{1}{2}$ and $3/2$, and where $\delta(p,n)$ is the proton-neutron mass difference. A semiempirical formula for Coulomb energy differences is given by Jänecke (Ja 60).

The nucleus we have chosen to study is Cl^{33} and the $T = 3/2$ state which we are looking for is the analogue of the ground state of P^{33}. The excitation of the analogue state calculated from the formula above is 5.5 MeV. The nucleus Cl^{33} can be reached by the reaction $P^{31}(He^3,n)Cl^{33}$ which has a ground state Q value of + 3.43 MeV. A state in Cl^{33} at 5.55 MeV has previously been reported by Hardy and Verrall (Ha 65) and by Poskanzer et. al. (Po 66). They both studied this nucleus by observing the delayed protons from the beta decay of Ar^{33}. From the superallowed nature of the beta decay to this state Hardy concludes that this state is the analogue of the ground state of Ar^{33} (or P^{33}). In addition, assuming that the spin of Ar^{33} is $\frac{1}{2}^+$, he assigns to the 5.55 MeV level spin and parity $\frac{1}{2}^+$. Hardy and Verrall also observed protons from a state in Cl^{33} at

7.55 MeV to which they assigned to properties T = $^3/_2$ and $J^\pi = \frac{1}{2}^+$, again basing their arguments on the small log.(ft) value for the beta decay feeding this state. This state together with several others was also seen by Poskanzer et. al. but they made no spin or isospin assignment to it.

If the nuclear force is charge independent the T = $^3/_2$ level structure in Cl^{33} should be the same as the level structure in the $T_z = {}^3/_2$ nucleus P^{33}. Shell model calculations by Glaudemans et. al. (Gl 64) have predicted that the ground state spin of P^{33} is $\frac{1}{2}^+$ and that there should be excited states at 1.37, 2.50, 3.00, 3.08 and 3.48 MeV with spins $^3/_2{}^+$, $^5/_2{}^+$, $^3/_2{}^+$, $^5/_2{}^+$ and $^3/_2{}^+$ respectively. Hardy's assignment of T = $^3/_2$, $J^\pi = \frac{1}{2}^+$ to a state in Cl^{33} at 7.55 MeV, which would be the analogue of a state in P^{33} at 2.0 MeV, does not fit in with Glaudemans' predicted level scheme. The energy level scheme of P^{33} has been determined experimentally by Currie and Evans (Cu 67) by means of the reaction $Si^{30}(\alpha,p)P^{33}$. In addition to the ground state they excited states at 1.43, 1.81 and 2.42 MeV, but made no spin determinations. The positions of the 1.43 and 2.42 MeV levels is in good agreement with Glaudemans' predicted states at 1.37 and 2.50 MeV. The 1.81 MeV level does not fit in with the calculations.

We have performed the reaction $P^{31}(He^3,n)Cl^{33}$ in order to check the isospin assignment of the 5.55 MeV state, to measure its spin, and also to investigate higher analogue states in Cl^{33}. From a measurement of the angular distribution of the neutrons from the 5.55 MeV state we should be able to make a spin and parity assignment. A state in Cl^{33} at 5.55 MeV is in a region of excitation where the level density is high and consequently one would expect a state at this energy to be only weakly excited. It is also unbound to proton decay to S^{32} and consequently would be expected to be broad. However, as we have said before, analogue states are expected to be preferentially excited by a (He^3,n) reaction and should therefore stand out strongly above the many $T = \frac{1}{2}$ levels. Also because of the isospin conservation law the proton decay of a $T = 3/2$ state will be inhibited with the result that the state will be narrow. These are some of the properties by which analogue states can be recognised. A further test would be by means of the reaction $S^{32}(d,n)Cl^{33}$. This reaction will only populate states in Cl^{33} with $T = \frac{1}{2}$. The appearance of a state in the (he^3,n) reaction and its absence in the (d,n) reaction would be a further indication of a $T = 3/2$ assignment.

Experimental Procedure

The reaction $P^{31}(He^3,n)Cl^{33}$ was performed at A.W.R.E. Aldermaston using the 6 MeV Van de Graaff accelerator. This machine is equipped with a pulsed source capable of producing pulses of charged particles of less than 2 ns. duration at a repetition rate of 5 Mc/sec. In addition the machine possesses a gas stripper enabling doubly charged helium ions to be accelerated to 10.5 MeV. For this experiment we used a pulsed beam of doubly charged He^3 ions with an energy of 9.00 MeV. The mean current reaching the target after pulsing was about 0.2 μa. Use was made of the Aldermaston time of flight spectrometer. The detector, which was a cell 5" in diameter and 2" thick containing the liquid scintillator Ne213, was placed at the end of a collimator which was on the symmetry axis of a large cylindrical tank of water [Fig. 5.1]. The completely shielded detector was suspended on a monorail which enabled it to move in a circular path round the target with a radius of about 5 metres. In front of this tank was a second tank also filled with water through the centre of which was an empty 5" diameter pipe. This tank too could be moved in a circle about the target. In this way the detector was well shielded against all neutrons except

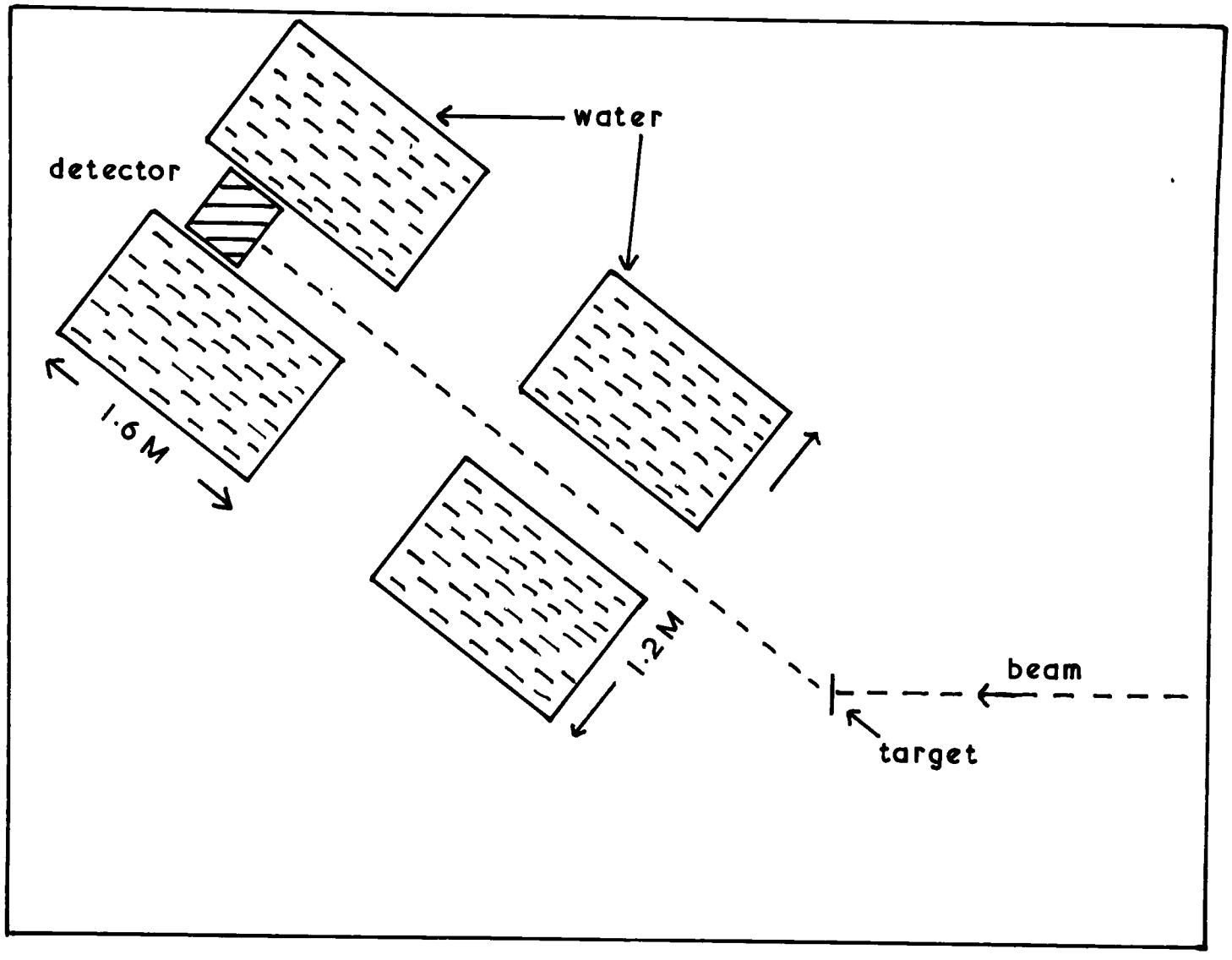

FIG 5.1

EXPERIMENTAL LAYOUT FOR $P^{31}(He^3,n)Cl^{33}$ REACTION

those arising from the target.

The stop pulse for the time sorter was derived from a pick up aerial through which the beam passed. This aerial which consists of a hollow cylinder placed just before the target, picks up a signal from the beam pulses as they pass through. The signal so derived is further amplified before being fed to a fast discriminator which produces standard pulses suitable for operating the time sorter.

The target was made by vacuum evaporation of pure red phosphorous to a thickness of 300 $\mu g/cm^2$ onto a thick tantalum backing. To avoid burning the target, the beam was made to scan a small circle over the target. A small deposit of carbon formed on the target during bombardment. A comparison with the yield from a 200 $\mu g/cm^2$ carbon target showed that the carbon build up amounted to about 7 $\mu g/cm^2$. The energy loss of a 9 MeV He^3 ion in this amount of carbon is about 3 keV. Due to the nature of the evaporation process the target also contained a small amount of oxygen as an impurity. Neither the carbon nor the oxygen impurities interfered with measurements on the analogue state, and in fact they provided very convenient calibration points for the spectra. The time calibration for the spectra was also measured by adding known lengths of delay cable into the stop channel

and observing the shift of a given peak on the spectra. The two calibrations agreed very well with each other, being 0.927 ns/channel.

Results and discussion

Time of flight spectra of the reaction $P^{31}(He^3,n)Cl^{33}$ taken at 5° and 20° with a flight path of 470 cms. are shown in Figs. (5.2) and (5.3). Neutron groups corresponding to the ground state and excited states of Cl^{33} at 0.8, 2.1, 2.85, 4.0, 5.55, 6.30 and 7.45 MeV have been identified from the reaction kinematics, together with neutron groups corresponding to the ground states of O^{14} and Ne^{18}. The ground state of Cl^{33} is not strongly excited at 5° since it is populated by an L = 2 transition. The most prominent feature of the spectra is the sharp neutron group corresponding to the state in Cl^{33} at 5.55 MeV. Using the O^{14} and Ne^{18} groups as calibration points, and allowing for the 50 keV energy loss of He^3 ions in the target, we find that the mean excitation energy of this state, obtained from all the spectra recorded, is 5.55 ± 0.02 MeV. The angular distribution of this state was measured from 0° to 80° and is shown in Fig. (5.4). The result is compared with angular distributions calculated using a version of the Hook and

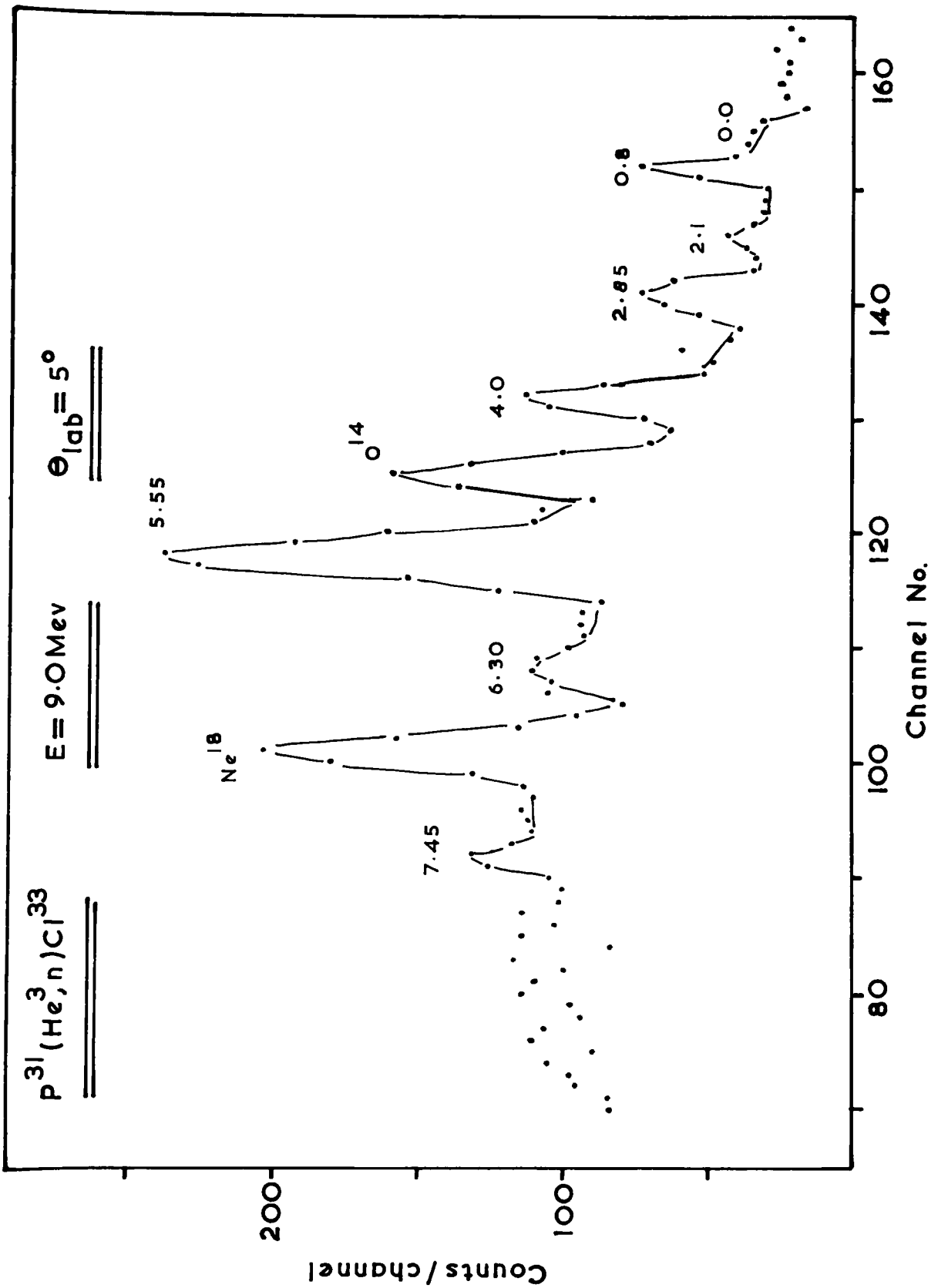
$p^{31}(He^3,n)Cl^{33}$
E = 9.0 Mev
$\theta_{lab} = 5°$
5.55
O^{14}
4.0
2.85
2.1
0.8
0.0
Ne^{18}
6.30
7.45
Counts / channel
200
100
80
100
120
140
160
Channel No.

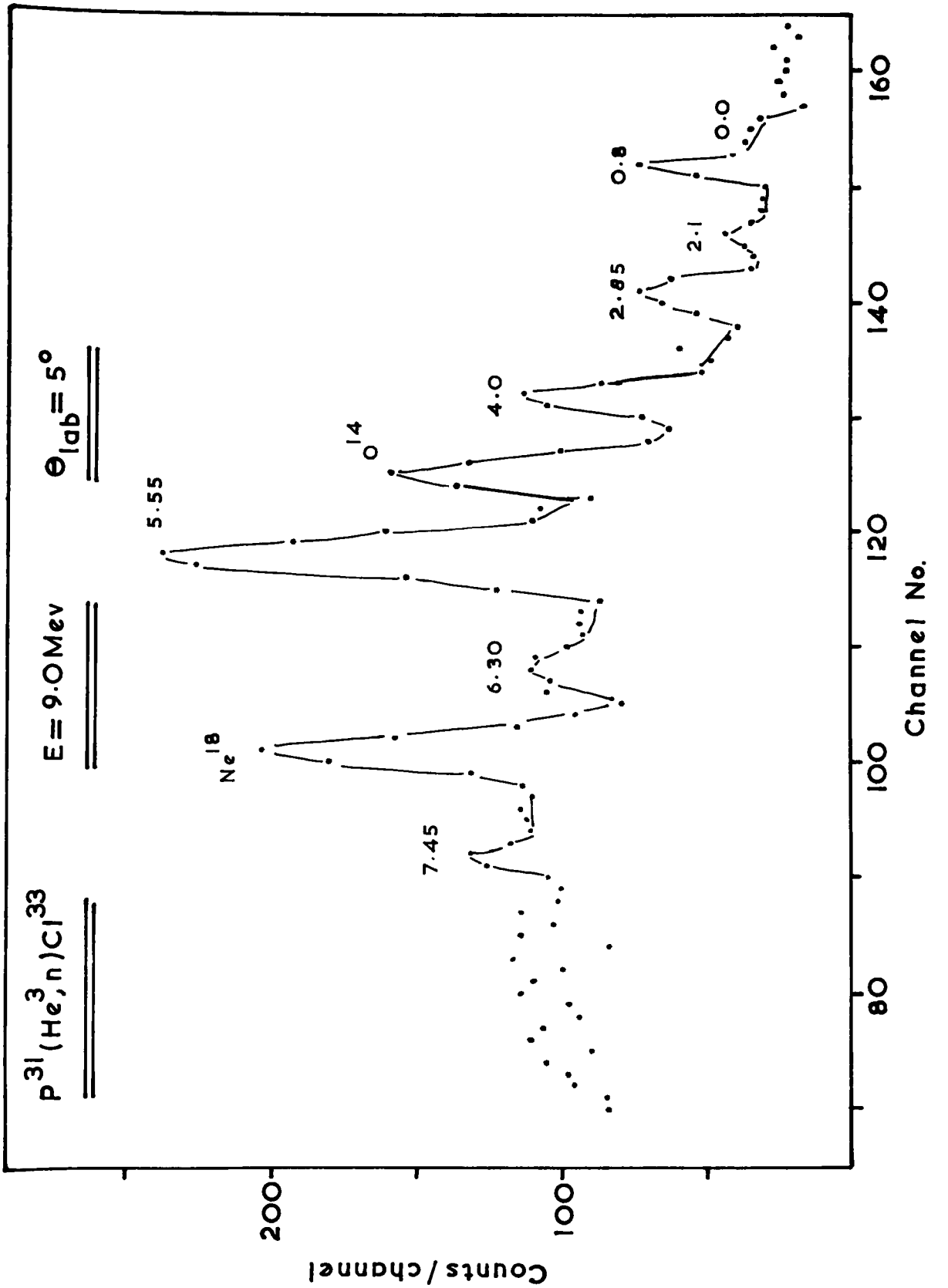
$P^{31}(He^3,n)Cl^{33}$
E = 9.0 Mev
$\theta_{lab} = 5°$
Ne^{18}
O^{14}
5.55
7.45
6.30
4.0
2.85
2.1
0.8
0.0
Counts / channel
Channel No.
100
200
80
100
120
140
160

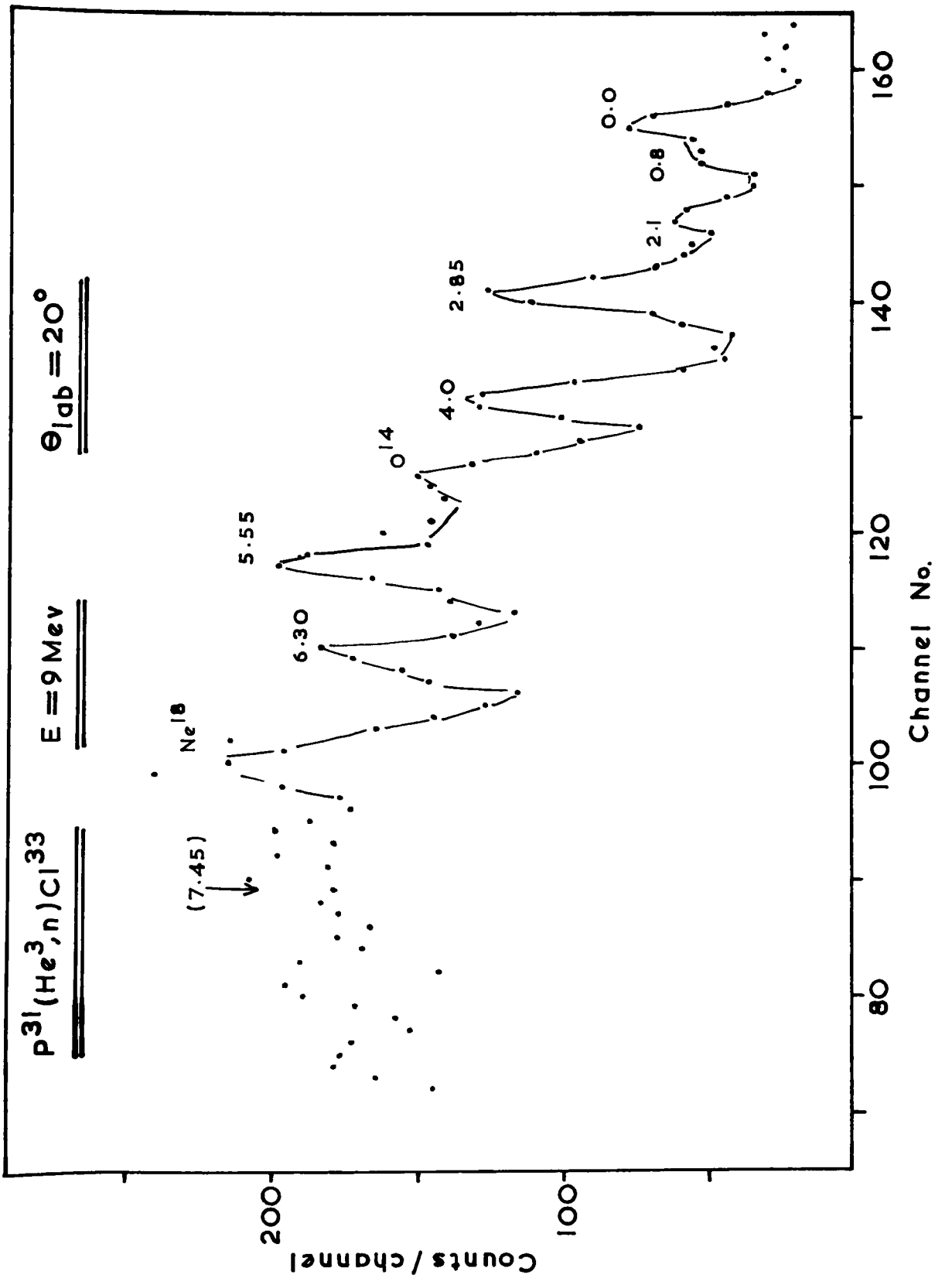
$P^{31}(He^3,n)Cl^{33}$
E = 9 Mev
$\theta_{lab} = 20°$
Ne^{18}
(7.45)
6.30
5.55
O^{14}
4.0
2.85
2.1
0.8
0.0
Counts / channel
200
100
80
100
120
140
160
Channel No.

FIG 5.4

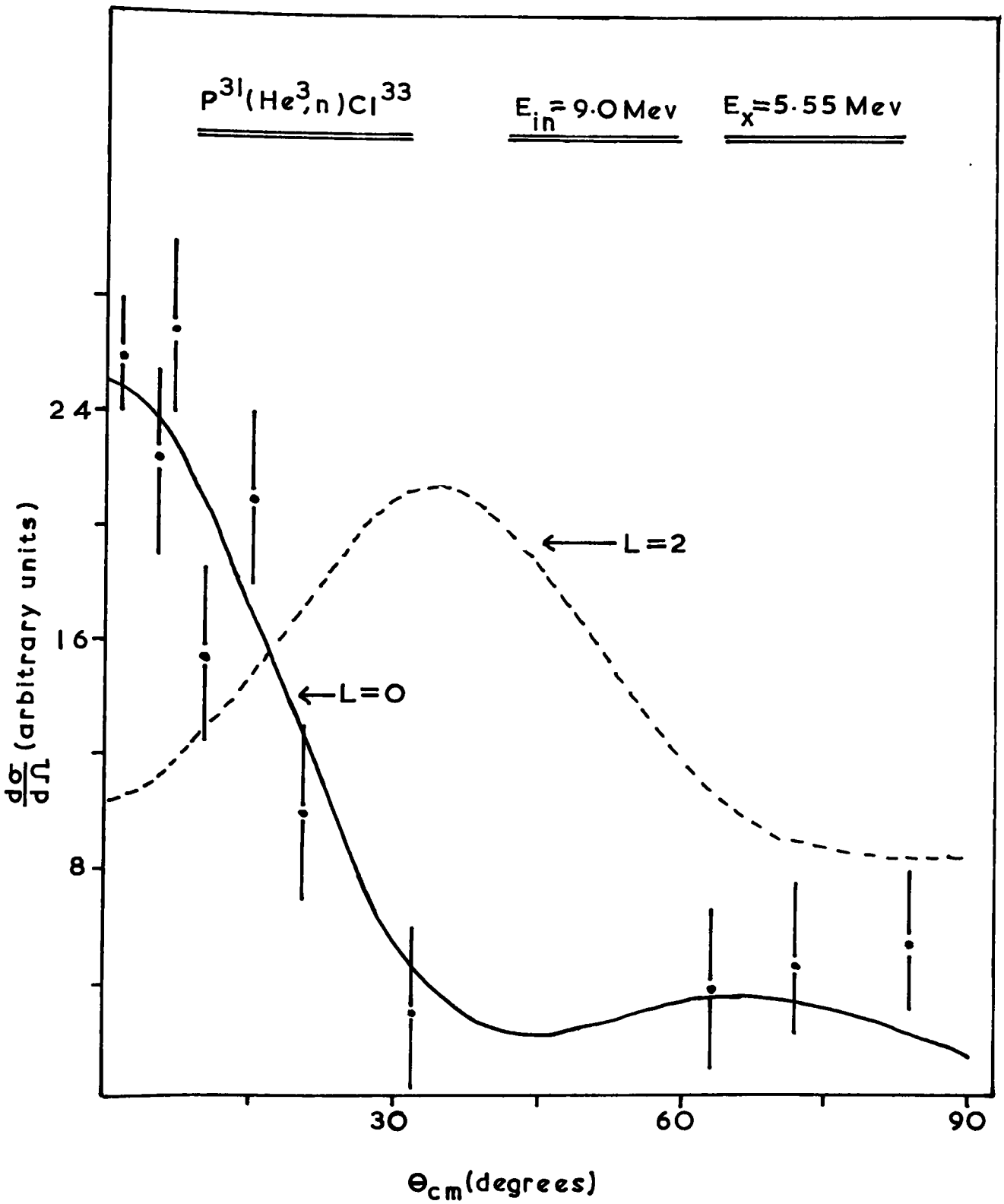
$P^{31}(He^3,n)Cl^{33}$
E_{in} = 9.0 Mev
E_x = 5.55 Mev
L=2
L=0
24
16
8
30
60
90
$\frac{d\sigma}{d\Omega}$ (arbitrary units)
θ_{cm} (degrees)

Mitra D.W.B.A. double stripping programme (Ro 64) written by Mr. M.J.L. Yates and arranged for the Atlas computer by Dr. J.C. Hardy and Dr. I.S. Towner. Figure (5.4) shows the result of calculations for L = 0 and L = 2 angular momentum transfer. The curve for L = 0 has been normalised to fit the experimental angular distribution at the peak. The experimental angular distribution clearly shows that the 5.55 MeV state is excited by an L = 0 transition. Therefore since the spin of the ground state of P^{31} is $\frac{1}{2}^+$ the spin of the 5.55 MeV state of Cl^{33} must also be $\frac{1}{2}^+$.

Of the other states in Cl^{33} excited by the reaction $P^{31}(He^3,n)Cl^{33}$ the ones of interest here are those seen at 6.30 and 7.45 MeV. These are probably the states seen in the delayed proton work of Poskanzer et. al. at 6.22 and 7.45 MeV, and by Hardy and Verrall at 7.55 MeV. As these states were populated by allowed beta transition from Ar^{33} which has the probable spin $\frac{1}{2}^+$, their spins and parities will be either $\frac{1}{2}^+$ or $3/2^+$. In our (He^3,n) work the 6.30 MeV state could be identified at every angle at which spectra were recorded, while the 7.45 MeV state was seen only at 0^o, 5^o, 10^o and possibly at 15^o and 20^o. Because of poor statistics it was not possible to obtain angular distributions for these states. Nevertheless we can make some tentative

spin assignments to them. Since the 7.45 MeV state is visible only at the very forward angles this suggests that it is being populated by an L = 0 transition. If this were so then its spin would be $\frac{1}{2}^+$. Hardy and Verrall assigned to this state the spin $\frac{1}{2}^+$ and also the isospin T = 3/2. As can be seen from Fig. (3.2) this state is sharp and so is not inconsistent with this isospin assignment. As mentioned in the introduction a T = 3/2 state at this excitation with spin $\frac{1}{2}^+$ does not fit in with Glaudemans' predictions, but it is possible that it is the analogue of the state in P^{33} seen at 1.81 MeV by Currie and Evans. Assuming the 7.45 MeV level to be a T = 3/2 state it would be the analogue of a state in P^{33} at 1.9 MeV.

We can identify the state at 6.30 MeV with the one observed by Poskanzer et. al. at 6.22 MeV. This state appeared to be more strongly excited at 20° and 30° than at 0° and 5° (compare Figs. (5.2) and (5.3)) and at 60° it was still excited with strength comparable with that at 0°. Using this argument we can tentatively say that the state is populated by an L = 2 transition. The ground state and 2.85 MeV state show a similar behaviour and these are known to be populated by L = 2 transitions since they have spins $3/2^+$ and $5/2^+$. An L = 2 transition would limit the spin of the

6.30 MeV state to $3/2^+$ or $5/2^+$, and since the state is also populated by an allowed beta transition from Ar^{33} its spin is further limited to $3/2^+$. There is no real evidence to identify this state with a T = 3/2 state except that it does appear to be strongly excited for an L = 2 transition. Its excitation (0.75 MeV in P^{33}) does not fit Glaudemans' predictions nor the experimental level structure of P^{33}.

Nevertheless we have strong evidence for the T = 3/2 nature of the 5.55 MeV state of Cl^{33}. Its excitation energy agrees well with the value calculated assuming charge independence. It is strongly excited by the reaction $P^{31}(He^3,n)Cl^{33}$. Its spin of $\frac{1}{2}^+$ is in full agreement with the value predicted by Glaudemans' calculations. A further piece of evidence comes from the reaction $S^{32}(d,n)Cl^{33}$. We performed this experiment at Oxford with deuteron energies of 8 MeV and 9 MeV using the same experimental technique as Mubarakmand (Mu 66) in his study of the low lying states of Cl^{33}. We were able to identify states in Cl^{33} below 4 MeV by this reaction but there was no strong neutron group visible above the continuum of neutrons, which is due to unresolved T = $\frac{1}{2}$ states in Cl^{33}, in the region of the spectra where the 5.55 MeV state was expected to lie (see (Fig. 5.5)). The non-appearance of the 5.55 MeV state in the $S^{32}(d,n)Cl^{33}$

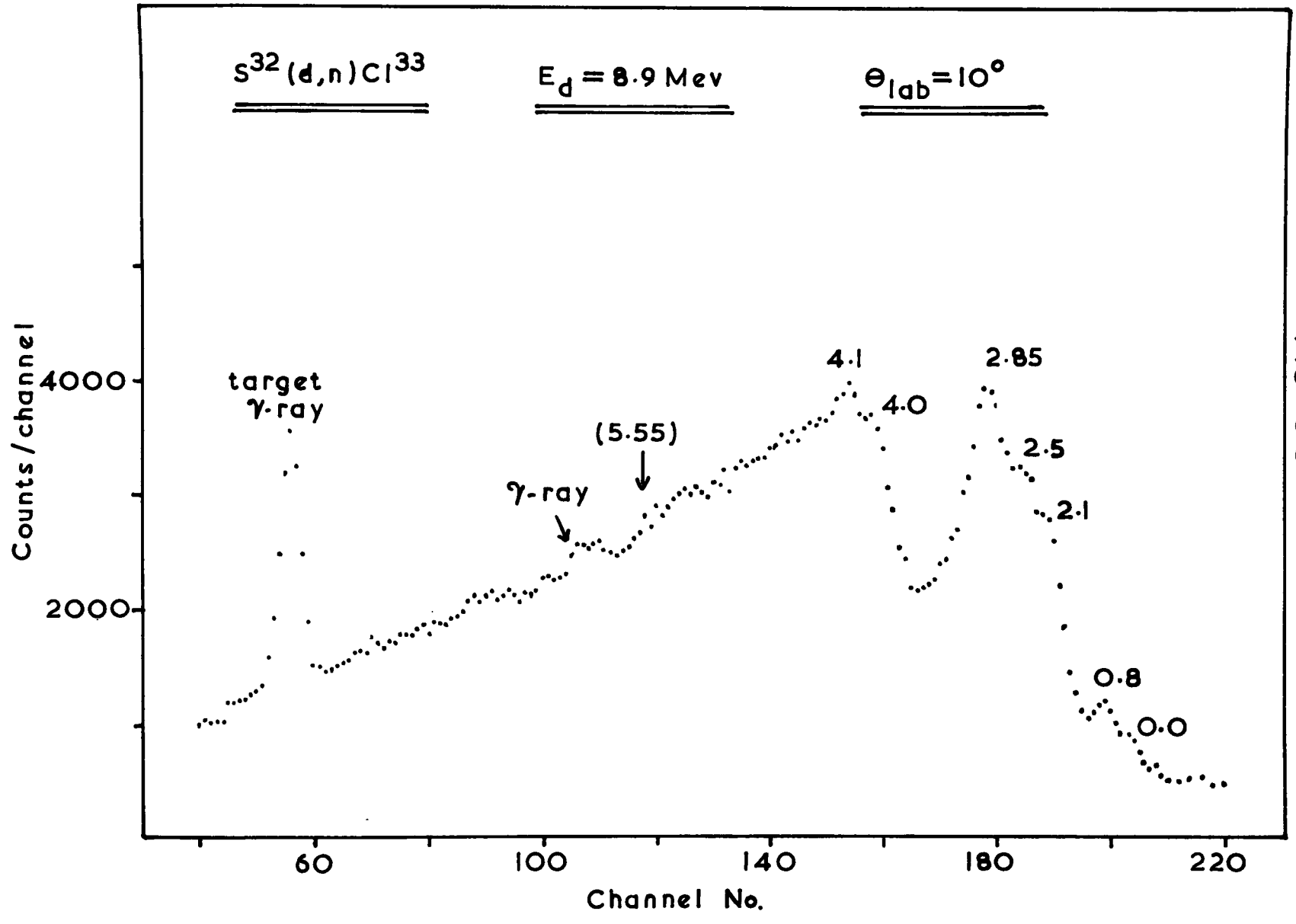
$S^{32}(d,n)Cl^{33}$
$E_d = 8.9$ Mev
$\theta_{lab} = 10°$
Counts / channel
4000
2000
target γ-ray
γ-ray
(5.55)
4.1
4.0
2.85
2.5
2.1
0.8
0.0
60
100
140
180
220
Channel No.

FIG 5.5

reaction is further evidence for its T = 3/2 nature. To all this evidence we can couple the observations of Hardy and Verrall and of Poskanzer, who found superallowed beta transitions to this state from Ar^{33}.

In Table (5.1) we summarise the properties of the Cl^{33} states at 5.55, 6.30 and 7.45 MeV obtained from this work and from the delayed proton experiments.

The first excited state in P^{33} is predicted by Glaudemans to lie at an excitation of 1.37 MeV and is found by Currie and Evans to be at 1.43 MeV. In Cl^{33} the analogue of this state is therefore expected to be at an excitation of 7.0 MeV assuming that the 5.55 MeV level is the analogue of the P^{33} ground state. Unfortunately such a state if excited by the (He^3,n) reaction would lie in that region of the spectra occupied by the strong neutron group from the $O^{16}(He^3,n)Ne^{18}$ reaction. Because of this we are unable to say anything about the existence of this state except to say that if it does exist it is not strongly excited by the (He^3,n) reaction.

We are not able to test the isobaric mass formula for the T = 3/2 quartet at mass 33 because the mass of Ar^{33} is not known accurately. The analogue state in S^{33} has been found at 5.483 ± 0.015 MeV by Dubois (Du 67) and so we are

TABLE 5.1

Excitation in Cl^{33} (MeV)			Spin, Parity and Isospin		
This work	(Ha 65)	(Po 66)	This work	(Ha 65)	(Po 66)
5.55 ± 0.02	5.55 ± 0.05	5.556 ± 0.020	$\frac{1}{2}^+, T=3/2$	$(\frac{1}{2}^+, T=3/2)$	$(\frac{1}{2}^+, T=3/2)$
6.30 ± 0.05		6.22 ± 0.03	$(3/2^+)$		
7.45 ± 0.05	7.55 ± 0.10	7.46 ± 0.09	$(\frac{1}{2}^+)$	$(\frac{1}{2}^+, T=3/2)$	

able to predict the mass of Ar^{33}. Using the mass formula the predicted mass excess of Ar^{33} is - 9.427 MeV.

C H A P T E R VI

CONCLUDING REMARKS

We have shown in this thesis how the neutron "time of flight" technique can be applied to a number of problems in nuclear structure. Neutron spectroscopy is not easy and at present it is not possible to get the same accuracy as can be achieved with charged particle spectroscopy. In view of this can it be said that "time of flight" is a useful tool? The answer to this question is "yes".

Quite often the most straightforward way to reach a particular nuclear state is via a reaction which involves the detection of neutrons. For example, we have measured the spin of the analogue state in Cl^{33} by means of the reaction $P^{31}(He^3n)Cl^{33}$. The nucleus Cl^{33} can also be formed by the reactions $S^{32}(He^3,d)Cl^{33}$, $S^{32}(\alpha,t)Cl^{33}$, $S^{33}(He,t)Cl^{33}$ and $Cl^{35}(p,t)Cl^{33}$ which involve only charged particles. However, the first two reactions cannot excite the analogue state while the last two have large negative Q values. The analogue state was first observed in the spectrum of delayed protons from Ar^{33}, but its spin could only be inferred from this experiment. By means of the (He^3,n) reaction we were able not only to confirm the $T = 3/2$ nature of this state but

also to measure its spin. There is plenty of scope for future work in the field of exciting analogue states by the (He^3,n) reaction. Two possible reactions for future study are $F^{19}(He^3,n)Na^{21}$ and $Mg^{25}(He^3,n)Si^{27}$.

As far as the determination of nuclear energy levels is concerned the reactions (p,n) and (He^3,t) are similar. The Q values are comparable, although always negative, so that in general, if one reaction is energetically possible then so is the other. However, in terms of the interpretation of experimental data such as angular distributions the (p,n) reaction is the more straightforward. The same model may be used to explain both reactions, but since He^3 nuclei and tritons are composite particles they will have complicated wavefunctions, thus making calculations for (He^3,t) reactions difficult unless approximations for the wave-functions are used. This difficulty does not arise with protons and neutrons as ingoing and outgoing particles. In some instances the (He^3,t) reaction is the only alternative to reactions involving neutrons for reaching a particular final nucleus. Such is the case with Be^6 which can only be formed by the reactions $Li^6(p,n)Be^6$, $He^4(He^3,n)Be^6$ and $Li^6(He^3,t)Be^6$. This nucleus was first investigated by means of the (p,n) reaction and only recently has the (He^3,t) reaction been used.

The (p,n) reaction is a useful tool for exciting isobaric analogue states in non-mirror nuclei [An 62]. The reaction can be pictured as one in which the incident proton undergoes charge exchange with a neutron in an unfilled shell in the target and then leaves as a neutron. The overall configuration of the final state is the same as that of the target except for an increase in charge of one unit. There is no transfer of spin or isospin. The Q value for the reaction to the analogue state is precisely the Coulomb displacement energy between the initial and final nuclei. It has also been found that the (p,n) reaction will selectively populate a state in the final nucleus which has the same angular momentum configuration as the target, but which differs in isospin by one unit. Such a state is known as a configuration state.

The third experiment reported in this thesis is a study of the delayed neutrons from Li^9. By means of this experiment we were able to locate states in Be^9 which, although predicted by the shell model, had not been found by reactions involving charged particles alone. We were also able to investigate the beta decay scheme of Li^9. Instead of looking for delayed neutrons we could have in principle looked for delayed alpha particles, but as the final nucleus

He^5 is not a sharp state the observation of particle groups associated with states in Be^9 would have been extremely difficult. The technique has previously been used to study the delayed neutrons from N^{17} [Gi 63] and by means of it several beta transitions to neutron unstable states in O^{17} were found.

The development of Van de Graaff accelerators with pulsed sources capable of producing pulsed beams with intensities of several micro-amperes has overcome to some extent two of the major drawbacks associated with time of flight experiments compared to charged particle spectroscopy. These drawbacks are the poorer energy resolution and the low real to background counting rate. The larger beam currents mean that the yield from the target is increased giving a better real to background ratio, and at the same time one can afford to use longer flightpaths so improving the energy resolution. When studying states with negative Q values one can in principle obtain very good energy resolution by using an incident beam energy which is just above the threshold for the state so that the neutrons leave the target with energies much less than 1 MeV. Now that intense pulsed beams are available use can be made of this effect to resolve closely spaced levels. The intense beams will permit the use of

targets with thicknesses of only a few tens of kilovolts or less instead of targets of the order of 100 keV thick. One does not observe this effect in charged particle spectroscopy since at the reaction threshold the outgoing charged particles have in general insufficient energy to penetrate the Coulomb barrier.

Another recent development is the construction of Van de Graaff accelerators capable of accelerating protons and deuterons to energies of 20 MeV or more. This will open up further fields of study for neutron spectroscopy. Probably the type of reaction with the most direct application in this energy region will be the (p,n) reaction. It should be possible to extend and improve on the work, initiated by the Livermore group using a cyclotron, on the study of isobaric analogue states and configuration states in non-mirror nuclei. By extending the study to heavier nuclei one can investigate to what extent isobaric spin is a good quantum number for heavy nuclei. One can also make precise measurements of Coulomb displacement energies and investigate the variation with atomic number. The field is wide open. "Time of flight" is a challenging but rewarding occupation.

A P P E N D I X

The Calibration of the Accelerators

At the commencement of this work neither of the Oxford accelerators had been calibrated. Since (p,n) threshold energies are easy to measure and since several of these thresholds are known accurately, they were used as calibration points. The relation between the proton resonance frequency in the magnetic field of the analysing magnet and the energy of the particles transmitted by the magnet is given by

$$E\left[1 + \frac{E}{2 m_o c^2}\right] = K \nu^2 \frac{Z^2}{m_o}$$

where E = energy of the particles

m_o = rest mass of the particles

Z = charge of the particles

ν = proton resonance frequency

K = a constant.

The object of the calibration experiments is to determine the magnet constant K. Briefly, this is done by finding the value of ν corresponding to each of the (p,n) threshold

energies used.

For these experiments the counter ratio technique was used (Ma 60). This required the use of two detectors; one which is preferentially sensitive to the slow, threshold neutrons, and one which is sensitive to neutrons of all energies. The slow counter consisted of three BF_3 counters, 7" long embedded in a disc of polythene 6" in diameter and 1" thick. The three counters were connected in parallel to increase the efficiency of the detector. Because of the small amount of moderator this detector is sensitive only to threshold neutrons, i.e., neutrons with energies of a few tens of kilovolts. The other counter, the fast counter, was made from one BF_3 counter 18" long embedded in a cylinder of paraffin wax 18" long and 8" in diameter. The large amount of moderator makes this detector sensitive to neutrons of all energies. The two detectors were arranged in tandem with the slow counter nearer the target and spaced so that they subtended approximately the same solid angle at the target.

The method of determining the position of the threshold is to plot the ratio of the counts in the slow counter to the counts in the fast counter against the magnet n.m.r. frequency in the region of the threshold. At the threshold

there is a sudden increase in the number of slow neutrons reaching the detectors with the result that the ratio increases sharply. This enables the threshold frequency to be found very accurately. The reactions chosen for the calibration experiments were as follows (Ma 66a)

Reaction	Threshold Energy
$Li^{7}(p,n)Be^{7}$	1.88056 ± 0.00013 MeV
$F^{19}(p,n)Ne^{19}$	4.2343 ± 0.0008 MeV
$Al^{27}(p,n)Si^{27}$	5.7969 ± 0.0038 MeV
$d(O^{16},n)F^{17}$	14.5255 ± 0.005 MeV

For the latter reaction O^{16} ions with charge states 3^{+} and 4^{+} were used enabling the magnet to be calibrated for equivalent proton energies of 25.627 ± 0.009 MeV and 14.519 ± 0.005 MeV respectively. Approximate values for the magnet constants had previously been determined by using 8.7864 MeV alpha particles from a ThC' source. The results of the threshold measurements gave the following values for the magnet constants for the two Oxford accelerators :-

Tandem $K = (2.270 \pm 0.001) \times 10^{-2}$

Injector $K = (8.984 \pm 0.004) \times 10^{-2}$

Figure (A.1) shows the result of plotting the counter ratio against frequency for the $Al^{27}(p,n)$ and the $d(O^{16},n)$ reactions. An interesting feature of the $d(O^{16},n)$ reaction is that due to the large centre of mass velocity the threshold neutrons leave the target with a lab. energy of nearly 1 MeV. As a result of this the slow to fast ratio suddenly decreases at the threshold instead of increasing as for the other reactions. This is due to an increase in the number of fast neutrons rather than slow ones. This also shows that the slow counter is indeed insensitive to fast neutrons.

FIG A·1

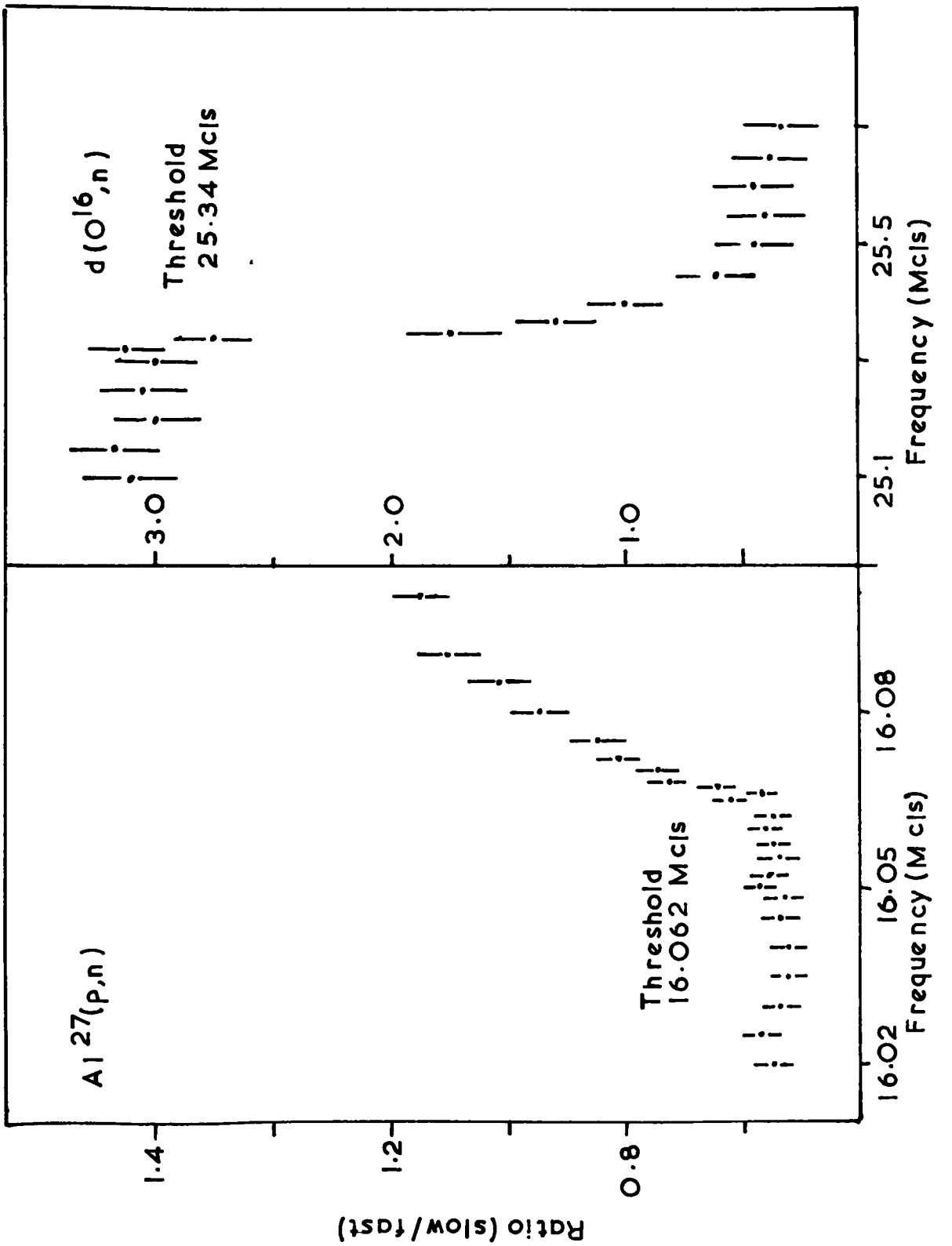
Al 27(p,n)
Threshold
16.062 Mcls
Frequency (Mcls)
16.02
16.05
16.08
d(O16,n)
Threshold
25.34 Mcls
Frequency (Mcls)
25.1
25.5
Ratio (slow/fast)
0.8
1.2
1.4
1.0
2.0
3.0

R E F E R E N C E S

Aj 59 F. Ajzenberg-Selove, C.P. Osgood and C.P. Baker. Phys. Rev. 116, 1521, 1959.

Aj 65 F. Ajzenberg-Selove, J.W. Watson and R. Middleton. Phys. Rev. 139, B592, 1965.

Al 60 K.W. Allen, E. Almquist and C.B. Bingham. Proc. Phys. Soc., 75, 913, 1960.

Al 63 D.E. Alburger, Phys. Rev., 132, 328, 1963.

An 62 J.D. Anderson, C. Wong and J.W. McClure. Phys. Rev., 126, 2170, 1962.

An 62a J.D. Anderson, C. Wong and J.W. McClure. Phys. Rev., 129, 2718, 1962.

Ba 60 R. Batchelor, W.B. Gilboy, A.D. Purnell and J.H. Towle, Nucl. Inst. and Methods, 8, 146, 1960.

Ba 61 R. Batchelor, W.B. Gilboy, J.B. Parker and J.H. Towle, Nucl. Inst. and Methods, 13, 70, 1961.

Ba 64 R.W. Bauer, J.D. Anderson and C. Wong, Nucl. Phys., 56, 117, 1964.

Ba 65 C.J. Batty, E. Friedman, P.C. Rowe and J.B. Hunt, Phys. Lett., 19, 35, 1965.

Ba 66 P.C. Barker, Nucl. Phys., 83, 418, 1966.

Be 63 G. Bellettini, C. Bemporad, C. Cerri and L. Foa. Nucl. Inst. and Methods., 21, 106, 1963.

Be 64 G. Bellettini, C. Bemporad, C. Cerri and L. Foa. Nucl. Inst. and Methods., 27, 38, 1964.

Bl 52 J.M. Blatt and V.F. Weisskopf. Theoretical Nuclear Physics, 1952.

Bo 58 G.F. Bogdanov, N.A. Vlasov, S.P. Kalinin, L.V. Rybakov and V.A. Sidorov. J. of Nucl. Energy 11, 8, 148, 1958.

Bo 63 R.R. Borchers and C.H. Poppe. Phys. Rev., 129, 2607, 1963.

Br 60 J.C. Brolley and J.L. Fowler., Fast Neutron Physics I, Ch. 1c.

Ch 66 F.O. Christensen and C.H. Cocke. Nucl. Phys. 89, 656, 1966.

Co 65 S. Cohen and D. Kurath. Nucl. Phys. 73, 1, 1965.

Co 67 W.F. Currie and J.C. Evans. Phys. Lett. 24B, 399, 1967.

Du 67 J.A.L. Dubois. Bull. Am. Phys. Soc., 12, 572, 1967.

Le 66 S.F. Eccles, C. Wong and J.C. Anderson. Phys. Lett. 20, 190, 1966.

Er 64 R.A. Eramjian. Phys. Lett. 12, 112, 1964.

Ga 59 F. Gabbard, R.M. Davis and T.W. Bonner, Phys. Rev. 114, 201, 1959.

Gi 63 J. Gilat, G.D. O'Kelley and A. Zichler. Bull. Am. Phys. Soc., 8, 320, 1963.

Gl 64 P.W.M. Glaudemans, G. Wiechers and P.J. Brussard. Nucl. Phys., 56, 548, 1964.

Gu 63 N. Gulyamov, B.V. Rybakov, and V.A. Sidorov. Soviet Physics J.E.T.P., 17, 1230, 1963.

Gu 67 N. Gulyamov, B.V. Rybakov, and V.A. Sidorov. Soviet Journal of Nuclear Physics, 4, 66, 1967.

Ha 63 W.D. Harrison and A.B. Whitehead. Phys. Rev., 132, 2607, 1963.

Ha 65 J.C. Hardy and R.I. Verrall. Can. J. of Phys. 43, 418, 1965.

Ha 65a J.C. Hardy, R.I. Verrall, M. Barton and I.S. Bell. Phys. Rev. Lett. 14, 376, 1965.

Ho 64 J.L. Honsaker, Bull. Am. Phys. Soc., 9, 527, 1964.

Ho 67 J.L. Honsaker, Nucl. Phys. A.90, 545, 1967.

In 53 D.R. Inglis. Rev. Mod. Phys. 25, 390, 1953.

Ja 60 J. Jänecke . Zeitschrift fur Physik. 160, 171, 1960.

Ja 65 J. Janecke. Nucl. Phys. 73, 97, 1965.

La 60 A.M. Lane, Rev. Mod. Phys., 32, 519, 1960.

La 66 T. Lauritsen and F. Ajzenberg-Selove, Nucl. Phys. 78, 1, 1966.

Le 55 S.H. Levine, M.L. Bender and J.H. McGruer. Phys. Rev., 97, 1249, 1955.

Ma 60 J.B. Marion and J.W. Bonner. Fast Neutron Physics, Part II, Ch. V o.

Ma 66 N. Mangelson, F. Ajzenberg-Selove, N. Reed and C.C. Lu. Nucl. Phys., 86, 137, 1966.

Ma 66a J.B. Marion. Rev. Mod. Phys., 38, 660, 1966.

Ma 67 V.S. Mathur and J.A. Nook., Nucl. Phys., A91, 305, 1967.

Mi 64 R. Middleton and D.J. Pullen., Nucl. Phys., 51, 50, 1964.

Mu 66 S. Mubarakmand. Thesis, Oxford University, 1966. and Nucl. Phys., A90. 82, 1967.

Ne 60 J.H. Neiler and W.M. Good. Fast Neutron Physics Part I, Ch. IV a.

Ne 60a M.C. Newns. Proc. Phys. Soc., 76, 489, 1960.

Ow 58 A.B. Owen., A.E.R.E. Harwell Report No. A/R/2712 1958. and I.R.E. Transactions on Nuclear Science, NS-5, No.3, 196, 1958.

Po 66 A.M. Poskanzer, R. McPherson, R.A. Esterland and P.L. Reeder. Phys. Rev., 152, 995, 1966.

Ro 64 J.A. Rook and D. Mitra. Nucl. Phys., 51, 96, 1964.

Ro 66 P.C. Rogers and H.H. Wegner., Phys. Rev. Lett. 17, 148, 1966.

Sa 64 G.R. Satchler. Nucl Phys. 55, 1, 1964.

Sa 66 G.R. Satchler. Nucl. Phys. 77, 481, 1966.

Sc 65 A. Schardeberg, H. Hansen, H. Weigmann and A. Flammersfeld. Zeitschrift für Physik. 188, 38, 1965.

Sw 60 C.D. Swartz and G.A. Owen. Fast Neutron Physics Part I, Ch. II D.

Ta 43 H. Taschek and A. Hemmendinger. Phys. Rev., 74, 373, 1948.

Ta 65 J. Takacs. I.E.E.E. Transactions in Nuclear Science 1965, and Rutherford Lab. Report NIRL/R/120.

Ve 66 R.I. Verrall, J.C. Hardy and R.E. Bell. Nucl. Inst. and Methods, 42, 253, 1966.

Wh 66 W. Whaling, Phys. Rev., 150, 836, 1966.

Wi 64a D.H. Wilkinson, Phys. Lett. 11, 243, 1964.

Wi 64b D.H. Wilkinson, Phys. Lett. 12, 348, 1964.

Wi 66 D.H. Wilkinson, J.T. Sample and D.E. Alburger. Phys. Rev., 146, 662, 1966.